Calhoun
Institutional Archive of the Naval Postgraduate School

Calhoun: The NPS Institutional Archive

DSpace Repository

Theses and Dissertations | 1. Thesis and Dissertation Collection, all items

2002-12

Megawatt class free electron lasers for naval application-short Rayleigh length and stability analysis

Ossenfort, William J., Jr.

Monterey, California. Naval Postgraduate School

http://hdl.handle.net/10945/3494

This publication is a work of the U.S. Government as defined in Title 17, United States Code, Section 101. Copyright protection is not available for this work in the United States.

Downloaded from NPS Archive: Calhoun

http://www.nps.edu/library

Calhoun is the Naval Postgraduate School's public access digital repository for research materials and institutional publications created by the NPS community. Calhoun is named for Professor of Mathematics Guy K. Calhoun, NPS's first appointed -- and published -- scholarly author.

Dudley Knox Library / Naval Postgraduate School
411 Dyer Road / 1 University Circle
Monterey, California USA 93943

NAVAL POSTGRADUATE SCHOOL
Monterey, California

THESIS

MEGAWATT CLASS FREE ELECTRON LASERS FOR NAVAL APPLICATION – SHORT RAYLEIGH LENGTH AND STABILITY ANALYSIS

by

William J. Ossenfort Jr

December 2002

Thesis Advisor:	William B. Colson
Second Reader:	Robert L. Armstead

Approved for public release; distribution is unlimited

THIS PAGE INTENTIONALLY LEFT BLANK

REPORT DOCUMENTATION PAGE			Form Approved OMB No. 0704-0188
Public reporting burden for this collection of information is estimated to average 1 hour per response, including the time for reviewing instruction, searching existing data sources, gathering and maintaining the data needed, and completing and reviewing the collection of information. Send comments regarding this burden estimate or any other aspect of this collection of information, including suggestions for reducing this burden, to Washington headquarters Services, Directorate for Information Operations and Reports, 1215 Jefferson Davis Highway, Suite 1204, Arlington, VA 22202-4302, and to the Office of Management and Budget, Paperwork Reduction Project (0704-0188) Washington DC 20503.			
1. AGENCY USE ONLY ***(Leave blank)***	**2. REPORT DATE** December 2002	**3. REPORT TYPE AND DATES COVERED** Master's Thesis	
4. TITLE AND SUBTITLE: Megawatt Class Free Electron Lasers for Naval Application – Short Rayleigh Length and Stability Analysis			**5. FUNDING NUMBERS**
6. AUTHOR William J. Ossenfort Jr.			
7. PERFORMING ORGANIZATION NAME(S) AND ADDRESS(ES) Naval Postgraduate School Monterey, CA 93943-5000			**8. PERFORMING ORGANIZATION REPORT NUMBER**
9. SPONSORING /MONITORING AGENCY NAME(S) AND ADDRESS(ES) N/A			**10. SPONSORING/MONITORING AGENCY REPORT NUMBER**
11. SUPPLEMENTARY NOTES The views expressed in this thesis are those of the author and do not reflect the official policy or position of the Department of Defense or the U.S. Government.			
12a. DISTRIBUTION / AVAILABILITY STATEMENT Approved for public release; distribution is unlimited			**12b. DISTRIBUTION CODE**

13. ABSTRACT ***(maximum 200 words)***

The free electron laser (FEL) is theoretically capable of scaling up to a MW class laser for naval point defense. At such high power levels, the FEL's optics could be damaged. An FEL operating with a short Rayleigh length reduces intensity at the mirrors; however, the performance of short Rayleigh length FELs is unknown. This thesis presents simulations of Thomas Jefferson Laboratories' proposed 100 kW FEL operating with a short Rayleigh length, and of a proposed 1 MW FEL undergoing shipboard induced mirror vibrations. In the 100 kW FEL, Rayleigh lengths of 0.1L to 0.5L (where L is the undulator length) were simulated. Weak field gain increases as Rayleigh length decreases, indicating that short Rayleigh length FELs will start from spontaneous emissions. Final FEL efficiency also increases as Rayleigh length decreases, with the exception of a spike at the typical Rayleigh length design value of 0.3L. For the 1 MW FEL system, the high operating current acts to stabilize the optical mode against vibrations that result in mirror tilts of 0 to 400 microradians, where final output power was reduced 80%. When used in conjunction with an active mirror alignment system, output power of the 1 MW FEL is unaffected.

14. SUBJECT TERMS Free Electron Laser, Short Rayleigh Length, Directed Energy Weapon, Mirror Stability			**15. NUMBER OF PAGES** 126
			16. PRICE CODE
17. SECURITY CLASSIFICATION OF REPORT Unclassified	**18. SECURITY CLASSIFICATION OF THIS PAGE** Unclassified	**19. SECURITY CLASSIFICATION OF ABSTRACT** Unclassified	**20. LIMITATION OF ABSTRACT** UL

NSN 7540-01-280-5500 Standard Form 298 (Rev. 2-89)
Prescribed by ANSI Std. 239-18

THIS PAGE INTENTIONALLY LEFT BLANK

Approved for public release; distribution is unlimited

MEGAWATT CLASS FREE ELECTRON LASERS FOR NAVAL APPLICATION – SHORT RAYLEIGH LENGTH AND STABILITY ANALYSIS

William J. Ossenfort Jr.
Lieutenant, United States Navy
B.S., Auburn University, 1994

Submitted in partial fulfillment of the
requirements for the degree of

MASTER OF SCIENCE IN PHYSICS

from the

NAVAL POSTGRADUATE SCHOOL
December2002

Author: William J. Ossenfort Jr.

Approved by: William B. Colson
Thesis Advisor

Robert L. Armstead
Second Reader

William B. Maier
Chairman, Department of Physics

THIS PAGE INTENTIONALLY LEFT BLANK

ABSTRACT

The free electron laser (FEL) is theoretically capable of scaling up to a MW class laser for naval point defense. At such high power levels, the FEL's optics could be damaged. An FEL operating with a short Rayleigh length reduces intensity at the mirrors; however, the performance of short Rayleigh length FELs is unknown. This thesis presents simulations of Thomas Jefferson Laboratories' proposed 100 kW FEL operating with a short Rayleigh length, and of a proposed 1 MW FEL undergoing shipboard induced mirror vibrations. In the 100 kW FEL, Rayleigh lengths of 0.1L to 0.5L (where L is the undulator length) were simulated. Weak field gain increases as Rayleigh length decreases, indicating that short Rayleigh length FELs will start from spontaneous emissions. Final FEL efficiency also increases as Rayleigh length decreases, with the exception of a spike at the typical Rayleigh length design value of 0.3L. For the 1 MW FEL system, the high operating current acts to stabilize the optical mode against vibrations that result in mirror tilts of 0 to 400 microradians, where final output power was reduced 80%. When used in conjunction with an active mirror alignment system, output power of the 1 MW FEL is unaffected.

THIS PAGE INTENTIONALLY LEFT BLANK

TABLE OF CONTENTS

I. INTRODUCTION 1

II. DIRECTED ENERGY SYSTEMS AND NAVAL SHIPS 3
A. DIRECTED ENERGY WEAPONS SYSTEMS 3
B. SHIPBOARD DIRECTED ENERGY WEAPONS 4
C. FREE ELECTRON LASERS 7
1. Overview of Free Electron Laser Operation 7
a. The Oscillator Type FEL with Energy Recovery in a Ring Configuration 7
b. The FEL in Other Configurations 10
2. Advantages of the Free Electron Laser for Naval Weaponization 12
a. Multi-mission 12
b. Increased Strike Potential 13
c. Fuel 13
d. Logistical Train 13
e. Lasing Medium 13
f. Tunable 14
g. Beam Quality 15
h. Reliability 15
i. Operating Cost 15
3. Disadvantages of the Free Electron Laser 16
a. Initial Cost 16
b. Power Requirements 17
c. Radiation 18

III. OTHER OPTIONS FOR ANTI-SHIP MISSILE DEFENSE 21
A. COUNTERMEASURES AND DECEPTION 21
1. Chaff 21
2. Infrared Decoy 22
3. The Rubber Duck 22
4. Electronic Attack 23
5. Maneuver 23
B. GUNS – THE PHALANX SYSTEM 24
C. MISSILES – THE SEA SPARROW 27
D. LASERS WEAPONS – THE TACTICAL HIGH ENERGY LASER (THEL) 29

IV. DESCRIPTION OF A SHIPBOARD FEL SYSTEM 33
A. OPERATIONAL DESCRIPTION 33
1. Required Power 33
a. Propagation of Light Through Maritime Atmosphere 33
b. The Energy Required to Kill a Missile is Exactly… 40

c. Defining Mission Success *42*
d. The Timeline *43*
e. So, How Much Power is Needed? *43*
2. Range 44
3. Modes of Operation/Operational Tempo 45
a. Cold *45*
b. Cold Standby *45*
c. Hot Standby *45*
d. Lasing *45*
B. PHYSICAL DESCRIPTION 46
1. Size and Weight 46
2. Electron Beam Subsystems 47
3. Light Beam Subsystems 48
4. Auxiliary Support Subsystems 49
a. Refrigeration System *49*
b. Fresh Water Cooling *49*
c. Radiation Shielding *49*
d. Flex/Vibration Control System *50*

V. FREE ELECTRON LASER THEORY 51
A. THE RESONANCE CONDITION - THE ELECTRON-PHOTON RACE 53
B. ELECTRON MOTION AND THE PENDULUM EQUATION 55
C. THE WAVE EQUATION – ELECTRON ENERGY BECOMES LIGHT 57
D. DIMENSIONLESS PARAMETERS 59
1. Dimensionless Time 60
2. Dimensionless Optical Field Strength 60
3. Dimensionless Electron Current 61
4. Dimensionless Phase Velocity 61
E. FEL GAIN 62
1. FEL Phase Space – Electron Bunching 64
2. Strong Field FEL Phase Space - Saturation 68
3. High Current FEL Phase Space 69

VI. SHORT RAYLEIGH LENGTH SIMULATIONS 73
A. SHORT RAYLEIGH LENGTH 73
B. TRANSVERSE WAVEFRONT SIMULATION 75
C. EFFECTS ON WEAK FIELD GAIN 79
D. EFFECTS ON FINAL OUTPUT POWER 80
E. VARYING ELECTRON BEAM SIZE 81
F. JEFFERSON NATIONAL LABORATORY SHORT RAYLEIGH LENGTH EFFORTS 84

VII. SHIPBOARD VIBRATION EFFECTS ON SHORT RAYLEIGH LENGTH FEL OPERATION 85

A. RESONATOR CAVITY STABILITY AND SHORT RAYLEIGH LENGTH....85
B. SIMULATION TECHNIQUE....85
C. SIMULATION RESULTS....87
D. INTERPRETATIONS AND CONCLUSIONS....89
VIII. CONCLUSION....91
APPENDIX A AN INTRODUCTION TO PHASE SPACE....93
LIST OF REFERENCES....97
INITIAL DISTRIBUTION LIST....101

THIS PAGE INTENTIONALLY LEFT BLANK

LIST OF FIGURES

Figure 1. Probability of Missile Fragments Hitting the Ship 5
Figure 2. Oscillator Type Free Electron Laser with Energy Recovery in a Ring Configuration 8
Figure 3. Oscillator Type Free Electron Laser Cavity 9
Figure 4. FEL in a linear configuration with energy recovery 11
Figure 5. Amplifier Type FEL 12
Figure 6. a) AN/SLQ-49 Chaff Buoy Decoy System, "Rubber Duck" 22
Figure 7. Phalanx Close-in weapons system 24
Figure 8. PHALANX hit probability 25
Figure 9. PHALANX bullet scatter at 1,000 meters 26
Figure 10. Launch of a Sea Sparrow Missile 28
Figure 11. THEL PTS beam director 31
Figure 12. THEL system in "transportable" form [HELTAWG, 2001] 32
Figure 13. Atmospheric extinction coefficients for horizontal transmission at sea level with 23.5 km visibility. Absorption by CO_2 and water are not included. 34
Figure 14. Transmittance of 1000 ft horizontal air path at sea level containing 5.7 mm precipitable water at 79° F 35
Figure 15. Coefficients of absorption, scattering, and extinction in a maritime atmosphere 36
Figure 16. Transmittable intensity through a maritime atmosphere 37
Figure 17. Extinction coefficient variation by wavelength at sea level for various atmospheric conditions. Absorption by CO_2 and water are not included. 38
Figure 18. Transmission of 1.06 μm light at sea level for various atmospheric conditions 39
Figure 19. High average current photoinjector 47
Figure 20. Electron Wiggle as a Result of the Undulator Field 52
Figure 21. Resonance 53
Figure 22. The Electron-Photon Race 53
Figure 23. FEL open and closed orbits plotted in phase space 64
Figure 24. FEL phase space evolution at resonance 65
Figure 25. FEL phase space evolution above resonance 67
Figure 26. Weak field FEL gain and phase spectra 67
Figure 27. Strong field FEL phase space evolution 68
Figure 28. High current FEL gain and phase spectra 70
Figure 29. High current FEL phase space evolution 71
Figure 30. Spot Size Picture 75
Figure 31. Weak Field Gain Simulation 77
Figure 32. Extraction Efficiency Simulation 77
Figure 33. Weak Field Gain Simulation Results 80
Figure 34. Strong Field Efficiency Simulation Results 81

Figure 35. Weak Field Gain vs. Electron Beam Radius....82
Figure 36. FEL Efficiency vs. Electron Beam Radius....83
Figure 37. Peak FEL Efficiency vs. Rayleigh Length at Any Electron Beam Radius....83
Figure 38. Mirror Tilt Simulation Results....86
Figure 39. Efficiency vs. Initial Electron Phase Velocity as a Function of Mirror Tilt q_m....87
Figure 40. 1 MW Efficiency vs. Mirror Tilt....88
Figure 41. 100 kW Tilted Mirror Efficiency and Gain....89
Figure 42. Simple pendulum closed-orbit phase space plot....93
Figure 43. Pendulum separatrix....94
Figure 44. Simple pendulum open-orbit phase space plot....95

LIST OF TABLES

Table 1. Comparison of Operational Cost of Point Defense Systems 16
Table 2. Comparison of Installation and Lifetime Cost of Point Defense Systems (Millions of Dollars) 17
Table 3. Comparison of Power Consumption of Point Defense Systems.....18
Table 4. Power *P* received from a 1 MW laser for various viewing conditions 39
Table 5. Comparison of Size and Weight of Point Defense Systems 46

THIS PAGE INTENTIONALLY LEFT BLANK

LIST OF ACRONYMS

AA	Anti-Air
ABL	Airborne Laser
ACTD	Advanced Concept Technology Demonstration
AFEL	Advanced Free Electron Laser at LANL
APDS	Armor Piercing Discarding Sabot
ASCM	Anti-Ship Cruise Missile
ASM	Anti-Ship Missile
BDA	Battle Damage Assessment
CIWS	Close-In Weapons System
CVN	Aircraft Carrier
CG	Guided Missile Cruiser
CW	Continuous Wave
C^3I	Command, Control, Communications and Intelligence
DC	Direct Current
DD/DDG	Destroyer
DF	Deuterium Fluoride
DSBTF	Defense Science Board Task Force
EAGLE	Evolutionary Aerospace Global Laser Engagement
ESSM	Evolved Sea Sparrow Missile
EW	Electronic Warfare
FAS	Federation of American Scientists
FEL	Free Electron Laser
FFG	Frigates
FY	Fiscal year
GAO	Government Accounting Office
GMVLS	Guided Missile Vertical Launch System
HEL	High Energy Laser
HELERP	High Energy Laser Executive Review Panel
HELSTF	High Energy Laser System Test Facility
IR	Infrared
JLAB	Thomas Jefferson National Accelerator Facilities
LANL	Los Alamos National Laboratories
LHA/LHD	Amphibious Assault Ships
LS	Laser Subsystem
LSD	Dock Landing Ships
MIRACL	Mid-Infrared Advanced Chemical Laser
M-THEL	Mobile Tactical High Energy Laser
NSSMS	NATO Sea Sparrow Missile System
NFF	Navy Fact File
PTS	Pointer Tracker Subsystem
PRF	Pulse Repetition Frequency
RAM	Rolling Airframe Missile
RF	Radio Frequency

SM	Standard Missile
SSTG	Ship's Service Turbine Generator
SWOIR	Super Walk-Off IR decoy
TBMD	Theater Ballistic Missile Defense
THEL	Tactical High Energy Laser
USAF	United States Air Force
USN	United States Navy

LIST OF SYMBOLS

Throughout this thesis, cgs units are used, except for the dimensionless variables mentioned below, which are defined in the text.

a_0	dimensionless optical field strength at the beginning undulator
a_t	dimensionless optical field strength at the end of the undulator
$\vec{A}$	vector potential
A_e	cross-sectional area of the electron beam
$\vec{B}$	vector sum of the undulator and optical magnetic fields
$\overrightarrow{B_S}$	optical magnetic field
$\overrightarrow{B_U}$	undulator magnetic field
c	the speed of light
c_{Al}	specific heat capacity of Al
e	charge of an electron
E_{bond}	bonding energy of each atom in a lattice structure
E_e	electron energy
E_{las}	accelerator output energy
E_{lat}	energy required to break apart 300 cm^3 of Al lattice
E_{melt}	energy required to melt 300 cm^3 of Al
E_{opt}	energy in the optical beam
E_s	optical electric field
DE/E	electron energy spread
$(DE/L)_{acc}$	acceleration gradient
f	FEL operating frequency
F	filling factor
G	optical gain
h_{FEL}	height of the FEL beam director above sea level
$h_{missile}$	height of an ASCM above sea level
I	instantaneous electron current
I_{avg}	average FEL current
I_{pk}	peak FEL current
j	dimensionless electron current
$\vec{J}_\perp$	transverse current density
k	optical wave number
k_0	undulator magnetic wave number
K	undulator parameter
l_e	electron pulse length
L	undulator length
L_{acc}	total accelerator length
L_{melt}	latent heat of melting for Al
L_{mod}	length of accelerator module

m	mass of an electron
M	atomic mass
N	number of undulator magnetic periods
N_A	Avogadro's number
N_e	number of electrons
$P(x)$	optical power at a range x
P_{acc}	Input Power
P_{inj}	injector input power
P_{out}	optical IR power out
q	bunch charge
Q	resonator quality factor
r	distance through which light must propagate
r_e	electron beam radius
$\vec{r}_i$	position of the i^{th} electron
R_{horiz}	farthest line of sight distance between the FEL beam director and the ASCM
R_m	mirror radius
S	resonator length
t	time
T	atmospheric transmittance
T_{amb}	ambient temperature
T_{melt}	melting temperature
$\vec{v}_e$	electron velocity through the FEL cavity
V	volume
W_{inj}	injector output energy
$W(z)$	optical waist
W_0	optical waist at mode focus
w_0	dimensionless optical beam waist
w_{mirror}	dimensionless optical spot radius at cavity mirror
z	longitudinal coordinate in the undulator
z_n	coordinate transformation = $z + ct$
z_0	dimensionless Rayleigh length
Z_0	Rayleigh length

$\vec{b}$	non-dimensional electron velocity
$b_\perp$	transverse component of $\vec{b}$
b_z	axial component of $\vec{b}$
d^3	three dimensional Dirac delta function
e	transverse emittance
$\hat{e}_1$	unit vector = $(\cos y, -\sin y, 0)$

$\hat{e}_2$	unit vector = $(-\cos y, -\sin y, 0)$
g	Lorentz factor
l	optical wavelength
l_0	magnetic period length
h	wiggler extraction efficiency
h_{rf}	accelerator efficiency
W	pulse repetition frequency
f	initial optical phase
r	density
r_e	density of electrons
y	optical phase
s	extinction coefficient
s_a	absorption coefficient
s_s	scattering coefficient
$s_{x,y}$	the dimensionless electron beam radius in the x and y dimension
q	pendulum phase position
t	dimensionless time
n	dimensionless electron phase velocity
n_0	initial electron phase velocity
n_s	phase velocity and phase of the FEL separatrix
z	electron phase
z_s	phase of the FEL separatrix

THIS PAGE INTENTIONALLY LEFT BLANK

ACKNOWLEDGMENTS

Plans fail for lack of counsel, but with many advisers they succeed.

– Proverbs 11:14

This thesis would not have been produced without tremendous support from so many of my family, friends, colleagues, and mentors.

To Professor Colson, who knows the secrets of the FEL, thank you for your endless patience. Thanks also to Professor Crooker and Professor Armstead. Your advice in editing and shaping this thesis were greatly appreciated. (In case you are wondering, the duck made it through after all.)

To Alan Todd, who loves living life, don't let the new kids forget what conferences are really about; and to George Niel, who somehow managed to explain physics while dancing with the stones (stick with the physics – trust me), thank you for your time, your friendship, and your willingness to help.

To my colleagues (cellmates) who obviously spent too much time playing with saran wrap to understand the game of football, I give much-deserved thanks. You made the time fun. To Thomas Campbell, who always gets the right answer, I'm still not sure if you helped keep me sane, or lost your sanity with me. Thanks for your friendship Super-G.

To my wife, Shelley, whose patience, support and love never gets recognized enough, I love you always. To my wonderful children, Ashley, Kali, Christian, and Trey, thanks for all the hugs. I am so glad you are mine.

Finally, I thank God, who healed me when I was broken, and taught me to love again. Thank you.

THIS PAGE INTENTIONALLY LEFT BLANK

I. INTRODUCTION

Point defense for a ship against modern anti-ship cruise missiles (ASCMs) requires faster weapons systems than are currently available. Improvements in anti-ship missile capability have reduced reaction times to seconds from detection until impact for a high-speed sea skimming missile. Directed energy weapons provide target engagement at the speed of light, thereby moving the ASCM destruction range away from the ship so that fragments generated from the missile kill will not hit the ship. The all-electric free electron laser (FEL) is theoretically capable of scaling up to a MW class laser needed for a naval point defense weapon. At such high power levels, the optics of a laser could easily be damaged. Simulations conducted for Jefferson Laboratories' proposed 100 kW FEL show that a short Rayleigh length will significantly reduce optical intensities seen at the mirror without significant degradation of laser performance. An FEL resonator, which must be tuned within microns of length, will be subject to ship-induced vibrations. Short Rayleigh length cavities are susceptible to optical mode rotations as a result of mirror instabilities. This thesis presents simulations that study the effect of vibrations that result in mirror tilt. This is the first time the effect of tilting the mirrors within an FEL has been examined. These simulations show that the high current necessary in a MW class FEL acts to stabilize the optical mode against vibrations that result in mirror tilt, and that when used in conjunction with an active mirror alignment system, output power is not affected.

Chapter II discusses current directed energy weapons programs, desired capabilities and needs of a shipboard high-energy laser, and introduces the free-electron laser. A basic operational description, as well as configurations and characteristics of a free-electron laser are discussed.

Chapter III discusses other options for shipboard defense, including countermeasures, deception, gunnery, missiles, and chemical lasers. The PHALANX close-in weapon system, Sea Sparrow missile system, and the tactical high-energy laser are examined in detail.

Chapter IV contains a description of a MW class FEL for shipboard use, including required power calculations, range, modes of operation, and a physical description.

Chapter V discusses the theory of operation of a free electron laser and establishes how electron beam energy is converted to laser light.

Chapter VI introduces the concept of using a short Rayleigh length optical cavity to reduce the optical intensity on the cavity mirrors. The transverse wavefront simulation used to analyze weak field gain and steady-state power is introduced. Simulations are presented with results applicable to the Thomas Jefferson National Accelerator Facilities' proposed 100 kW FEL using a short Rayleigh length. The compiled results represent the work of LT Thomas Campbell, Mr. Ivan Ng, and myself. I conducted simulations studying specific Rayleigh lengths. These results were originally presented at the 23rd International FEL Conference in Darmstadt, Germany, and has been published in Nuclear Instruments and Methods in Physics Research [Ossenfort, 2002].

Chapter VII examines the impact of mirror oscillations induced by shipboard vibrations. The transverse wavefront simulation is again used to examine weak-field gain and steady-state power. The results represent the work of LT Thomas Campbell and myself. I conducted the simulations for specific mirror vibration angles. These results were originally presented at the 24th International FEL Conference in Chicago, Illinois, and will be published in 2003.

The capabilities of a directed energy weapon are different from any other Navy system. The ability to strike a lethal blow at the speed of light with such precision would provide a new force in point defense, as well as a quick-response precision weapon in the fight against anti-symmetric threats. With continued research into the effects of the high-power short Rayleigh length FEL, and in creating compact laser components, a MW class system appears to be achievable within a decade.

II. DIRECTED ENERGY SYSTEMS AND NAVAL SHIPS

A. DIRECTED ENERGY WEAPONS SYSTEMS

The United States has thrived militarily by fielding the best-trained, best-equipped war fighting force on any battlefield. Directed energy in the form of high-energy lasers (HELs) introduces an entirely unique capability to today's fighting force. No existing weapon system possesses the ability to precisely deliver lethal amounts of damage limited only to a specific location on a target. Lasers offer the ability to selectively destroy a small volume of a target accurately. The ability to deliver this energy on target while causing no damage to the immediate area surrounding the target, gives unprecedented flexibility in target selection. This precision in delivery will allow targets previously considered difficult, such as an anti-aircraft gun on top of a civilian apartment complex or a jet-ski zooming through a crowded harbor, to be lethally struck without causing unnecessary casualties or undesired damage to the building.

Within the next two decades, it is possible that lasers will form a key component in all battle spaces, including systems incorporated into aircraft, ground vehicles, ships, and space. Advances in computing power and simulations have allowed the rapid maturity of directed energy weapons such that many systems are being tested in a prototype status. Examples are the Mid-Infrared Advanced Chemical Laser (MIRACL) and Tactical High Energy Laser (THEL) systems for tactical anti-missile defense, and the Army's ZEUS counter-munitions system used to neutralize surface-laid mines and unexploded ordnance. The Airborne Laser program (ABL) for theater ballistic missile defense (TBMD) and M-THEL, a truck mounted mobile version of THEL, are under construction and scheduled for testing this decade. Other projects are in various stages of design, such as the Evolutionary Aerospace Global Laser Engagement (EAGLE) system to relay a laser beam generated elsewhere to a target by bouncing the beam off several mirrors installed on satellites orbiting the earth.

General Larry D. Welch, USAF (Ret.), and Mr. Donald C. Latham, members of the Defense Science Board [Welch, 2001], summarized well the potential for directed energy to significantly affect the battle spaces of modern warfare:

> HEL systems offer speed-of-light engagement of a variety of targets with the potential to produce a range of precisely controlled effects, as well as the potential of deep magazines, low cost per shot (or per kill), and reduced logistical footprint.

B. SHIPBOARD DIRECTED ENERGY WEAPONS

Naval warship weaponry has historically been designed using a magazine of ballistic shells or missile weapons. Offensive weapons, such as five-inch guns or TOMAHAWK cruise missiles, and defensive systems, such as the PHALANX close-in weapons system or STANDARD missiles, use gunnery or rocketry to send the kill vehicle (i.e. – explosive warhead or bullet) toward the target.

However there are several reasons to pursue an HEL system as a maritime weapon. Perhaps the most compelling is that today's defense against anti-ship missiles (ASMs) is taxed to the limit, yet faster, more capable ASMs are still being developed. New supersonic, low flying cruise missiles have dramatically reduced the time a ship has to track and engage an incoming threat missile. For example, the SS-N-26 Oniks, a Russian deployed ASM, can exceed Mach 3.5 upon approach to its target, while racing just a few feet above sea level [Jane's (b), SS-N-22 Sunburn/SS-N-26 Oniks]. The low flying altitude makes detection more difficult, allowing the missile to get in closer to the ship before detection. If this missile can be detected 12 miles from the ship, which is unlikely given the low flying altitude, the ship would have only 18.5 seconds to identify and track the threat, determine a firing solution, authorize weapons free, and engage the ASM with enough time to allow the defensive weapon to shoot down the incoming ASM threat. It is in this last step of engagement/shoot-down of the ASM that directed energy weapons could significantly enhance ship's defense. Modern anti-ASM missiles have speeds of Mach 2 (Rolling Airframe Missile (RAM)) to Mach 2.5 (Sea Sparrow) [Jane's (c), Spruance Class Destroyers]. This means that the ASM will be able to close over half the range to the ship prior to intercept, *after the ship has launched its defensive missiles!* Shorter ASM destruction range is significant because at the moment a missile is destroyed, it will no longer be able to fly a controlled course and detonate, but will now continue on as several large flying pieces of ASM. Essentially, the ASM has been converted from a guided bomb to a kinetic energy ballistic weapon. Figure (1) shows the

probability of any one missile fragment striking a ship as a function of the range at which the ASM was destroyed. This simulation assumes a Mach 1.2 (400 m/s) inbound ASM cruising at a height of 32 m, a relatively simple target. This simulation generates random sizes and air drag coefficients for each fragment.

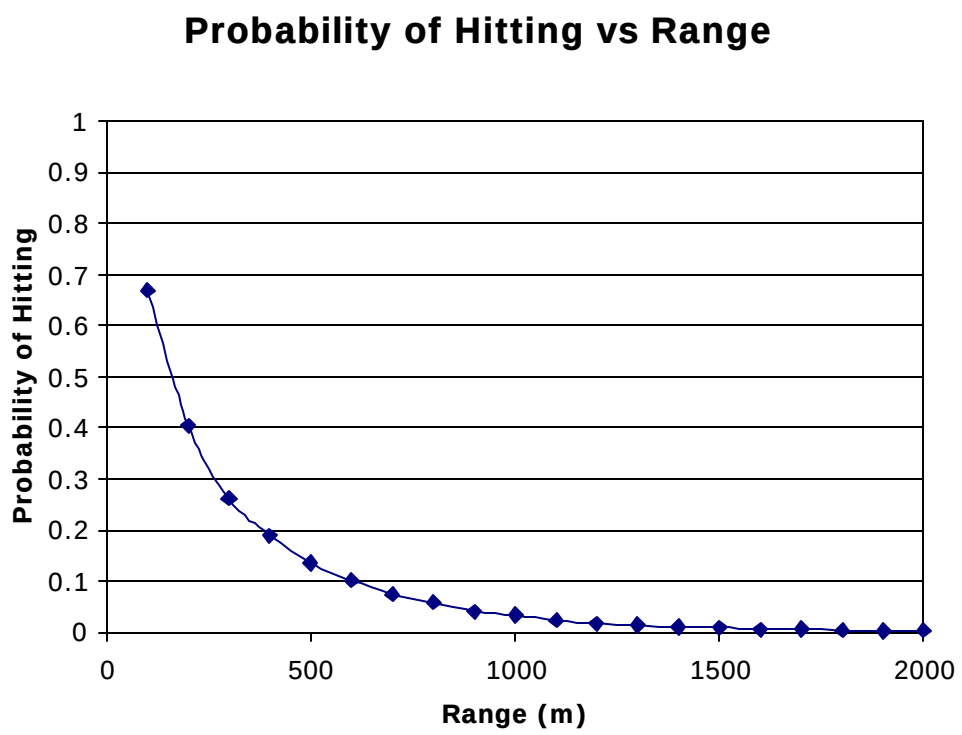

Figure 1. Probability of Missile Fragments Hitting the Ship

Outside of 1000 meters, the probability of missile fragments hitting the ship remains near zero, with less than a 1% change in probability per one hundred meters change in range. The probability begins to rapidly rise inside of seven hundred meters, changing from 7% at 700 meters to 67% at 100 meters. Using even the best-case scenarios, PHALANX Close-In Weapons System (CIWS) will statistically kill the Mach 1.2 ASM at a range of only 300 meters. Figure 1 gives a 26% chance of any one fragment hitting the ship if originating from a Mach 1.2 missile destroyed 300 meters from the ship. Since many fragments may result from the destruction of an ASM, the likelihood of some fragments hitting the ship are high. Each fragment carries enough kinetic energy to cause damage to unarmored components such as personnel, antennae, or sensitive radar equipment. An in-depth discussion of PHALANX is presented in Chapter III, Section B.

As better ASMs further strain the capabilities of current ship defense systems, the ASM/anti-ASM engagement will continue to move toward the ship. Not only does close engagement raise the chances of ASM detonation upon the ship, but as seen in Figure 1, significantly raises the likelihood of ASM fragments striking the ship, which can cause substantial damage or loss of life even with a successful kill of the ASM. An HEL system moves this engagement out because the anti-ASM mechanism moves at the speed of light. This near instantaneous engagement means the ASM can be destroyed several seconds earlier, resulting in a smaller chance of damage to the ship by either warhead detonation or impact by destroyed missile fragments.

This reason alone would justify further research into the development of HEL technologies for ship's defense, but an HEL offers many other advantages as well. In addition to point defense, a high-powered laser has the inherent ability to be utilized as an offensive weapon against any type of target if desired. Unlike most weapons systems, an HEL is not optimized to work against a specific type of target, such as a missile or a tank, but can strike any target equally well. An HEL is designed to deliver more energy to a target than the target can accept. Whether slow or fast, on land, air, or sea, large or small, if the ship can detect it, an HEL can engage it. For example, a highly maneuverable small watercraft such as an unmanned remotely controlled jet ski is a formidable challenge to all current ship's weapons systems, but could be easily targeted with a laser.

Perhaps the most under appreciated aspect of HEL systems is the ability to utilize the laser optics for high-resolution visual surveillance on any line-of-sight contact. Improved visualization capability would allow real-time contact identification, battle damage assessment (BDA), or just a closer look at an unknown object or activity. The laser's beam director, which is normally used to aim the laser at its target, is essentially a large telescope. The Sea Lite Beam Director, which is part of the High Energy Laser System Test Facility (HELSTF) at White Sands Missile Range, New Mexico, is currently being used at long ranges to positively identify targets and confirm the kill of ASMs [DSBTF, pp. 87].

The emergence of all-electric ship designs, the success of prototype missile defense systems, and the rapid maturity of HEL systems and simulations all indicate that

a shipboard HEL is possible. The multi-mission capability, controlled lethality, and impressive surveillance capability make a shipboard HEL desirable. The improvements in ASM technology makes a shipboard HEL missile defense necessary. It is for these reasons that the Commander in Chief, U.S. Atlantic Fleet, Admiral Robert Natter, has stated to the Chief of Naval Operations [Natter, 2001].

> It is my hope that [the Navy] can move quickly toward developing, demonstrating, and acquiring an effective laser weapon system for out forces. I request, therefore, that we pursue this technology aggressively.

C. FREE ELECTRON LASERS

The free electron laser (FEL) offers a unique set of attributes such as wavelength selection, all electric operation, and scalability to extremely high powers, all of which suggest that further research toward a compact, high-powered FEL system could provide the Navy with a viable HEL weapons system within ten years [DSBTF, pp. 89].

1. Overview of Free Electron Laser Operation

There are several operational configurations for a free electron laser. Fundamentally, each configuration must contain four processes: 1) freeing electrons from a cathode surface for use in an electron beam, 2) acceleration of the electron beam to high energy, 3) passing high energy electrons through a lasing cavity containing a spatially periodic magnetic field which produces an optical wave, and finally 4) disposing of the electrons. Steering magnets are used to guide the electron beam through the FEL system.

Section (*a*) contains a discussion of an oscillator type FEL with energy recovery in a ring configuration. While no weapons-grade FEL has been constructed, parameters discussed here for the purpose of explanation are suitable. Other common configurations will be compared to this laser in Section (*b*).

a. The Oscillator Type FEL with Energy Recovery in a Ring Configuration

The "lifetime" of an electron in the free electron laser can be traced from birth to death as the red path in Figure 2.

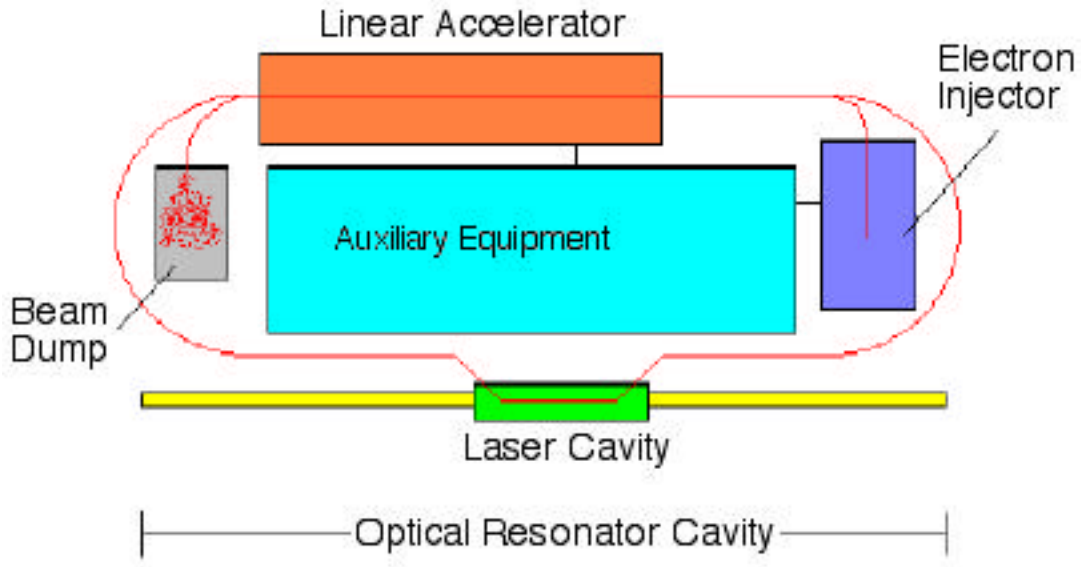

Figure 2. Oscillator Type Free Electron Laser with Energy Recovery in a Ring Configuration

Many electrons are initially generated in the electron injector. Electrons can be freed from a metallic surface by thermionic emission (heating the cathode surface until some electrons have enough energy to become free) or, more commonly, by photoemission (pulsing a laser upon the cathode surface). A strong electric field at the output of the electron injector collects the free electrons and accelerates them toward the input of the linear accelerator. The electrons leave the injector at approximately 7 MeV in short pulses with a repetition rate determined by the laser pulse frequency - 750 MHz for the example laser used in this discussion.

The electron beam gains all of its energy in the linear accelerator. Radio frequency (RF) super-cooled superconducting modules are used to create *very* strong electric fields, possibly as high as 20 MV/m. The operating frequency of the accelerator is synchronized with the injector laser pulses so that when the electrons arrive in the accelerating cavity, an electric field is applied to accelerate the electrons up to an energy of 187 MeV, about 99.999% the speed of light. In the accelerator, each electron pulse will become slightly tighter bunched together, with a pulse frequency remaining at the injector laser pulse frequency, 750 MHz.

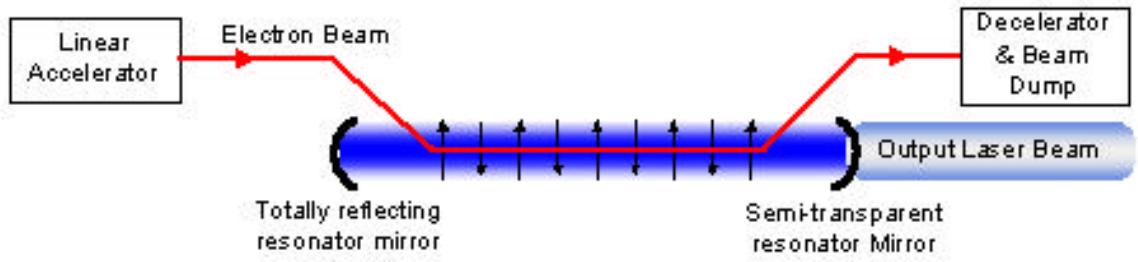

Figure 3. Oscillator Type Free Electron Laser Cavity

The high-energy electron beam is now passed into the lasing cavity, where it travels through a series of opposing magnets, called an undulator. The following is a general overview of the physics that occurs inside an FEL cavity. A more thorough discussion is presented in Section V.

As the electrons pass through the spatially oscillating magnetic field set up by the undulator shown in Figure 3 they will be accelerated, wiggling back and forth according to the Lorentz force law. The lateral acceleration of relativistic electrons results in radiation (light) being emitted along the axis of the undulator. The emitted light is now bounced back and forth between the mirrors at either end of the lasing cavity. As the reflected light crosses the undulator from its second reflection (so that it is traveling in the same direction as the electron beam), another electron pulse is sent through the undulator. These new electrons wiggle due to the undulator fields, but are now in the presence of the previously created light beam as well. The electric and magnetic fields from the light will also interact with the electron beam, stimulating additional light created coherently with the original light. This process is repeated until the resultant electric field created by the light reaches saturation, where further growth of light intensity is matched by cavity losses. One of the end mirrors of the cavity is partially transmissive, allowing some fraction of the light to pass through with each reflection. The light that escapes the cavity is used as a weapon.

At saturation, the electrons will lose a few percent of their energy in creating the light in the laser cavity, dependant on undulator design and electron beam characteristics. After the electrons have passed through the undulator, they are again steered through a 180° turn and returned to the accelerator. The electrons enter the

accelerator field at a phase that causes the electrons to be slowed down, giving up their energy to the accelerator's electric field. The energy the electrons give up is stored in the accelerator and given to the next batch of electrons that passes through. This process of recycling the energy from "used" electrons (dubbed "energy recovery") was recently used at Thomas Jefferson National Accelerator Facilities (JLAB). Energy recovery gives two significant advantages. First, since energy from one electron bunch is used to speed up the next electron bunch, the amount of energy that must be supplied by a separate power source to the accelerator during operation of the FEL is dramatically reduced. Less obvious, but perhaps more significant for naval applications, is that the electrons are slowed to less than 10 MeV before being steered to the beam dump. The beam dump is used to stop the electrons after the accelerator slows them. This is usually nothing more than a cooled block of metal. As the electrons are stopped, they will emit radiation. The type of radiation emitted depends on how much energy the electrons have prior to stopping. Since most of the electron beam energy has been given to the accelerator during energy recovery, the electrons that enter the beam dump only have enough energy to create electromagnetic radiation, which can be easily shielded to protect personnel and equipment. Without energy recovery, neutron radiation would be created. Neutrons are more difficult to shield, significantly more harmful to personnel, and will cause equipment to become radioactive.

b. The FEL in Other Configurations

Figure 4 shows another FEL configuration with energy recovery. This method of operation eliminates the magnetic turnarounds found in the ring configuration used to return the electrons back to the original accelerator cavities. The electrons are sent to a second accelerator in-line with the first and the lasing cavity. Additionally, a second electron gun can be added to the end, allowing a "cross-firing" of electrons, with each accelerator cavity being used to decelerate electrons fired from the opposite end.

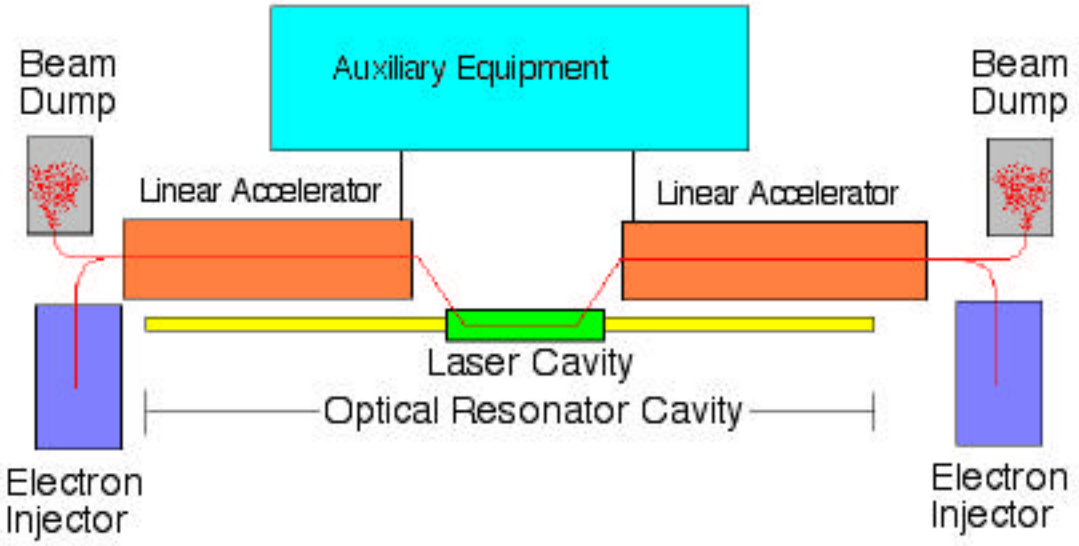

Figure 4. FEL in a linear configuration with energy recovery

The additional size and cost of adding a second linear accelerator makes this configuration undesirable in most laboratory settings. The additional length in the dimension of the lasing cavity is undesirable for shipboard designs, which could be as long as 16 meters in a ring configuration.

Another configuration being researched at Los Alamos National Laboratories (LANL) is the Advanced Free Electron Laser (AFEL), is a single-pass, high-power high-gain FEL design using an amplifier cavity rather than a resonator cavity [LANL.gov]. Amplifier FELs are designed to extract as much energy as possible from the electron beam in just one pass. The amplifier configuration shown in Figure 5 shows that the light beam does not bounce back and fourth between mirrors, but immediately exits the lasing cavity.

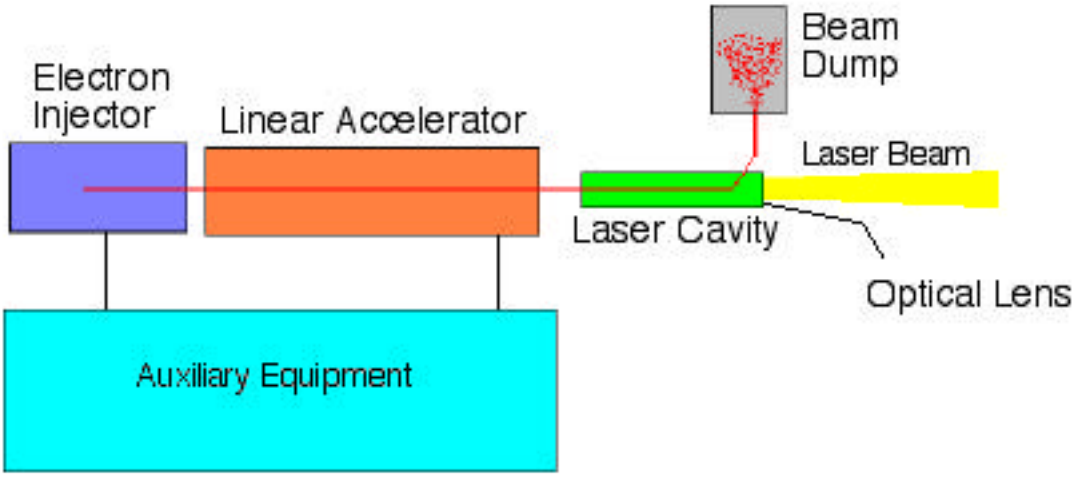

Figure 5. Amplifier Type FEL

One disadvantage of the amplifier FEL as a Naval weapon is that so much energy is removed from the electron beam in the laser cavity, the electron beam is dispersed enough so that energy recovery cannot be done. This provides the undesirable complication of much higher radiation levels, with possible neutron creation at the beam dump.

2. Advantages of the Free Electron Laser for Naval Weaponization

Chemical, free electron, and solid-state lasers have been identified as having the potential to achieve high enough power levels for weaponization. The Defense Science Board Task Force (DSBTF) favors additional research of the free electron and solid-state lasers for maritime self-defense based upon projected electrical power available onboard navy ships. Chemical lasers, however, have been determined to be a poor choice for shipboard use based upon poor selection of operating wavelengths and fuel handling and storage requirements. [DSBTF, pp. 89]

a. Multi-mission

An FEL would contain attributes enabling engagements over a wide spectrum of threats and threat scenarios. The FEL is not a specialized weapon system such as PHALANX, TOMAHAWK, or RAM. Unlike most weapons systems, an FEL is not optimized to work against a specific type of target. While most commonly discussed in a point-defense role, an FEL is not limited to it.

The FEL's missions are not even limited to weapon related tasks. The laser optics can be used for high-resolution visual surveillance on any line-of-sight contact. Real-time contact identification, battle damage assessment (BDA), or a closer look at an unknown object or activity can be done with the laser's beam director.

b. Increased Strike Potential

With the introduction of the FEL as an anti-missile asset, presumably the ship would not be as dependent upon other systems such as the SM-2 (STANDARD missile system) fulfilling an anti-missile role. The number of SM-2's loaded in launcher cells could be reduced, allowing additional TOMAHAWK strike missiles to be carried by the ship. This increase in strike capability gives the battle commander options to use additional force during a strike, or to extend the time he is able to remain on station capable of conducting strike missions before needing to port for TOMAHAWK reloading.

c. Fuel

The FEL uses only electricity for operation. No bullets, missiles, or chemical storage tanks are needed for sustained fire. As long as the ship is capable of electric power generation, the laser can shoot. This gives the ship a highly reliable source of munitions that never has to stop firing to be reloaded. Ships without all-electric capability may be required to recharge stored energy systems periodically.

d. Logistical Train

Many of today's most commonly used systems such as TOMAHAWK are limited by how many are onboard the ship, or in the national inventory. When a ship has expended the TOMAHAWK's onboard, it must leave station and pull into port to replenish its supply. The HEL's logistics train consists only of the fuel needed to operate the ship's turbine generators. Ship's fuel is regularly loaded today while remaining on station. As long as the ship has fuel, the ship has both an offensive and defensive capability.

e. Lasing Medium

Most lasers use a lasing medium such as CO_2, Deuterium Fluoride (DF), or a silicon substrate, to provide electrons that can be excited and emit light. During the

lasing process, the lasing medium will heat up. The higher the output power of the laser, the more the medium will heat up. This heat must be removed for sustained operation. Current high-power chemical lasers such as THEL or MIRACL vent the hot lasing gas through a cooler and refuel the laser with fresh unheated fuel. Often, this exhaust is toxic and highly corrosive. The FEL uses electrons in a vacuum, and has no other medium to heat up. Since no medium has to be vented, the FEL has no toxic exhaust plume to dispose of and no medium to overheat, and does not require refueling.

f. Tunable

Not all light travels through the atmosphere in the same way. The ability of a laser to deliver lethal energy to a target is affected by the air it travels through. The atmosphere itself becomes the new medium for the laser light after it leaves the ship. Some wavelengths will become almost completely absorbed in a short distance, while other wavelengths will pass through the atmosphere with only a small fraction of original beam energy lost.

The problem of absorption becomes much worse when considering very high-powered laser beams. The more energy passed through the air, the more energy is absorbed. If the air absorbs enough energy rapidly, it will heat up, causing a change in the air density. The localized change in air density will form a divergent atmospheric lens that will de-focus the laser beam, resulting in the laser energy becoming too spread out to destroy the target. The process of the laser light becoming spread out as a result of localized atmospheric heating is known as thermal blooming.

Lasers that use a lasing medium are constrained to a few, very specific wavelengths determined by the medium used. In an FEL, the wavelength of the radiation is determined by the electron beam energy and undulator design parameters. For the proposed Naval FEL system, infrared light of 1.06 μm is used to minimize atmospheric absorption of the laser energy while keeping the laser beam out of the visible spectrum. An examination of absorption of 1.06 m light absorption is presented in Section IV.A.1.

g. Beam Quality

The oscillator FEL generates a pulsed, high-brightness coherent wave front that gives excellent optical beam control properties. The coherent wave front allows for sharp focusing of the optical beam upon a target.

h. Reliability

FEL's have been in operation throughout the world for decades. Since the FEL system is entirely electrical (except the refrigeration plant), limited maintenance is required for sustained operation. JLAB's 10 kW FEL upgrade, which is similar in design to proposed weapons system but on a smaller scale, projects a capability for 10,000 hours (over 13 months) of continuous operation without a scheduled maintenance shutdown [Neil]. The FEL's anticipated uptime of > 99% is impressive when compared to the PHALANX system that has an average fleet wide availability of just 76% for FY97-99 [GAO, 2000]. Even when functioning, the PHALANX system can only fire for 5 seconds continuously before needing to cool down, and must be secured for reload after less than 20 seconds of operation [NFF, Phalanx].

Unlike a missile system such as RAM or STANDARD, a light beam does not suffer from reliability issues. While rocket motors, guidance systems, fusing systems, or warhead detonation can fail in a physical system, a light beam has no failure mechanisms. Once successfully "launched", the light beam will propagate to its target (with absorption and scattering losses).

i. Operating Cost

Unlike missiles, no upgrade to the weapon (light) is needed. Throughout the lifetime of a weapons system, several upgrades are typically introduced, and current inventories of missiles are regularly rotated to upgrade the hardware. For example, solid rocket propellant has a usable shelf-life limit, and then must be replaced. Since the FEL has no munitions, there is no cost of maintaining and upgrading the munitions.

The cost of operating the FEL is extremely low. Once installed, the only expense when firing an FEL is the cost of the fuel required to generate power. The projected wall-plug efficiency of an FEL is approximately 10%. To generate a 1 MW

beam for 5 seconds with a 10% efficient FEL, 50 MJ of energy are required from the ship.

$$Energy\ Required = \frac{(Power)(Time)}{efficiency} = \frac{(1\text{MW})(5\text{s})}{0.10} = 50\text{MJ} \qquad (1.1)$$

Fuel oil contains 113.5 MJ/gal. A fully loaded LM-2500 turbine generator can extract 41.5 MJ/gal (36.6% efficiency). Using a cost of $1.40 per gallon of fuel oil, the cost of operation for a 5 second engagement of the FEL is only $1.68.

$$Cost = \frac{(Energy\ Needed)(Cost\ per\ Gallon)}{Energy\ \ From\ Generator\ per\ Gallon}$$

$$Cost = \frac{(50\text{MJ})(\$1.40/\text{gal})}{41.5\text{MJ/gal}} = \$1.68 \qquad (1.2)$$

Table 1 highlights the extent of savings realized during usage of the FEL system compared to other anti-missile options [Ng, pp. 8; NFF, (b)]. Over a 30-year lifetime of ship, millions of dollars are saved in operating expenses. (Lifetime costs in Table 1 assume a 30-year ship lifetime, 20 PHALANX shots per year of 225 rounds each, and 3 RAM firings a year.) With so low a cost of engagement, live fire training could be done whenever live fire is authorized.

	FEL	PHALANX	RAM
Cost per Engagement	$1.68	$13,500 Assumes 225 rounds	$0.9 Million Assumes 2 missiles
Shooting Cost Over a Lifetime	$5,040	$8.1 Million (note 1)	$40 Million

Table 1. Comparison of Operational Cost of Point Defense Systems

3. Disadvantages of the Free Electron Laser

a. Initial Cost

While the cost of operating an FEL once installed is extraordinarily low, the initial cost of installation is substantial. Current technology cannot currently provide a

suitable electron beam for use in an FEL weapon, nor has the required optics been produced, but a projected cost of $55 million is projected to install a 1 MW FEL onboard a ship [Todd, (a)]. The $55 million includes anticipated costs plus a 30% contingency. Table 2 compares initial expense of point defense systems [Ng, pp. 8].

	FEL	PHALANX	RAM
Installation Cost for 1st Unit on a Ship	$55	Mount = $3.2 Ammo = $0.1 Total = $3.3	Launcher = $7.9 Missiles = $7.6 Total = $15.5
Installation Cost for Additional Units on the Same Ship	$15 (adds an additional beam director)	Total = $3.3 (adds an additional PHALANX mount)	Total = $15.5 (adds additional missiles and launcher)

Table 2. Comparison of Installation and Lifetime Cost of Point Defense Systems (Millions of Dollars)

Once generated, the laser beam can be transported throughout the ship via the optical transport system to any of several beam directors on the ship. Multiple beam directors could be used to provide a 360° firing arc around a ship, just as multiple PHALANX units are used today. The additional cost of installing additional firing mounts is just the cost of transport optics and an additional beam director.

b. Power Requirements

Modern warships currently have less than ten percent of their power generation capability in a form of electrical power usable to ships' systems. The remainder of the power is reserved solely for the ship's propulsion turbines. Today's weapons draw little power from the ship, using instead internal batteries, fuels, and propellants to develop the required energy to transport the munitions toward a target. In many cases, such as missiles or explosive shells, explosives are incorporated into a warhead, which generate additional energy to damage the target. All of these sources of power are separate from the ship. Many types of directed energy weapons, such as solid state or free electron lasers, would demand substantially more electrical power from the ship than current weapons systems. In today's fleet, this would require additional energy

storage systems, such as capacitor banks or flywheels. Future all-electric ship designs such as DD-21 will allow all of the ships' power generation capability to be distributed as needed between ships' systems and propulsion, eliminating the ship's inability to supply the power required by an HEL system.

	FEL	PHALANX	RAM
Power Required during Engagement	10 MW	70 kW	< 10 kW
Power Required during Standby	1 MW	18 kW	< 10 kW

Table 3. Comparison of Power Consumption of Point Defense Systems

In addition to the increased power required for operation shown in Table 3, [McWhite, pp. 3; Jane's (f), Raytheon Phalanx CIWS] the nature of the power demanded by an FEL is unique. The FEL engagement will typically last about 5 seconds, with an additional 10 MW required during this time. Ship's Service Turbine Generator (SSTG) used to provide naval electric plants with power are not designed to provide the short, huge power surges of 10MW on only a few seconds notice. Even when the ability to meet the FEL power demands can be met, some form of stored energy may be required to temporarily supply power until an additional SSTG can be brought on line to service FEL power demands.

c. Radiation

Radiation is generated any time a charged particle is accelerated. Indeed, the FEL's laser beam is the radiation from the acceleration of electrons in the laser cavity. But there are many stages in the life of an FEL electron beam in which undesirable radiation is created. For the design considered (187 MeV electron beam with 1m radius turning bends), synchrotron radiation in the form of x-rays are produced when the electron beam is steered. The piping walls surrounding the electron beam provide sufficient shielding for these X-rays. When the electron beam is dumped, Bremsstrahlung radiation (in addition to neutron radiation if no energy recovery is used) is created. This

radiation must be properly shielded to prevent exceeding personnel exposure limits or activation of surrounding equipment.

THIS PAGE INTENTIONALLY LEFT BLANK

III. OTHER OPTIONS FOR ANTI-SHIP MISSILE DEFENSE

A. COUNTERMEASURES AND DECEPTION

All point defense systems, including Phalanx, HEL, and anti-missile missiles (RAM, Sea Sparrow, and Standard), seek to destroy threat missiles in flight so they cannot strike their intended targets. But destroying the threat missile is not the only way to avoid getting hit; you can also try to make the missile miss the ship. For a missile to successfully strike a target, it must first find the target. While this seems obvious, locating the ship can be made difficult for the missile. Target localization is usually done with a radar subsystem mounted in the nose of the missile, and is frequently augmented with the use of an infrared seeker. Most countermeasures attempt to foil the missiles ability to detect the intended target through distraction (providing a confusing radar and infrared picture to the missile) and/or seduction (providing an alternate, highly attractive target to the missile). Proper deployment of chaff, when combined with maneuver (discussed in Section III.A.5 below), can be very effective at confusing radar seeker systems.

1. Chaff

Chaff consists of small shards of highly reflective metal strips, usually aluminum, launched from a countermeasures system. Chaff is designed as either a seduction or a distraction round. A seduction round is made to give a sharp radar return from a small area in an attempt to fool the incoming missile into thinking a tight chaff cloud is a ship and thus "seduce" the missile away from the ship. Distraction rounds are made to give a radar return from a large cloud of objects, thus raising the background noise level of radar. The goal is to create a large radar "white noise" area so that the return from the ship cannot be picked out of the large mass of radar signals returned from the chaff. Multiple chaff rounds can be fired simultaneously into different areas to force the missile to choose which general area of strong radar return belongs to its actual target [Jane's, (d) Hycor naval decoy rounds].

2. Infrared Decoy

An infrared (IR) seeker is used aboard many anti-ship missiles as a second set of eyes. A ship burning fuel as it makes its way across the cool ocean provides a large IR signal that is easily seen against a cool ocean background. Since the IR seeker does not rely on a radar return, an IR seeker cannot be distracted or blinded by chaff. Because it is difficult to white out an IR sensor over a large area, flares are used exclusively as seduction rounds, meant to lure the missile away from the ship. Many chaff rounds designed to be deployed away from the ship now include a parachute deployed flare or a floating canister that contains a flame source. Advanced flare rounds such as the Super Walk-Off IR (SWOIR) decoy have been developed that release a series of short-time heat sources further and further from the ship in an attempt to trick the missile into following the decoy away from the ship [Jane's, (d), Hycor naval decoy rounds].

3. The Rubber Duck

a)

b)

Figure 6. a) AN/SLQ-49 Chaff Buoy Decoy System, "Rubber Duck"
b) Yellow "Rubber Ducky" – Makes bath-time so much fun!

Figure 6 shows two versions of the "rubber duck". Known throughout the fleet as "the Rubber Duck", the AN/SLQ-49 Chaff Buoy Decoy System consists of two inflatable, radar-reflecting buoys designed to produce a strong radar return similar to a ship. A 5-meter line connects the buoys, with each buoy having its own self-inflating life raft type container that inflates when the decoy is launched. Each buoy contains an antennae network designed to re-radiate the missile's radar signals. This creates a highly attractive radar target to the missile's homing systems, seducing the missile away from the ship's actual radar return. [FAS, (a)][Jane's, (e), Tarawa]

4. Electronic Attack

The magnitude of the anti-ship cruise missile (ASCM) threat suddenly came to the forefront in 1970 when Egypt sank the Israeli destroyer ELATH using a Soviet SS-N-2 STYX ASCM. For a relatively low cost, a small military force could effectively challenge highly valued assets of a much stronger military asset. In response to the new cruise missile threat, the US Navy began development of the AN/SLQ-32 Electronic Warfare (EW) system. The AN/SLQ-32 is the US Navy's standard threat detection, analysis, and jamming system. Capable of simultaneous engagement of multiple threats, the AN/SLQ-32 analyzes threat radars and determines attack missile geometry. The EW system then determines the best countermeasure tactics to use against the threat missile. The EW system is capable of both automatic and semi-automatic jamming and countermeasures coordination to alter the ASCM trajectory. In the semi-automatic mode, operator action is required to initiate active jamming or launch countermeasures. [FAS, (b)] [Jane's, (d), AN/SLQ-32(V)]

5. Maneuver

Modern missile systems respond to jamming and countermeasures in many different ways. Some will attempt to maneuver to reacquire the original target, while others will become strongly attracted to seduction countermeasures. If a ship stops dead in the water within a chaff cloud, some missiles will avoid the chaff looking for the ship while others will head straight for the cloud since it provides the strongest return signal. Sometime the Commanding Officer may want to turn the ship so that the most anti-missile weapons can be brought to bear on the incoming missile, while other times it may be better to turn the ship so as to provide the smallest radar cross Section. The AN/SLQ-32 Electronic Warfare system provides recommendations of the best course and speed tactic to minimize the possibility of ASCM homing on the ship. [FAS, (b)] [Jane's, (d), AN/SLQ-32(V)]

B. GUNS – THE PHALANX SYSTEM

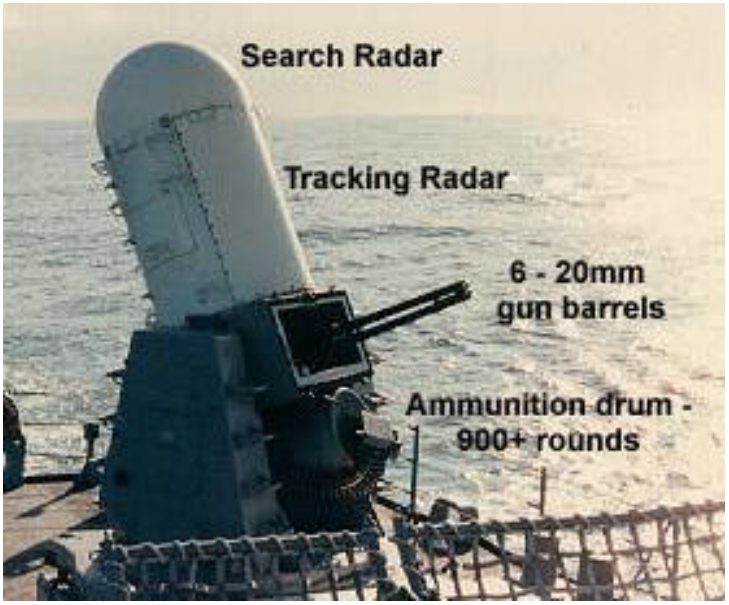

Figure 7. Phalanx Close-in weapons system

The PHALANX system shown in Figure 7 is the Navy's close-in defense system against incoming missiles. PHALANX is an M-61A1 Gatling gun system that shoots hundreds of bullets at an incoming missile in an attempt to disable the missile prior to impact with the ship. PHALANX is capable of sustaining fire rates up to 4,500 shots per minute for a total of 1,550 rounds before requiring a reload, however the PHALANX gun barrel will begin overheating after about five seconds (375 rounds) of continuous fire [Colson, (d)]. Overheating is usually not a concern for single missile intercepts, since a Mach 1 missile engagement from 2,000m continuously until impact with the ship would last approximately 6 seconds, using 450 shots, and most ASCMs are faster than Mach 1. PHALANX shoots high density Armor Piercing Discarding Sabot (APDS) Tungsten or depleted Uranium rounds design to shred the incoming missile [NFF (a)]. The PHALANX system is designed to begin engagement at 2,000 m, but the probability of the destruction of an actual incoming missile is extremely unlikely beyond a few hundred meters.

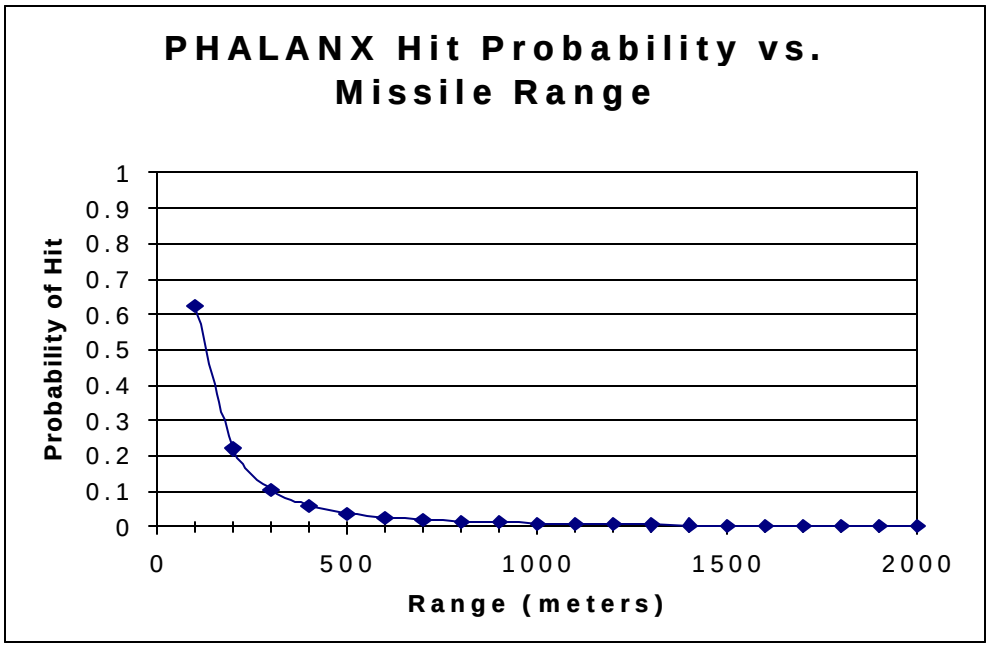

Figure 8. PHALANX hit probability

Figure 8 shows the probability of any one PHALANX projectile hitting a missile as a function of missile range. Many sources or error can affect the proper aim point of a gun, such as gun mount stability, wind, target speed and direction, firing solution accuracy, and internal gun vibrations generated while the gun shoots. Even very small errors can result in substantial projectile miss distances down range. To minimize aiming errors, PHALANX incorporates a closed loop fire control system that uses radar to track the outgoing bullets, determines the miss distance, and then changes the gun aim point to correct the observed error. This closed loop system will correct for many of the previously mentioned effects [Jane's (f), Raytheon Phalanx CIWS], however inconsistency in the firing solution and internal gun vibrations cannot be corrected by this method. Figure 8 assumes PHALANX can correct all errors in aim point to within 0.002 radians (3.5×10^{-5} degrees) and that PHALANX is shooting at a missile of radius 20 cm heading directly toward the ship. Even using this extremely accurate solution, PHALANX has less than a 1% chance of a projectile hitting at ranges outside of 1,000 m. Simulation using a Gaussian distribution with an error of 0.002 radians shows typical bullet scatter at 1,000 m is given in Figure 9.

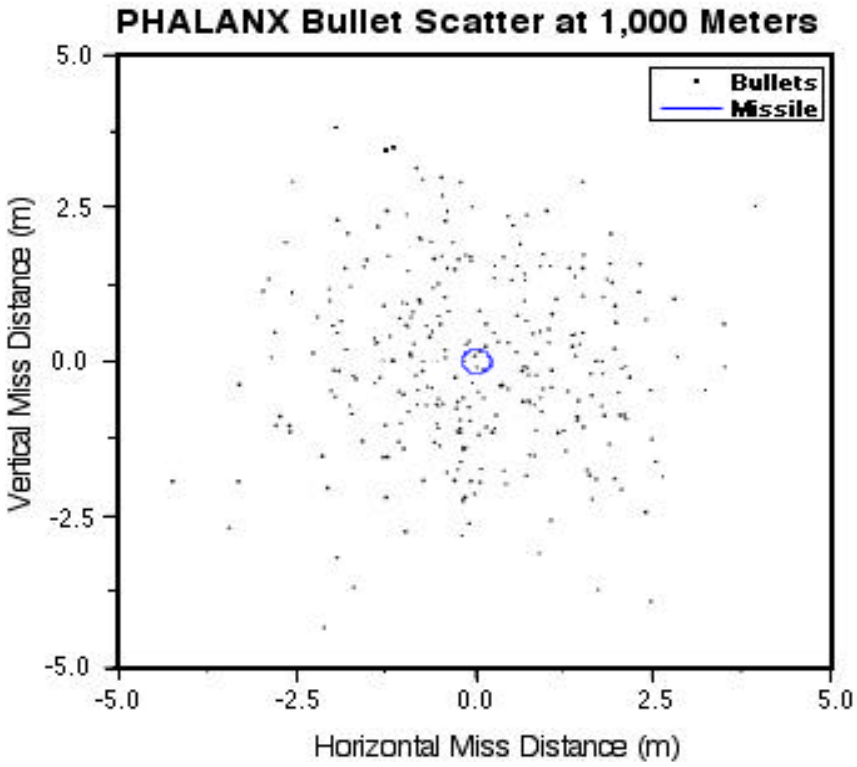

Figure 9. PHALANX bullet scatter at 1,000 meters

Compounding this problem is that typically the missile must acquire 5 to 10 hits before it is destroyed. The time it takes to acquire several hits usually means the missile is allowed to approach to within a few hundred meters of the ship before the missile is successfully "killed". When PHALANX destroys a missile, the missile will break up into many pieces. At this point, the missile becomes hundreds of kilograms of missile parts traveling at Mach 1.2 straight toward the ship. As shown in Figure 1 (pp. 3), if a missile is killed at a range of 300 m, each piece has a 26% chance of impacting the ship. At Mach 1.2, even smaller fragments carry enough kinetic energy to cause extensive damage to unarmored components such as personnel, antennae, or sensitive radar equipment. While PHALANX may keep the ship from complete loss, a few "successful missile kills" could cause enough damage to render the ship combat ineffective.

C. MISSILES – THE SEA SPARROW

The most capable type of defense against an ASCM in the fleet today is another missile. The Navy uses a layered missile defense system consisting of the rolling airframe missile (RAM), the standard missile (SM), and the Sea Sparrow missile.

The RAM is a short-range (10 km) add-on point defense missile system designed to supplement the PHALANX and Sea Sparrow systems [Jane's (g), RIM-116 RAM]. Over 1,000 RAM Block 1 missiles and 83 RAM launcher systems have been ordered for installation aboard Amphibious Assault Ships (LHA/LHD), Dock Landing Ships (LSD), Frigates (FFG), and Destroyers (DD/DDG), and Aircraft Carriers (CVN) [NFF (b)].

There are two major types of Standard missile systems used for anti-missile defense, the SM-1 (medium range) and the SM-2 (extended range). The standard missile system is one of the Navy's most reliable weapons [NFF (d)], and can be used either in air defense or in limited anti-ship missions. The SM-2 missile system is found on board Ticonderoga Guided Missile Cruiser (CG-47) and Arleigh Burke (DDG 51) class ships, and the SM-1 is on board the Oliver Hazard Perry (FFG 7) class ship [Jane's (b), RIM-66/67/156/300 Standard Missile 1/2/3/4/5].

In the mid-1950's, the US Navy sought a more capable air defense weapon than traditional short-ranged anti-air (AA) guns. The Navy first attempted to modify the Army's successful RIM-64 Mauler surface-to-air system, but converting the tail-chase Mauler missile to a head-on engagement missile needed for most naval engagements proved difficult. In December 1964, the Navy began development of the RIM-7 Sea Sparrow missile, a modified version of Raytheon's Sparrow III air-to-air missile. In 1968 the United States entered into an agreement with Denmark, Norway, and Italy for development of a joint missile defense system, dubbed NATO Sea Sparrow missile system (NSSMS). Today, 17 countries use the NSSMS, which includes the launcher, automated fire control, and the improved RIM-7H missile shown in Figure 10, as the primary means of anti-missile defense onboard capital ships [Jane's (b), RIM-7 Sea Sparrow/RIM-162 Evolved Sea Sparrow]. In contrast to the great success of the Standard missile system availability, the GAO reports an average NSSMS uptime of only 80.3%

over the 3-year period of FY 97 – FY 99 [GAO]. At a cost of $165,400 per missile, Sea Sparrow is considered a low-cost anti-missile missile [NFF (c)].

Figure 10. Launch of a Sea Sparrow Missile

The Sea Sparrow is a highly maneuverable radar guided surface-to-air missile, with a high explosive warhead. As anti-ship missiles have become more formidable, the capabilities of Sea Sparrow have changed to better engage emerging threats. Originally a medium-range missile (55 km), recent versions of Sea Sparrow trade range for exceptional maneuverability and seeker enhancements. Called the "dog-fight modification" [NFF (d)], Sea Sparrow is a Mach 2.5 missile limited to 16 km range, but capable of 30g maneuvers (RIM-7H). The most recent versions of Sea Sparrow missile include substantial radar enhancements needed to find very low-altitude targets in sea clutter (RIM-7P), with some versions incorporating IR sensors (RIM-7R). [Jane's (b), RIM-7 Sea Sparrow/RIM-162 Evolved Sea Sparrow]

In September 2002, Raytheon delivered the first Evolved Sea Sparrow missile (ESSM) to the US Navy, which is expected to begin deployment throughout the fleet in the spring of 2003. This most recent upgrade to the RIM-7 provides significant

improvements to all aspects of the missile, earning the new NATO designation RIM-162. Capable of 18 km engagements with a speed of Mach 3.6, the ESSM has an improved electronic suite that eliminates Sea Sparrow's required 4-minute warm up time and allows up- and downlinks between the missile and its associated fire control system. Advanced modes of operation include launch-on-search, delayed illumination, and home-all-the-way. These flight mode improvements will allow each tracker/illuminator to control up to 3 missiles, rather than the currently allowed 1 missile per tracker. ESSM will remain compatible with current NSSMS launchers, but will also be packaged in a quad-pack launcher that fits into existing vertical launch systems for use onboard ships with the Aegis system. [Jane's (b), RIM-7 Sea Sparrow/RIM-162 Evolved Sea Sparrow]

D. LASERS WEAPONS – THE TACTICAL HIGH ENERGY LASER (THEL)

The concept of using lasers as weapons is not new. In the early 1970s, all branches of the United States military had an HEL program to determine the potential missions and effectiveness of lasers on the battlefield [Anderberg, pp. 1]. Chemical, free electron, and solid-state lasers have been identified as having the potential to achieve power levels high enough for use as a weapon. In their report of June 2001, the Defense Science Board Task Force found that an HEL system would provide a new level of flexibility and possess attributes that are particularly valuable in both existing and future security environments [DSBTF, pp. 89]. A brief description of solid-state and chemical laser operation is provided below. An introduction to free electron laser operation is provided in Section I.C.1.a (pp. 5-8) and will not be repeated here.

Both solid state and chemical lasers use the transition of bound electrons between energy levels (called energy states) to create laser light photons. Quantum mechanics explains that atoms can only be at certain, specific energy states. The allowed energy states are unique for every type of atom, and only certain energy state transitions can be made. When an atom transits to a lower energy level, it must emit energy; similarly, atoms must absorb energy to transit to a higher energy state. The energy emitted or absorbed from the atoms is in the form of photons, which are basically small packets of light. The type of atoms used in the lasing medium determines the allowed energy state transitions that can occur, thereby fixing the wavelength of light the medium can

generate. In a CO_2 laser, CO_2 molecules are making transitions to generate photons; in a solid-state laser, semiconductor atoms are generating photons.

Just as the rest of nature does, atoms seek the lowest energy level. All laser systems excite atoms and then allow the excited atoms to transit back to a lower energy state, causing the emission of photons. The more atoms that can be made to make the transition down, the more photons created, and therefore the higher the output power of the laser. Solid state lasers use a voltage applied to semiconductor atoms to excite electrons, while chemical lasers use a chemical reaction to produce excited electrons. The photons that result as the excited electrons transition to a lower energy state are collected and focused, creating a laser beam.

The Tactical High Energy Laser (THEL) is a specific high-power chemical laser system designed to become a military weapon. A description of the THEL system is presented to illustrate a typical laser system.

The Nautilus project is a joint United States-Israeli effort to determine the feasibility of using an HEL for missile defense. The Nautilus project used the 2.2MW MIRACL laser system and the Sea Lite beam director to demonstrate the feasibility of shooting down artillery rockets with high-powered lasers [Jane's (g), Ground Based Laser]. On 9 February 1996, MIRACL destroyed an in-flight artillery rocket. In May 1996, THEL was designated as an Advanced Concept Technology Demonstration (ACTD) program. The ACTD program links scientists with warfighters to quickly determine if cutting edge technology can significantly enhance battlefield capabilities [Eash, 2000]. Located at HELSTF, the THEL system is a follow-on program to the Nautilus project. The goal of the THEL ACTD program is to develop a weapons system that is capable of supporting Israel's requirement to defend against rocket artillery attacks on northern Israeli cities from Hezbollah forces in southern Lebanon. During June of 2000, just 4 years after program creation, THEL shot down an in-flight Katyusha rocket on its first attempt. Since then, the THEL prototype has engaged in over twenty-five single- and multiple-122 mm Katyusha rocket salvo shoot-downs [HELERP, pp. 14-15]. The successful shoot-downs of multiple Katyusha rockets completed the ACTD portion of THEL research. Subsequent battlefield simulations conducted by the Army Air

Defense Artillery Center predict a 90-100% success rate against a coordinated attack utilizing ground-launched cruise missiles, and an 80-90% success rate against rockets, mortars, and artillery rounds [Eash, 2000].

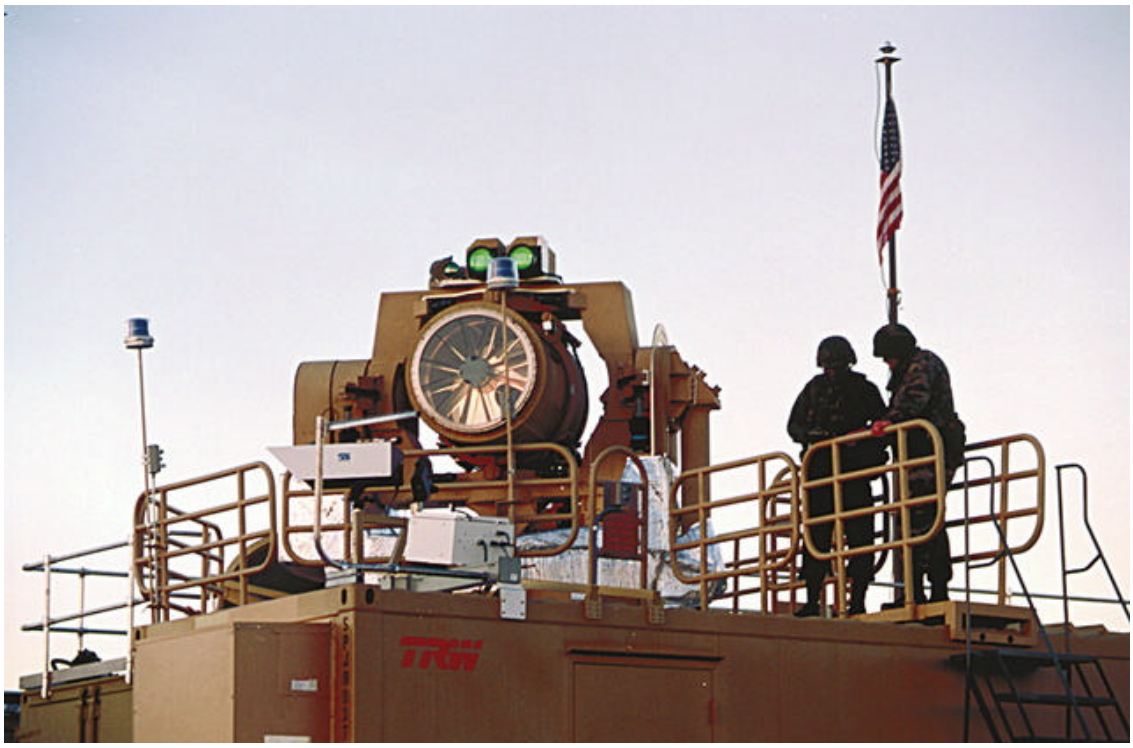

Figure 11. THEL PTS beam director

THEL consists of 3 subsystems: 1) the Command, Control, Communications and Intelligence (C^3I) subsystem, 2) the Laser Subsystem (LS), and 3) the Pointer Tracker Subsystem (PTS) shown in Figure 11. The THEL radar, used for search, acquisition, and fire control, is part of the C^3I subsystem. Once operational, THEL requires only 2 people to man C^3I for operation – a commander and a gunner. C^3I can be operated in three modes: 1) manual – all targets must be designated and engaged by the commander, 2) semi-automatic – all functions operate automatically except manual firing of the laser, and 3) fully automatic – the commander or gunner must intervene to prevent weapon engagement. The LS, like MIRACL, is a continuous wave (CW) deuterium fluoride (DF) laser operating in the infrared spectrum at 3.8μm. While not achieving the power attained by the MIRACL system, THEL LS generates adequate power at high rates of fire, sufficient to meet Israeli weapons systems requirements for artillery rocket defense at a

range of 5-10km [Jane's (g), Ground Based Laser]. The PTS points the laser and focuses the beam on the designated target, and provides visual target tracking for final target verification and damage assessment [Schwartz, 2001]. THEL has successfully integrated an HEL into a packaged system with demonstrated capability to detect, track, point and shoot a high-powered laser to destroy airborne missile threats.

Figure 12. THEL system in "transportable" form [HELTAWG, 2001]

Many THEL program parameters are classified, but it is expected to serve as a short-to-medium range anti-missile platform [Jane's (g), Ground Based Laser] with a deep magazine, possibly 30 or more engagements [Eash, 2000]. The estimated cost of $3,000 per engagement is substantially less than current anti-missile engagement costs [White, pp. 1]. In its current "transportable" form shown in Figure 12, THEL is moved in several semi-truck containers, which must be unpacked and setup before operation is possible. In this transportable form, Israel has expressed interest in deployment of up to 13 THEL units around its northern cities. The US Army and the Israeli Defense Ministry continue efforts toward the creation of a highly mobile, combat ready version for use with armored and infantry divisions. The Mobile Tactical High Energy Laser (M-THEL) is scheduled for demonstration in three to five years [Jane's (a), pp. 186].

IV. DESCRIPTION OF A SHIPBOARD FEL SYSTEM

A. OPERATIONAL DESCRIPTION

1. Required Power

In determining the best power for the design of an anti-ship laser, several factors must be taken into account. Atmospheric effects can impose both upper and lower design limits. The desired affect on the target, as well as acceptable dwell time of the laser must also be considered when determining required laser power.

a. Propagation of Light Through Maritime Atmosphere

As discussed in Section I.C.2.f, the atmosphere effects laser light propagation in at least three significant ways: absorption, scattering, and thermal blooming. Atmospheric transmittance T is the fraction of the light that is transmitted from the ship that reaches the target. The atmospheric transmittance T is given by:

$$T = e^{-a\,r} \tag{4.1}$$

where a is the extinction coefficient and r is the distance through which the light must propagate. The extinction coefficient is a function of wavelength, and is the sum of the coefficients of absorption and scattering.

$$a = a_a + a_s \tag{4.2}$$

The fraction of energy lost to absorption and scattering per unit length traveled is a function of the concentration of atmospheric particles, including aerosols, ozone, CO_2, and water in the air. Figure 13 [RCA, pp. 85] shows the effects of scattering from all typical atmospheric components, as well as absorption from ozone. (Figure 13 uses s in place of a. They are identical.)

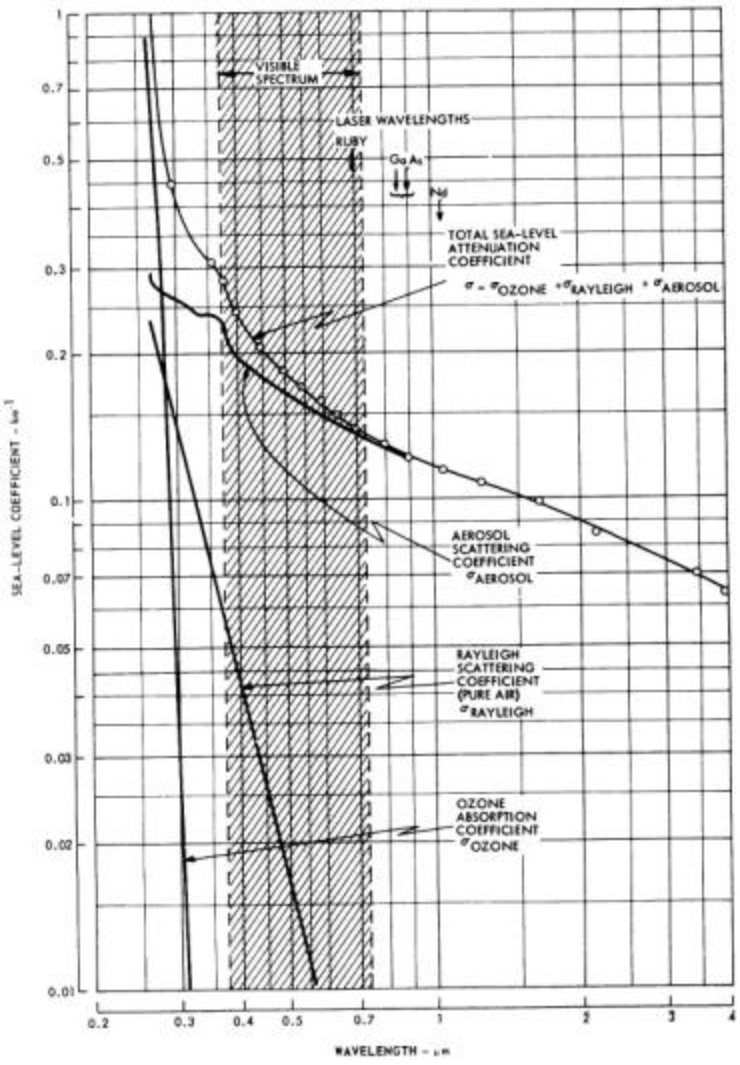

Figure 13. Atmospheric extinction coefficients for horizontal transmission at sea level with 23.5 km visibility. Absorption by CO_2 and water are not included.

At ultraviolet wavelengths (< 0.36 μm), absorption of light by ozone forces a to become very large, resulting in poor atmospheric transmittance. According to Figure 13, the longer the wavelength the lower the value of a, and the higher the transmission should be.

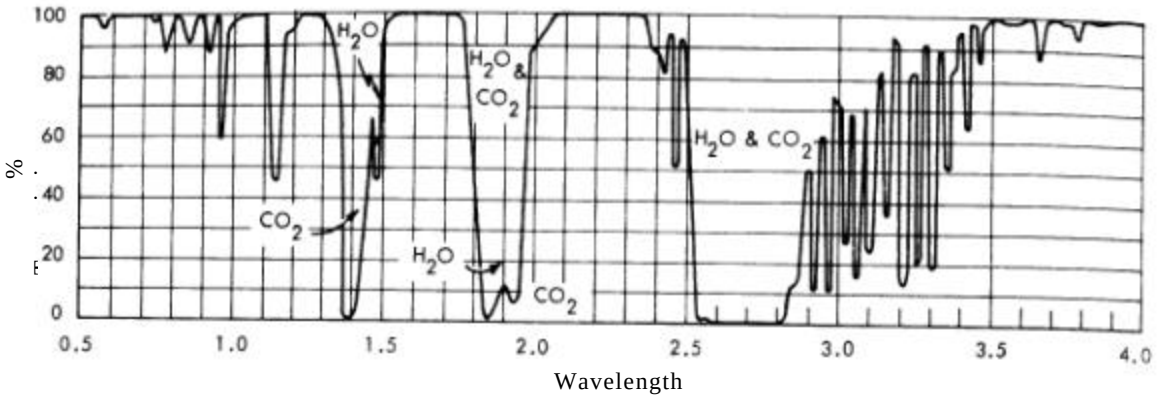

Figure 14. Transmittance of 1000 ft horizontal air path at sea level containing 5.7 mm precipitable water at 79° F

Figure 14 [RCA, pp. 84] shows the transmission over 1,000 feet when water and CO_2 are included. Even over such a short distance, there are many observable transmission plateaus that occur throughout this spectrum (i.e.- 1.06 μm, 1.65 μm, and 2.3 μm) where the light is well transmitted, while other nearby wavelengths are almost completely absorbed (i.e. – 1.38 μm, 1.92 μm, and 2.7 μm). Any high-powered laser must operate on one of the high transmission plateaus so that the laser light will make it to the target without being absorbed by water or CO_2. A maritime atmosphere, however, contains many more aerosols than the typical atmosphere analyzed in Figures 13 and 14. The absorption spectrum for all elements contained in a maritime atmosphere is very complex. Figure 15 [Stock, 2001] gives coefficients of scattering, absorption, and extinction for 0.5-10 micrometer wavelengths in an atmosphere that contains typical maritime aerosols.

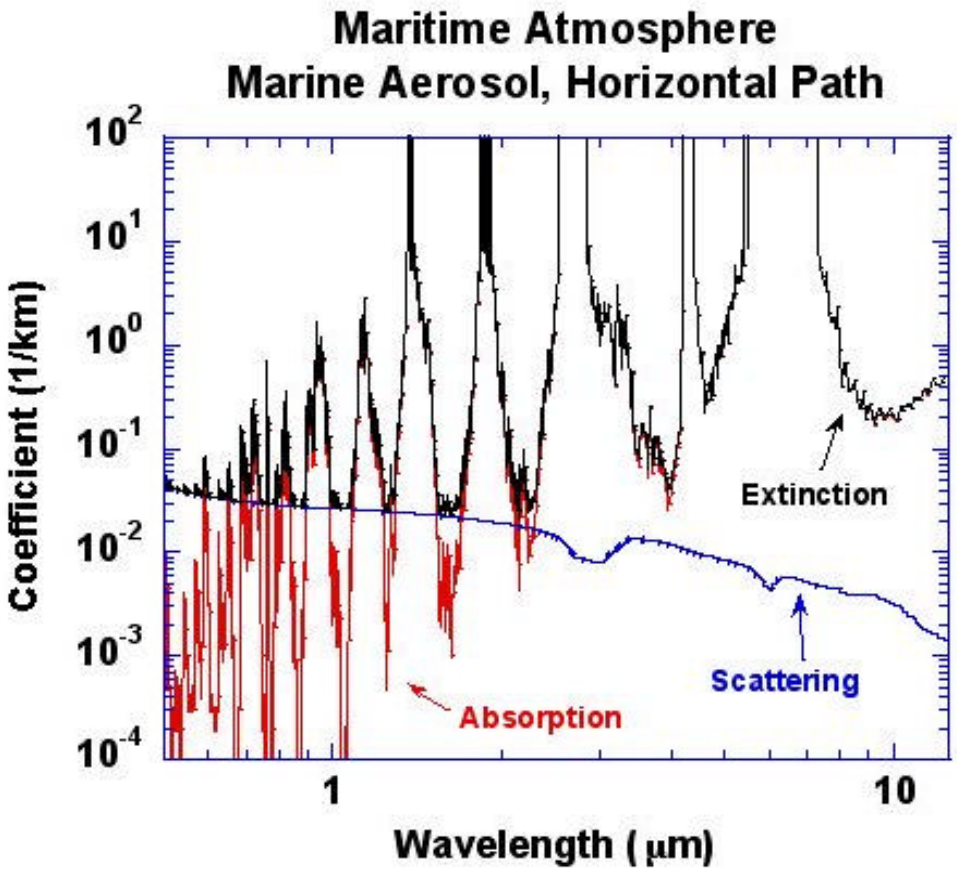

Figure 15. Coefficients of absorption, scattering, and extinction in a maritime atmosphere

As noted in Figure 13, the scattering coefficient generally decreases as wavelength increases. However, with the introduction of maritime atmosphere aerosols, Figure 15 shows many spikes in the absorption coefficient (and thus the extinction coefficient) across 1-10 micron wavelengths. The wavelengths corresponding to the minimum extinction coefficients in Figure 15 are 1.62 μm, 1.25 μm, and 1.06 μm, in order from least to greatest extinction coefficient.

If Figure 15 was the end of the story, 1.62 μm would be the optimal wavelength for use for maritime HEL applications, however with scattering and absorption understood, we must now consider the effect of thermal blooming, which becomes significant for very high-powered laser beams. Thermal blooming is a highly nonlinear process; its effects are negligible until a "critical power density" is reached. When attempting to transmit more power than the critical power density, the blooming

effect will rapidly cause the spreading of the beam. As the beam spreads, the beam intensity (W/cm^2) rapidly drops, so that at very high-transmitted powers—those beyond critical power density levels—the laser beam intensity received at the target can actually drop as laser power increases.

Since thermal blooming occurs as a result of absorption (not scattering), a lower coefficient of absorption causes a slower heating up of the air column and delays the onset of blooming. Comparing the coefficients of absorption for the previously noted wavelengths that have the lowest coefficients of extinction (1.62 μm, 1.25 μm, and 1.06 μm), Figure 15 shows that 1.06 μm, has the lowest coefficient of absorption, followed by 1.25 μm, then 1.62 μm. Figure 16 [Stock, 2001] shows the peak intensity transmittable as a function of wavelength, including the effects of scattering, absorption, and thermal blooming, assuming a 10 m/s crosswind, and confirms that 1.06 μm is the optimal wavelength for maximum intensity transmission to the target.

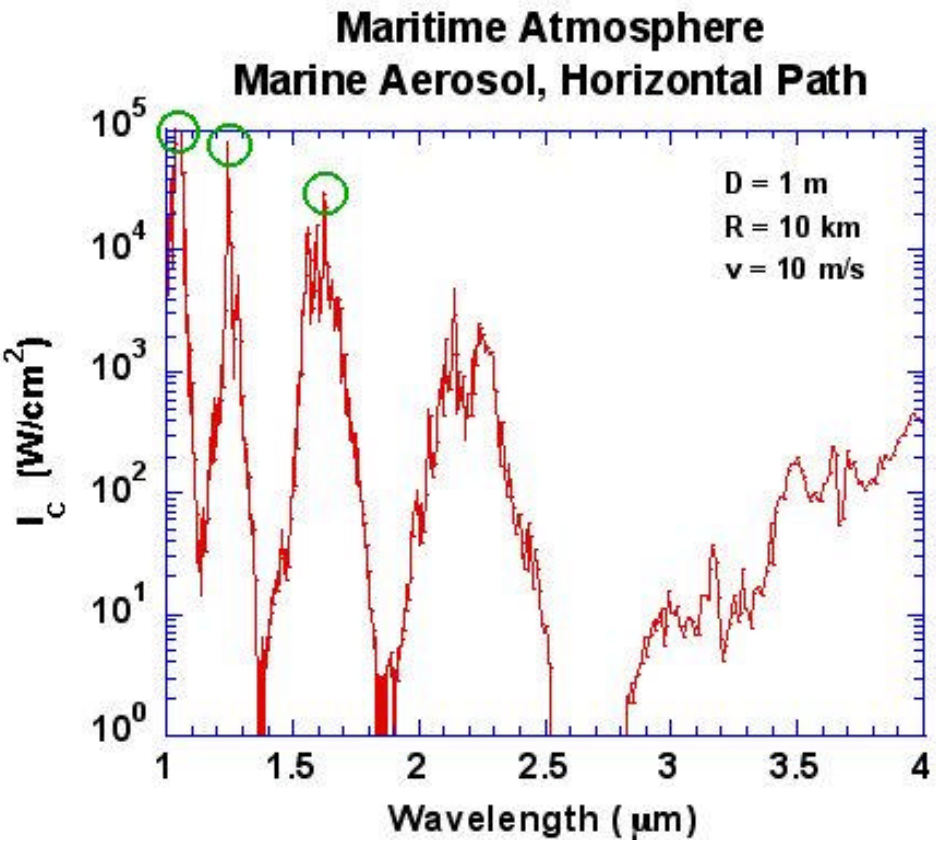

Figure 16. Transmittable intensity through a maritime atmosphere

With the wavelength of operation determined, we can now refer back to Figure 13 to find a value for the total extinction coefficient $a = 0.144$ km^{-1}. But Figure 13 assumes "standard clear" visibility of 23.5 km. Varying the atmospheric conditions will cause significant changes in the value of a, as shown in Figure 17 [RCA, pp. 88].

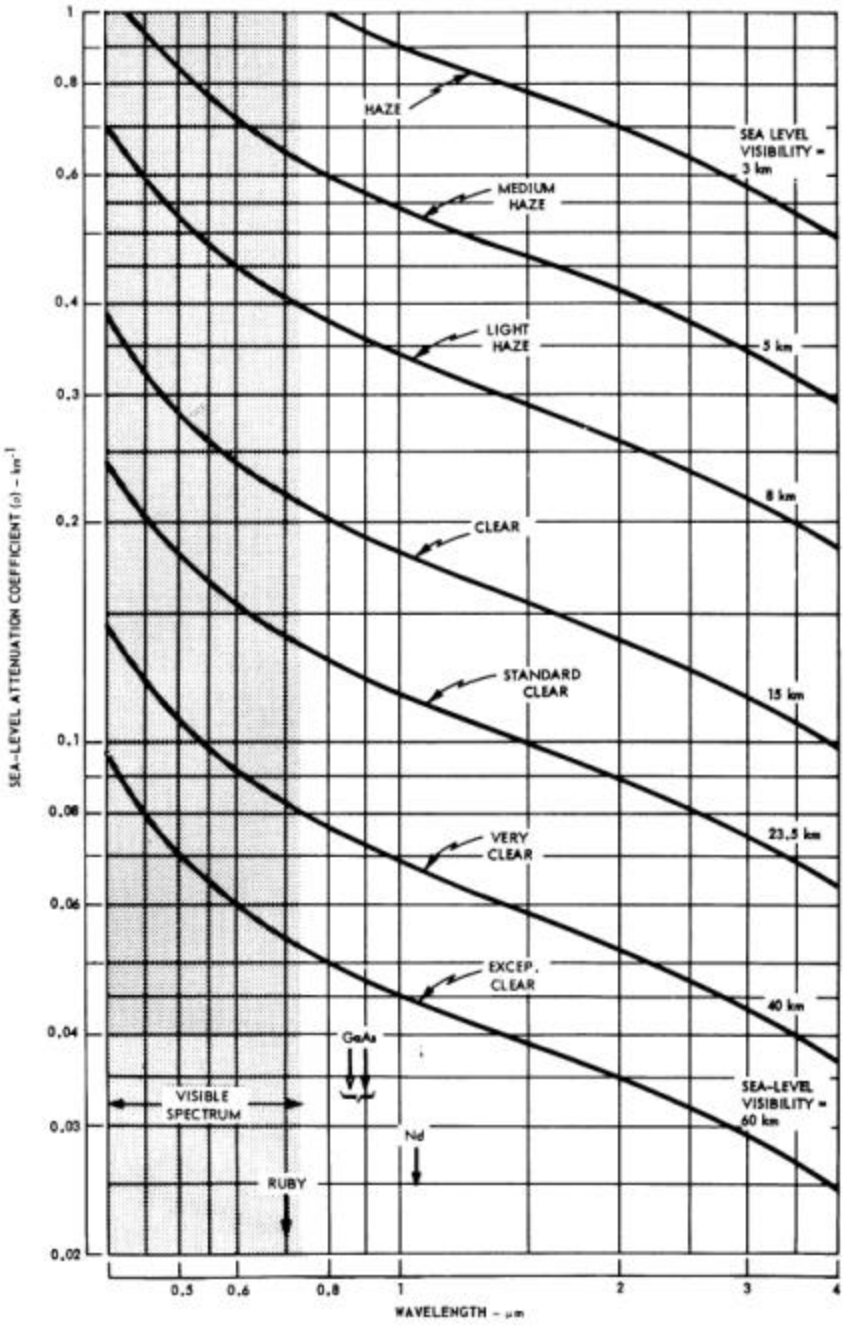

Figure 17. Extinction coefficient variation by wavelength at sea level for various atmospheric conditions. Absorption by CO_2 and water are not included.

Figure 18 plots transmission T as a function of range (equation 4.1 from above), using different values of s associated with various atmospheric conditions from Figure 17. Maritime weather conditions can impose significant range limitations upon a laser weapon. Table 4 gives the power received at the 5 and 10 km for various visibility conditions assuming 1 MW laser is fired from the ship.

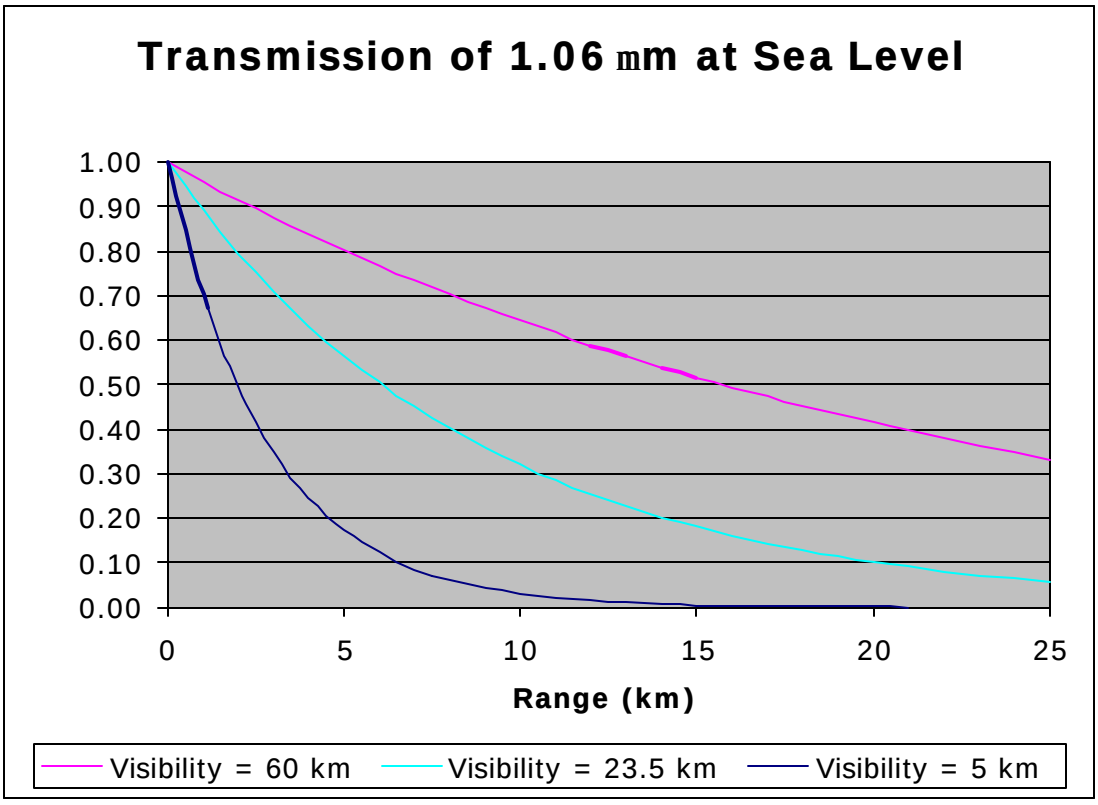

Figure 18. Transmission of 1.06 μm light at sea level for various atmospheric conditions

Viewing Conditions	P(5 km)	P(10 km)
Exceptionally Clear (visibility = 60 km)	803 kW	644 kW
Standard Clear (visibility = 23.5 km)	566 kW	320 kW
Medium Haze (visibility = 5 km)	174 kW	30 kW

Table 4. Power P received from a 1 MW laser for various viewing conditions

There is a great deal of uncertainty in the understanding of atmospheric conditions in maritime environments. While the data presented here is believed to be accurate given today's knowledge of oceanic atmospheres, it is far from complete. Much data exist concerning transmission of laser light over land, but, as presented here, ocean environments can be significantly more complex than those over dry land. Winds, surf, and ocean spray significantly contribute to aerosols, thus altering the absorption and scattering characteristics of light. Many regions of the ocean's atmosphere have never been studied in detail, so the absorption and scattering coefficients are not fully known. While many aspects of atmospheric transmission are common to all environments, local aerosols may differ, creating unique and unknown absorption spectrum. Without a better understanding of oceanic atmospheric transmission, the ability to transmit lethal amounts of energy to a target is unknown. The tunability of an FEL while operating makes the FEL well poised to adapt to many environments, but knowing exactly the optimum wavelength for transmission in local regions is necessary to maximize the full potential of a laser weapon. Additional research in over ocean atmospheres would be useful in determining whether a shipboard FEL system is the best answer in combating future missile threats.

b. The Energy Required to Kill a Missile is Exactly…

A missile may be killed quickly (< 1 second) by just a few kilowatts if an IR seeker is utilized by the missile. Since the IR window that is transparent to the ship's IR signature would also let the IR laser beam enter the missile's electronics. With the guidance electronics destroyed, the missile would be unable to find and kill its intended target. This type of engagement, where the target missile is not destroyed but instead is rendered unable to complete its mission, is called a "soft kill". Relying on soft kill engagements, similar to relying purely on countermeasures response, leaves the ship commander with a nagging concern that a missile designed to destroy his ship is still moving at Mach speed in the area.

A successful FEL engagement should result in a "hard kill", where the missile (or remaining fragments) splash harmlessly into the sea far from the ship. A hard kill can be achieved in a number of ways. A laser can heat the explosives carried by the missile until they detonate, resulting in a catastrophic and satisfying "boom" that blows

the missile to smithereens. On other missiles, the same result is achievable by heating the missile's fuel tanks. Still others may be most rapidly destroyed by cutting the flight control surfaces of the missile. Specifying the amount of energy required to kill a missile is not straightforward even when the best way to attack the missile is known. Lasers interact differently with different materials. Also, the effects of ultra-short FEL laser pulses are not fully understood. Even the type and thickness of paint the missile is coated with can alter the laser-missile interaction.

Although the amount of energy necessary to destroy a missile is not exact, some approximations can be made. The first assumption is that if ≈ 300 cm^3 of material can be removed from the missile, the missile will become aerodynamically unstable, creating aerodynamic forces that will cause it to break apart and tumble into the ocean. The following calculations assume the missile is aluminum (Al). Two estimates of the energy required to remove 300 cm^3 of Al are: 1) A determination of the energy required to melt 300 cm^3 solid Al, or 2) A determination of the energy required to break the bonds of 300 cm^3 of Al lattice.

The energy required to melt 300 cm^3 of Al is given by

$$\begin{aligned} E_{melt} &= (rV)_{Al}\left[(T_{melt} - T_{amb})\, c_{Al} + L_{melt}\right] \\ &= \left(2.7\frac{\text{g}}{\text{cm}^3}\right)(300\text{cm}^3)\left[(660\text{K} - 323\text{K})\left(1.05\frac{\text{J}}{\text{gK}}\right) + 400\frac{\text{J}}{\text{g}}\right] \\ &= 610\text{kJ} \end{aligned} \qquad (4.3)$$

where r, V, c_{Al}, and L_{melt} are the density, volume, specific heat capacity, and latent heat of melting for Al, respectively. The value 610 kJ assumes that as soon as the material melts, it is removed by some mechanism (such as air drag forces) without requiring any more energy from the laser. In reality, some atoms will absorb more energy before leaving the melted cavity, while other unmelted portions will be swept away with fully melted sections of metal.

The energy required to remove each atom from the Al lattice can be found from equation 4.4, where N_A is Avogadro's number and E_{bond} = 3.4 eV [Kittle, pp. 74] is the bonding energy of each Al atom that must be overcome to remove the atom from the lattice structure

$$E_{lat} = \frac{(V r)_{Al} N_A E_{bond}}{M}$$

$$E_{lat} = \frac{(300\text{cm}^3)\left(2.7\frac{\text{g}}{\text{cm}^3}\right)\left(6.02\text{x}10^{23}\frac{\text{atoms}}{\text{mole}}\right)\left(3.4\frac{\text{eV}}{\text{atom}}\right)\left(\frac{\text{eV}}{1.602\text{ J}}\right)}{27\frac{\text{g}}{\text{mole}}} \qquad (4.4)$$

$$E_{lat} = 9.82\text{MJ}$$

Both order-of-magnitude approximations indicate that mega joules of energy are needed. The 1 MW THEL and the 2 MW MIRCL are both capable of shooting down a missile within a few seconds, supporting the estimation that a few MJ are required. I will assume 2 MJ of energy is required for a missile kill.

c. Defining Mission Success

Mission success can now be defined as the ability to deliver 2 MJ to the target over a few seconds at a range sufficient so that missile fragments have less than a 2% chance of striking the ship. According to Figure 1, this means the missile must receive 2 MJ before it gets within 1,200 m of the ship.

Choosing 2% is fairly arbitrary, but is reasonable. In a highly stressed anti-missile environment where several missiles are fired at a ship in an attempt to saturate missile defenses, perhaps 2 missiles might penetrate the STANDARD/Sea Sparrow anti-missile shield. In this case, the reaction time of the FEL must be extremely quick as the incoming anti-missiles would already be within 10 km. If each missile is assumed to produce 10 fragments with enough mass and kinetic energy to be of concern, than a total of 20 fragments will be produced. The 10 fragments from the first missile killed have < 0.1% probability of hitting the ship since the first missile is killed many kilometers (>4.0) from the ship. Each fragment from the second missile, killed at the worst acceptable range of 1,200 m, has a 1.7% chance of striking the ship. In this scenario, the ship would have an 84% chance of not being hit by any fragments at all. While 0% chance of hit is desirable, it is not realistic given that 2 missiles have already penetrated to within 10 km without being damaged.

d. The Timeline

Modern ASCMs can exceed Mach 3.5. Since the FEL system must be capable of dealing with evolving future threats, I will assume a Mach 5 missile threat. A Mach 5 missile traveling straight at a ship, first engaged by an FEL at 10 km from the ship, will travel for 5.3 seconds before the missiles is inside 1,200 m.

In this time, 2 MJ must be transmitted to the first missile, the FEL given 0.5 seconds to switch targets after the first missile is killed, then the FEL must deliver 2 MJ to the second missile before it closes to within 1,200 m.

e. So, How Much Power is Needed?

The power determined below is meant to serve as an order-of-magnitude approximation only. It is very possible that substantially lower powers could accomplish mission objectives, but it could also be that a higher power is required than assumed. This uncertainty, however, is not unique to a FEL system. Most high-tech weapons systems are so complex and expensive that probability-of-kill assessments must be made to estimate operational success, and those assessments are made on well-understood electronics and fusing systems. In the case of the FEL, neither the interactions of ultra-short pulse lasers on high-velocity missile targets nor the propagation of laser light through maritime atmospheres are fully understood, and thus the "derived" required power must be taken with a grain of salt.

Some of the assumptions for this ASCM engagement scenario include:

- Two Mach 5 missiles are heading straight for the ship
- Propagation losses are in accordance with a standard clear day (Section III.A.1.a)
- Missiles are killed when 2 MJ reach the missile (Section III.A.1.b)
- The second missile is killed at 1,200 m, maintaining < 2% chance of any missile fragment impacting the ship (Section III.A.1.c)
- Total engagement time is constrained by the Mach 5 ASCM closure to within 1,200 m and includes a 0.5 second FEL retargeting time (Section III.A.1.d),
- The FEL begins engagement when the missiles reach 10 km from the ship.

In the above ASCM engagement scenario, a shipboard FEL must be 2 MW or greater to achieve mission success with both missiles. With a 2 MW FEL, the first missile will be destroyed at 4.3 km from the ship, and the second at 1,200m.

Several designs for a multi-MW class FEL are being considered. The FEL at JLAB has achieved the world's highest power to date, reaching 2.1 kW. JLAB's FEL is currently shut down to install a high-power modification that should achieve over 10 kW in 2003. Assuming success of the 10 kW upgrade, JLAB will shut down again in 2005 to install an upgrade designed to reach 100 kW. Research beyond 100 kW will be done at a missile test range where operational testing as an anti-missile weapon system can occur [JLAB.org].

2. Range

The laser is a line-of-sight weapon. Line of sight range can be estimated by

$$R_{horiz} \approx 3.57 \frac{\text{km}}{\sqrt{\text{m}}} \left(\sqrt{h_{FEL}} + \sqrt{h_{missile}} \right), \tag{4.5}$$

where R_{horiz} is the line of sight range in km, h_{FEL} and $h_{missile}$ are the heights of the FEL beam director and missile respectively, measured in meters above sea level. If a beam director is placed 16 m high on a ship, and the ASCM cruises at 4 m, the FEL beam director can see the missile at a line of sight range of 21 km.

While a light beam can travel to the horizon, the power delivered diminishes exponentially with range. Figure 18 shows that even in "exceptional clear" weather (as defined in Section IV.A.1.a), just 40% of the laser beam's energy is delivered to a range of 20 km. Only 20% of the originally transmitted energy makes it to 20 km on a "standard clear" day. With moderate haze, virtually no energy is propagated to 20 km.

Despite the reduction in power delivered at long ranges, it is not necessarily a poor decision to shoot at long-range targets. The cost of operation of the FEL is only a few dollars for a several second engagement, and the FEL has no limit on the number of times it can be fired. The lower probability of missile destruction at long range is better than no possibility of successful engagement when the FEL is not fired.

3. Modes of Operation/Operational Tempo

The point defense FEL system envisioned will be delivered to the ship as a sealed unit. No shipboard maintenance would be required; the FEL unit would be exchanged in port periodically, perhaps every 3-5 years. The FEL would have 4 modes of operation: cold, cold standby, hot standby, and lasing. [McWhite, pp. 3]

a. Cold

In port, if the FEL were not fully shutdown for maintenance, the FEL would be kept in a "cold" mode. The cryoplant would be cooled to 4K, with approximately 500kW required from the ship for operation of the cooling plants. Approximately 1 day would be required to transition from a completely shutdown condition to cold mode. [McWhite, pp. 3]

b. Cold Standby

Cold standby is an at-sea condition for use when no threats are in the area. In cold standby, the cryomodules are further cooled to 2K, and all FEL subsystems are made ready for operation. Cold standby mode will require approximately 1 MW of power. Transition from cold to cold standby would take approximately 1 hour. [McWhite, pp. 3]

c. Hot Standby

In hot standby, the FEL is a "trigger pull" away from lasing. The electron injector is operating, making an electron beam that is being continuously dumped prior to acceleration. Hot standby requires approximately 4 MW of power. The transition from cold standby to hot standby will require about 2 minutes. [McWhite, pp. 3]

d. Lasing

Just as the name implies, the FEL is lasing and shooting at a target. The electron beam is now being accelerated through the accelerator and sent to the FEL lasing cavity to create light. While lasing, the FEL would draw 10 MW of power continuously. Transition from hot standby to lasing occurs in a fraction of a second. [McWhite, pp. 3]

B. PHYSICAL DESCRIPTION

A MW class FEL consists of several subsystems, which can be divided into three main categories: electron beam control, light beam control, and auxiliaries. The majority of the FEL systems would be packaged in a box made to drop into a ship, similar to the PHALANX system. An FEL has no preferential orientation, and could be installed vertically or horizontally. Some portions of the system could be distributed to nearby locations on the ship. Both a cylindrical and a box shape are being considered. The FEL box would require tie-ins to cooling water, electrical power, control signals, and laser output. Adequate acquisition, and fire control systems are common aboard naval vessels and will not be discussed in this paper.

1. Size and Weight

Table 5 [Todd, (a), (b), & (c); Jane's (b), GMVLS Mk 41; NFF, Phalanx] shows the FEL is similar in both size and weight to a PHALANX unit or a VLS missile system. VLS launcher systems are loaded as modules of 8-missile cells, with some ships carrying up to 122 TOMAHAWK, STANDARD, ESSM, or RIM-7 quad pack missiles. Ship configuration and mission will determine how many of each missile type are actually carried. I have assumed a load of 20 SM-2's for air defense, but fewer or more could be carried.

	FEL (Assume 2 Beam Directors)	PHALANX (Assume 2 units)	STANDARD Missile System (Assume 20 SM-2 Load Out)
Size	FEL: 96 m^3 Beam Director: 16 m^3 each Total: 128m^3	Gun Mount: 32 m^3 each Ammo Stowage: 25 m^3 each Each Unit: 57 m^3 Total: 114 m^3	2.8 m^3 each Total: 66.5 m^3
Weight	23,000 kg (estimate)	6,170 kg each Total: 12, 340 kg	Missiles: 20 @ 1,500 kg each = 30,000 kg Launcher: 11,775 kg Total: 41,775 kg

Table 5. Comparison of Size and Weight of Point Defense Systems

2. Electron Beam Subsystems

The electron beam control subsystems generate, accelerate, steer, and dispose of a highly energetic beam. The major components of electron beam control consist of the injector, accelerator, electron beam transport, and the beam dump. Operation of the electron injector and the accelerator are discussed in Section II.C.1.a (pp. 6), and will not be repeated here. The electron beam is transported in steel tubing maintained at a very high vacuum to prevent the electrons from scattering off the air.

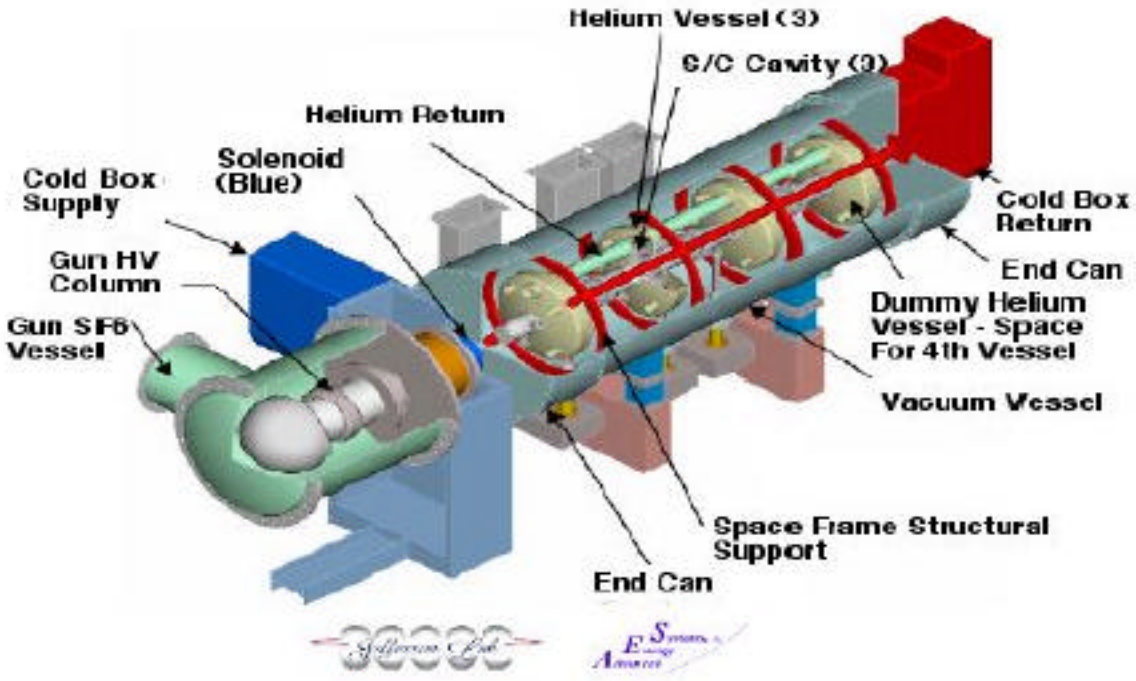

Figure 19. High average current photoinjector

One proposed electron injector shown in Figure 19 [Todd, (d)] is a DC photocathode injector with an estimated cost of $450,000, and would operate with the following characteristics:

Injector Output Energy	W_{inj}	7 MeV
Bunch Frequency	W	750 MHz
Bunch Charge	q	600 pC
Average Current	I_{avg}	450 mA
Peak Current	I_{pk}	2.4 kA
Input Power	P_{inj}	3.5 MW

The accelerator is estimated to cost $3.0 M, and would operate with the following characteristics [Todd, (d)]:

PRF frequency	W	750 MHz
Acceleration Gradient	$(DE/L)_{acc}$	18 MeV/m
Number of Modules		2
Length of Accelerator Module	L_{mod}	5.0 m
Total Accelerator Length	L_{acc}	10.0 m
Output Energy	E_{las}	187 MeV
Exit Bunch Pulse Length	l_e	250 fsec
Input Power	P_{acc}	3.8 MW
Accelerator Efficiency	h_{rf}	60%
Transverse Emittance	e	2π mm-mrad

The heat generated at the beam dump is removed by ship-supplied fresh-water. During lasing operations, the beam dump must be capable of receiving nearly 3 MW of power continuously. [Todd, (d)]

3. Light Beam Subsystems

The major components of the light beam subsystems are the undulator, cavity mirrors, light beam transport, and beam director. The light beam control subsystems consists will generate about 10 MW of IR power in the laser cavity (consisting of the undulator and cavity mirrors) and transport 3 MW of that light to a beam director outside the ship, where it can be focused on a target.

An IR undulator design typically costs around $0.5 M [Todd, (d)]. One proposed MW class IR lasing cavity would operate with the following parameters [Colson (a); Todd, (d)]:

Undulator Length	L	60 cm
Number of Magnetic Periods	N	20
Magnetic Period Length	l_0	3.7 cm
Magnetic Field Strength	B_u	1 T
Wiggler Extraction Efficiency	h	3.5%
Resonator Length	S	12 m
Optical Beam Waist	w_0	50 μm
Optical Spot Size at Mirror	w_{mirror}	2.6 cm
Optical IR Power Out	P_{out}	2 MW
Electron Energy Spread	DE/E	14 %

The FEL beam generated would supply beam directors at any location, either a forward or aft, port or starboard. The beam director will take light from the beam transport subsystem and focus it onto the target. At least two beam directors would likely be placed on the ship to provide 360-degree coverage for point defense. By utilizing adaptive optics, wavefront distortion caused by atmospheric turbulence can be virtually eliminated. Including the required targeting systems and adaptive optics, each beam director will cost about $15 M.

4. Auxiliary Support Subsystems

Auxiliary systems are those that enable the systems described above to function. They include refrigeration, freshwater cooling, radiation shielding, vibration/flex control, and possibly electrical storage, depending on the ship's electrical configuration.

a. Refrigeration System

Cooling of the RF cavity is required to reduce losses in the accelerator while generating a high voltage gradient for acceleration. At an estimated $2 M, cooling components will require a liquid helium refrigeration plant to maintain the electron injector and accelerator at required 2 K for super-conductivity. The resonator mirrors will also require cooling to remove any absorbed energy to prevent excessive mirror face warping.

b. Fresh Water Cooling

Ultimately, the ocean is the preferred final heat sink for an FEL system. A fresh-water cooling system capable of sustained 5 MW heat removal capacity would be used to cool the refrigeration system, beam dump, RF generator. Fresh water is used to minimize corrosive effects on cooled components, and the heat is transferred through a heat exchanger to seawater. Many similar-scale cooling systems are already used in shipboard engine rooms today.

c. Radiation Shielding

High-energy radiation will be generated in the RF cavities, electron beam bends, and the beam dump. Shielding of shipboard personnel and equipment from gamma radiation is accomplished through lead and steel surrounding all sources of radiation, but

the amount of shielding required will depend on the proximity of these systems to berthing and working areas.

d. Flex/Vibration Control System

Ship-generated vibrations as well as ship flexing can cause mirror vibrations and motion of precisely aligned components. Proper mounting can decouple most of the shipboard vibrations from the FEL system. The FEL resonator mirrors must be maintained within a few microns for the FEL to operate. Therefore, an active mirror alignment system will be required to prevent misalignment of the laser cavity and optical transport mirrors.

V. FREE ELECTRON LASER THEORY

As an electron travels through an undulator in the presence of light, it will feel three forces – one from the undulator's static magnetic field and one each from the optical magnetic and electric fields. The electron will accelerate according to the relativistic Lorentz force equation [Jackson, pp.572]

$$\frac{d\left(g\vec{b}\right)}{dt} = -\frac{e}{mc}\left(\overrightarrow{E_S} + \vec{b}\times\vec{B}\right) \tag{5.1}$$

where e and m are the charge magnitude and mass of an electron respectively, c is the speed of light, $\overrightarrow{E_S}$ is the optical electric field, $\vec{B}$ is the vector sum of the undulator magnetic field $\overrightarrow{B_U}$ and the optical magnetic field $\overrightarrow{B_S}$. The undulator magnetic field is taken to be purely transverse and circularly polarized, with strength B and a period $l_0 = 2p/k_0$. The optical field is a circularly polarized plane wave that would be emitted by an electron in the field $\overrightarrow{B_U}$. These fields are given by

$$\overrightarrow{E_S} = E\left(\cos y\ ,\ \text{-}\sin y\ ,\ 0\right) \tag{5.2}$$

$$\overrightarrow{B_S} = E\left(\sin y\ ,\ \cos y\ ,\ 0\right) \tag{5.3}$$

$$\overrightarrow{B_U} = B\left(\cos\left(k_0 z\right),\ \sin\left(k_0 z\right),\ 0\right) \tag{5.4}$$

where $y = kz - wt + f$, with optical wave number $k = 2p/l = w/c$, optical wavelength l, optical frequency w, and optical phase f. The Lorentz factor g and the electron velocity $\vec{b}c$ are related by

$$g = \frac{1}{\sqrt{1-\frac{v_e^2}{c^2}}} = \frac{1}{\sqrt{1-b^2}}, \tag{5.5}$$

where $\vec{v}_e$ is the electron velocity. At 187 MeV, the electrons are traveling very near the speed of light, resulting in b = 0.9999925 and g = 365.

Energy exchange between the electrons and light occurs when the electron velocity has a resonant velocity component in the direction of the optical electric field. The optical electric field is perpendicular to the direction of propagation. Since the light and the electron beam travel in the same direction, no energy exchange would occur naturally. The undulator magnetic field wiggles the electrons, creating a component of the electron's velocity in the transverse direction parallel to the optical electric field as shown in Figure 20. Electrons will spiral through the helical undulator fields given by equation 5.2. For visual clarity, planar fields are illustrated in Figure 20 resulting in electrons oscillating in two dimensions through the undulator rather than spiraling.

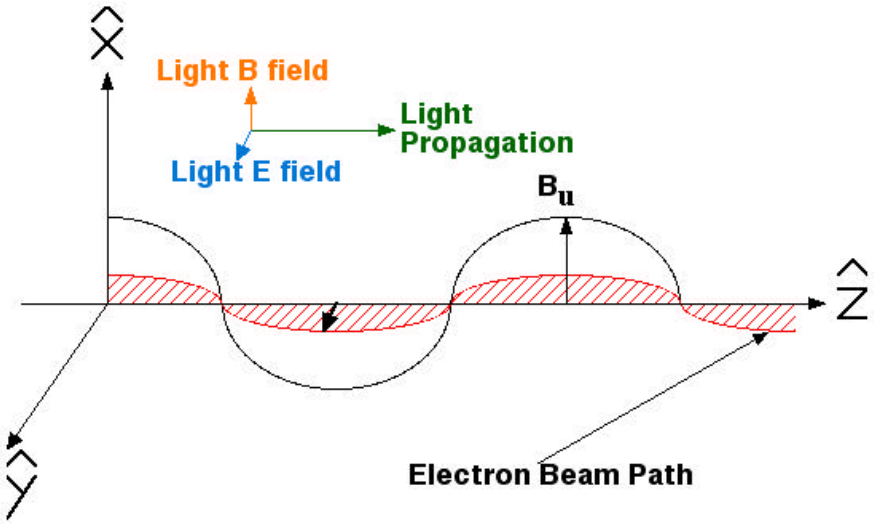

Figure 20. Electron Wiggle as a Result of the Undulator Field

This alignment between the electron's transverse motion and the optical electric field allows the electron to exchange energy with the light, given by [Jackson, pp.572]

$$\frac{\partial g}{\partial t} = -\frac{e}{mc}\vec{b} \bullet \vec{E} \tag{5.6}$$

Equation 5.6 shows that maximum energy exchange between the electron beam and the optical field occurs when the electron's wiggling motion occurs in phase with the optical field. This condition is called resonance, and is examined next.

A. THE RESONANCE CONDITION - THE ELECTRON-PHOTON RACE

The light beam travels down the undulator at the speed of light, slowly passing over an electron. When the energy (and therefore the speed) of the electron is such that one wavelength of light passes over the electron as the electron travels through one undulator period, then the oscillations of the electron are in phase with the optical electric field; the laser is in the "resonance condition". Figure 21 illustrates FEL resonance, where a wavelength of light (blue) passes over an electron (red) in one magnetic wavelength λ_0 of the undulator (green).

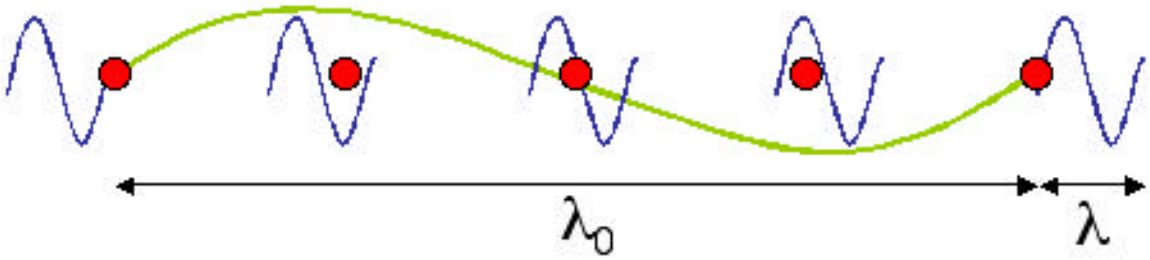

Figure 21. Resonance

Electrons enter the undulator and begin radiating light. One wavelength of light is created as the electron wiggles through one undulator period in a distance λ_0. As shown in Figure 22, the light created at the beginning of the undulator period (the leading edge of the created wave) has traveled a distance l_0/b_0 (by traveling at speed c for a time $l_0/b_z c$), while the electron has only traveled a distance λ_0.

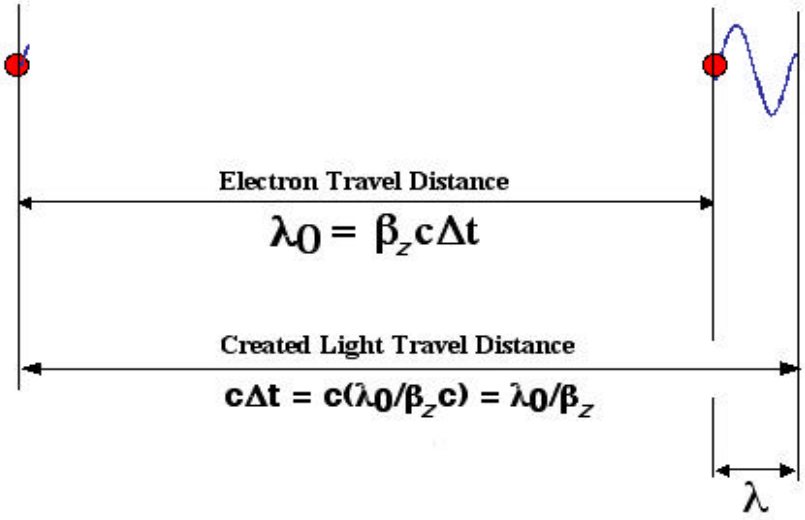

Figure 22. The Electron-Photon Race

One emitted light wavelength l is then given by the difference between these distances

$$l = \frac{l_0}{b_z} - l_0 = l_0\left(\frac{1}{b_z} - 1\right) = l_0\left(\frac{1-b_z}{b_z}\right). \tag{5.7}$$

From equations 5.5,

$$b^2 = 1 - g^{-2}. \tag{5.8}$$

However, b^2 can be decomposed into a transverse components $b_\perp^2$ and an axial component b_z^2 as

$$b^2 = b_\perp^2 + b_z^2. \tag{5.9}$$

It will later be shown that

$$b_\perp^2 = \frac{K^2}{g^2} \tag{5.10}$$

where the undulator parameter is $K = eB_{rms}l_0 / 2\pi mc^2$, and $B_{rms} = B/\sqrt{2}$. From equations 5.8, 5.9, and 5.10, b_z is found to be

$$b_z = \sqrt{1 - \frac{1+K^2}{g^2}} \approx 1 - \frac{1+K^2}{2g^2} \tag{5.11}$$

when $g >> 1$. Substituting b_z from equation 5.11 into equation 5.7, and recognizing that $(1+K^2)/2\gamma^2 << 1$ gives an emitted wavelength l

$$l = l_0\left(\frac{1-\left(1-\frac{1+K^2}{2g^2}\right)}{1-\frac{1+K^2}{2g^2}}\right) = l_0\left(\frac{\frac{1+K^2}{2g^2}}{1-\frac{1+K^2}{2g^2}}\right)$$

$$l \approx l_0\left(\frac{1+K^2}{2g^2}\right). \tag{5.12}$$

B. ELECTRON MOTION AND THE PENDULUM EQUATION

The last section presented a qualitative understanding of energy transfer from the electron beam to the light wave. In this section, we develop a better understanding of electron motion and light propagation through the undulator to describe FEL operation more quantitatively.

Substituting the light and undulator fields from equations 5.2, 5.3, and 5.4 into the Lorentz force equation 5.1, the transverse components can be written as

$$\frac{d(g\beta_x)}{dt} = -\frac{e}{m_e\, c}\left(E_{sx} + \beta_z \times B_{uy} + \beta_z \times B_{sy}\right),$$

$$\frac{d(g\beta_x)}{dt} = -\frac{e}{m_e\, c}\left(E_s(1-\beta_z)\cos(y) - B_u \beta_z \sin(k_0\, z)\right), \qquad (5.13)$$

$$\frac{d(g\beta_y)}{dt} = -\frac{e}{m_e\, c}\left(-E_s(1-\beta_z)\sin(y) + B_u \beta_z \cos(k_0\, z)\right). \qquad (5.14)$$

Recognizing $-E_s(1-\beta_z) << B_u \beta_z$, equations 5.13 and 5.14 then combine into one transverse equation

$$\frac{d(g\,\overrightarrow{\beta_\perp})}{dt} = -\frac{e\,B\,\beta_z}{m_e\, c}(-\sin(k_0\, z),\ \cos(k_0\, z),\ 0). \qquad (5.15)$$

Integration gives

$$\overrightarrow{\beta_\perp} = -\frac{e\,B\,l_0}{g\ m_e\ c^2\ 2\,p}(\cos(k_0\ z),\ \sin(k_0\ z),\ 0). \qquad (5.16)$$

where constants of integration are set equal to zero assuming perfect injection into helical orbits. Defining the undulator parameter $K = eB\,l_0 / 2p\,m_e c^2$, $\beta_\perp$ then becomes

$$\beta_\perp = -\frac{K}{g}(\cos(k_0\ z),\ \sin(k_0\ z),\ 0). \qquad (5.17)$$

Using 5.17, the energy exchange equation 5.6 can then be written as

$$\frac{dg}{dt} = -\frac{e}{m_e\, c}\left(-\frac{K}{g}\cos(k_0\, z),\ -\frac{K}{g}\sin(k_0\, z),\ \beta_z\right)\cdot E_s\left(\cos y, -\sin y, 0\right). \qquad (5.18)$$

Conducting the dot product, equation 5.18 simplifies to

$$\frac{dg}{dt} = \frac{e\ K\ E_s}{g\ m_e\ c}\ \cos(k_0\ z + y\ ). \tag{5.19}$$

Defining the electron phase z

$$z = (k+k_0)\ z - w\ t, \tag{5.20}$$

equation 5.19 can be written

$$\frac{dg}{dt} = \dot{g} = \frac{e\ K\ E_s}{g\ m_e\ c}\ \cos(z\ + f)\ . \tag{5.21}$$

Taking the time derivative of equation 5.11 and solving for $\dot{g}$ gives

$$\dot{g} = \frac{g^3\ b_z\ \dot{b}_z}{\left(1+K^2\right)}. \tag{5.22}$$

$\dot{b}_z$ is found by taking two time derivatives of the electron phase z ,

$$\dot{z} = (\mathrm{k}+\mathrm{k}_0)v_z - w = (\mathrm{k}+\mathrm{k}_0)c\,b_z - w\ ,$$

$$\ddot{z} = (\mathrm{k}+\mathrm{k}_0)c\,\dot{b}_z\ ,$$

$$\dot{b}_z = \frac{\ddot{z}}{(\mathrm{k}+\mathrm{k}_0)c}. \tag{5.23}$$

Substituting equation 5.23 into equation 5.22 for $\dot{b}_z$ gives

$$\dot{g} = \frac{g^3\ b_z\ \ddot{z}}{\left(1+K^2\right)(k+k_0)c}\ . \tag{5.24}$$

Equation 5.24 can be simplified by recognizing that $k_0 << k$ for relativistic electrons, so $(k+k_0)c \approx kc = w$. Recalling also that $b_z \approx 1$ reduces equation 5.24 to

$$\dot{g} = \frac{\ddot{z}\ g}{2w_0}. \tag{5.25}$$

Using equations 5.21 and 5.25, and solving for $\ddot{z}$ gives

$$\ddot{z} = 2w_0 \frac{eKE_s}{g^2 m_e c} \cos(z + f). \tag{5.26}$$

Equation 5.26 describes the electron microscopic motion in the presence of light, and is mathematically the same as the simple pendulum equation. Pendulum motion suggests that an examination of phase space may be useful in understanding the operation of an FEL. Phase space will be explored further in Section IV.E (FEL Gain) below.

C. THE WAVE EQUATION – ELECTRON ENERGY BECOMES LIGHT

Having determined how electrons respond in the presence of a light wave, we can now turn our attention to the effect of the electrons upon the light wave. In terms of the vector potential $\vec{A}$, light will propagate according to the inhomogeneous wave equation [Jackson, Eq. 6.52]

$$\left(\nabla^2 - \frac{1}{c^2} \frac{\partial^2}{\partial t^2} \right) \vec{A} = -\frac{4p}{c} \vec{J}_\perp \,, \tag{5.27}$$

where $\vec{J}_\perp$ is transverse current density due to the oscillations of electrons passing through the undulator. For a circularly polarized plane wave, $\vec{A}$ is represented as

$$\vec{A} = \frac{E_s}{k} \left[\cos(y), \; -\sin(y), \; 0 \right]. \tag{5.28}$$

Assuming slowly varying fields (therefore neglecting higher order terms), the second derivatives of $\vec{A}$ from equation 5.27 yields

$$\frac{\partial^2 \vec{A}}{\partial z^2} = \frac{2}{k} \frac{\partial E_s}{\partial z} \left(k + \frac{\partial f}{\partial z} \right) (\cos y, -\sin y, 0) + \frac{1}{k} \left(k + \frac{\partial f}{\partial z} \right)^2 E_s (-\sin y, -\cos y, 0) \tag{5.29}$$

$$\frac{\partial^2 \vec{A}}{\partial t^2} = \frac{2}{k} \frac{\partial E_s}{\partial t} \left(\frac{\partial f}{\partial t} - w \right) (\cos y, -\sin y, 0) + \frac{1}{k} \left(\frac{\partial f}{\partial t} - w \right)^2 E_s (-\sin y, -\cos y, 0). \tag{5.30}$$

Substituting equations 5.29 and 5.30 back into 5.27 gives

$$2\left(\frac{\partial}{\partial z}+\frac{1}{c}\frac{\partial}{\partial t}\right)E_s\left(\cos y,-\sin y,0\right)+2E_s\left(\frac{\partial}{\partial z}+\frac{1}{c}\frac{\partial}{\partial t}\right)f\left(-\cos y,-\sin y,0\right)=\frac{-4p}{c}\vec{J}_\perp . \quad (5.31)$$

Transforming coordinates to $z_n = z + ct$ reduces the derivatives of equation 5.31 so that

$$\left(\frac{\partial}{\partial z}+\frac{1}{c}\frac{\partial}{\partial t}\right)=\frac{1}{c}\frac{\partial}{\partial t} \quad (5.32)$$

Defining unit vectors $\hat{e}_1 = \left(\cos y,-\sin y,0\right)$ and $\hat{e}_2 = \left(-\sin y,\cos y,0\right)$ allows equation 5.32 to be simplified and separated into two component wave equations

$$\frac{\partial E_s}{\partial t}=-2p\left(\vec{J}_\perp \bullet \hat{e}_1\right) \quad (5.33)$$

$$E_s\frac{\partial f}{\partial t}=-2p\left(\vec{J}_\perp \bullet \hat{e}_2\right). \quad (5.34)$$

The transverse current density $\vec{J}_\perp$ is the sum of all the individual electron's perpendicular currents

$$\vec{J}_\perp=-ec\sum_i \vec{b}_\perp d^3(\vec{x}-\vec{r}_i)\frac{Kec}{g}=\sum_i(\cos(k_0\ z),\ \sin(k_0\ z),\ 0)\,d^3(\vec{x}-\vec{r}_i) \quad (5.35)$$

where $\overrightarrow{b_\perp}$ is defined in equation 5.17, $d^3(..)$ is the three dimensional Dirac delta-function, and $\vec{r}_i$ is the position of the ith electron. Substituting equation 5.35 into the component wave equations 5.33 and 5.34 and performing the dot product gives

$$\frac{\partial E_s}{\partial t}=-\frac{2p\,Kec}{g}\sum_i \cos(k_0\ z+y\ )\,d^3(\vec{x}-\vec{r}_i) \quad (5.36)$$

$$E_s\frac{\partial f}{\partial t}=\frac{2p\,Kec}{g}\sum_i \sin(k_0\ z+y\ )\,d^3(\vec{x}-\vec{r}_i). \quad (5.37)$$

Average over a small volume of the electron beam with the electron density r_e constant, and convert the summation to an average over electron phases ζ (denoted by <..>), and use $k_0 z + y = z + f$. Equations 5.36 and 5.37 become

$$\frac{\P E_s}{\P t} = -\frac{2p Kec r_e}{g}\left\langle \cos(z + f)\right\rangle \tag{5.38}$$

$$\frac{\P f}{\P t} = -\frac{2p Kec r_e}{g E_s}\left\langle \sin(z + f)\right\rangle . \tag{5.39}$$

Equation 5.38 shows the change in optical field strength E_s, while equation 5.39 shows the evolution of the optical phase f. Both are dependent upon the undulator through *K*, the average over electron phase, and the instantaneous electron *I* given by

$$I = ec r_e \left(A_e \right), \tag{5.40}$$

where A_e is the cross-sectional area of the electron beam. Equation 5.39 also shows that the rate of change in f decreases as E_s increases. The dependence of f upon z is seen more clearly when combining equations 5.36 and 5.37 as the real and imaginary parts of

$$\frac{\partial}{\partial t} E_s \, \mathrm{e}^{if} = -\frac{2p Kec r_e}{g}\left\langle \mathrm{e}^{-iz} \right\rangle . \tag{5.41}$$

D. DIMENSIONLESS PARAMETERS

At this point, equations 5.26 and 5.41 represent the response of the electrons to the presence of light and the conversion of electron energy into light. With these coupled differential equations, an analysis of FEL operation can be performed. Converting the parameters of equations 5.26 and 5.41 to dimensionless values accomplishes three worthwhile achievements. First, equations 5.26 and 5.41 are bulky, with many fixed constants. For convenience, properly gathering constants could simplify these equations. Second, by converting to "dimensionless" variables, the resulting FEL equations would yield general results, needing only conversion to specific parameters to determine desired parameters for specific cases. Finally, since thousands of electrons are included in a single pulse, the amount of math required to determine meaningful results requires

numerical analysis on a computer. Since many thousands of calculations will be performed upon input parameters, choosing variables with values near unity minimizes numerical errors. Time, optical field strength, electron current density, and phase velocity can be recast in dimensionless form to greatly simplify equations 5.26 and 5.41.

1. Dimensionless Time

A dimensionless time parameter t is defined to describe the position of the electrons in an undulator of length L, such that $t = ct/L$. A single pass through the undulator is now described by t going from 0 to 1. Derivatives with respect to t will be indicated with an open circle above the function, as

$$\frac{d(X)}{dt} = \frac{L}{c}\frac{d(X)}{d\,t} = \mathring{X}\ , \tag{5.42}$$

A second derivative with respect to t is given by $\mathring{\mathring{X}}$. Transforming the electron pendulum equation 5.26 and the optical wave equation 5.41 into dimensionless time gives

$$\mathring{\mathring{z}} = \frac{L^2}{c^2}\ddot{z} = 2w_0\frac{eKE_sL}{g^2 m_e c^3}\cos(z + f) \tag{5.43}$$

$$\frac{\partial}{\partial t}E_s\ \mathrm{e}^{if} = \frac{L}{c}\frac{\partial}{\partial t}E_s\ \mathrm{e}^{if} = -\frac{2p\ K\ Le r_e}{g}\left\langle \mathrm{e}^{-iz}\right\rangle. \tag{5.44}$$

2. Dimensionless Optical Field Strength

From equation 5.43, w_0 can be expressed as $k_0 c = (2p/l_0)c$, and $L = N l_0$. Equation 5.43 can then be simplified by defining the dimensionless optical field strength as

$$|a| = \frac{4p\ Ne\ K\ E_s L}{g^2\ m_e\ c^2}. \tag{5.45}$$

The intensity of the laser light, which is proportional to $E_s{}^2$, is then also proportional to a^2.

The dimensionless pendulum equation used to describe electron motion then becomes

$$\boxed{\ddot{z} = \dot{n} = |a| \cos(z + f)} \tag{5.46}$$

The optical wave equation should also examine the change in dimensionless optical field strength a rather than E_s. Multiplying both sides of equation 5.44 by a / E_s and defining $a = |a| \, e^{if}$ results in

$$\frac{\partial}{\partial t} a = -\frac{8p^2 K^2 L^2 N e^2 r_e}{g^3 m_e c^2} \left\langle e^{-iz} \right\rangle \tag{5.47}$$

3. Dimensionless Electron Current

The last simplification to be made is to define the dimensionless current j as the coefficient of the electron average in equation 5.47,

$$j = \frac{8p^2 K^2 L^2 N e^2 r_e}{g^3 m_e c^2} \tag{5.48}$$

This results in the compact optical wave equation

$$\boxed{\frac{\partial}{\partial t} a = \dot{a} = -j \left\langle e^{-iz} \right\rangle} \tag{5.49}$$

4. Dimensionless Phase Velocity

In studying the phase space (Section IV.E.1 below) of the electron beam, the phase velocity of the electrons as well as the electron phase must be considered. The dimensionless phase velocity is the time derivative of the electron phase z. From equation 5.20,

$$v = \dot{z} = L\left[\left(k + k_0\right) b_z - k\right], \tag{5.50}$$

Note that n is zero when the FEL is operating at resonance and the electron velocity is $b_z = k/(k + k_0)$. When b_z is greater than $k/(k + k_0)$, n is positive. When b_z is less than $k/(k + k_0)$, n is negative.

E. FEL GAIN

The gain in the optical field strength per pass G is expressed mathematically as

$$G = \frac{a_1^2 - a_0^2}{a_0^2}, \tag{5.51}$$

where a_0 and a_1 are the optical field strength at the beginning (t = 0) and end (t = 1) of the undulator respectively. While equation 5.51 intuitively makes sense, it is mathematically easier to utilize energy conservation to determine the optical gain. As the electrons lose energy, the light beam gains energy. The change in electron energy E_e is given by

$$\Delta E_e = \Delta g \; mc^2 . \tag{5.52}$$

The change in electron energy is proportional to the change in electron phase velocity from equation 5.50, which is expressed as

$$\Delta v = L\left(k + k_0\right)\Delta b_z \approx L \; k \; \Delta b_z . \tag{5.53}$$

By substituting $L = N \, l_0$ and equation 5.12 into equation 5.53,

$$\Delta v \approx N \frac{2g^2 l}{1 + K^2} \; k \; \Delta b_z$$

Substituting equation 5.22 in difference rather than differential form, Δn becomes

$$\Delta v = 4 \; p \; N \frac{\Delta g}{g \; b_z} \approx 4 \; p \; N \frac{\Delta g}{g} . \tag{5.54}$$

The average change in electron energy $\Delta \bar{n}$ is expressed as

$$\overline{\Delta v} = 4 \; p \; N \frac{\overline{\Delta g}}{g} . \tag{5.55}$$

Solving for Δg and substituting the result into equation 5.52 gives an average change of electron energy

$$\overline{\Delta E_e} = g \, mc^2 \frac{\overline{\Delta v}}{4 \; p \; N} . \tag{5.56}$$

Equation 5.56 represents the change in energy that each electron will undergo. Assuming constant electron density r_e, the number of electrons dN_e in an incremental volume of the optical wave dV is given by

$$dN_e = r_e F dV , \tag{5.57}$$

where F is the filling factor representing the ratio of the cross-sectional areas of the electron and the optical beam. The total change in electron beam energy in an incremental volume of optical beam is then the value found from equation 5.56 times the number of electrons given in equation 5.57

$$\overline{\Delta E_{bm}} = \left(\overline{\Delta E_e}\right)\left(dN_e\right) = g\, mc^2 \frac{\overline{\Delta v}}{4\ p\ N}\left(r_e F dV\right). \tag{5.58}$$

The optical energy E_{opt} in a cylindrical unit volume of the optical beam is given by

$$dE_{opt} = \frac{E_s^2}{4p} dV . \tag{5.59}$$

FEL gain is then given by

$$G = -\frac{\overline{\Delta E_{bm}}}{dE_{opt}} = \frac{g\, mc^2 \overline{\Delta v}\, r_e F dV / 4\ p\ N}{E_s^2 dV / 4p}. \tag{5.60}$$

Equation 5.60 can be simplified by substitution of the dimensionless field at the beginning of the undulator a_0 and the dimensionless current j,

$$G = -\frac{2Fj\overline{\Delta v}}{a_0^2} \tag{5.61}$$

Equation 5.61 assumes low gain, so that the optical field a_0 is nearly constant. In weak optical fields where $|a| < \pi$, $\overline{\Delta v}$ can be estimated using perturbation theory to get [Colson (c), pp. 21]

$$G = -\frac{2Fj}{n_0^3}\left[\cos\left(n_0 t\right) + \frac{n_0 t}{2}\sin\left(n_0 t\right) - 1\right]. \tag{5.62}$$

The following sections analyze the FEL in phase space and assume the reader is familiar with interpreting phase space diagrams. An introduction to phase space plots is provided in Appendix A.

1. FEL Phase Space – Electron Bunching

For an FEL, the height of the separatrix is $2\sqrt{|a|}$, and the electron phase space coordinates are the electron phase z and the electron phase velocity n. Open and closed orbits in FEL electron phase space are shown in Figure 23 [Colson (b), pp. 27].

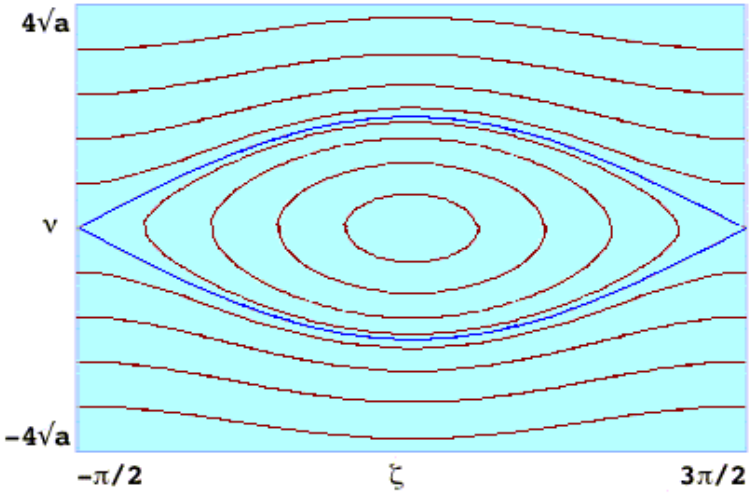

Figure 23. FEL open and closed orbits plotted in phase space

The pendulum equation 5.46, restated below, describes the energy transfer process in an FEL.

$$\boxed{\ddot{z} = \dot{n} = |a|\cos(z + f)} \tag{5.46}$$

Note that the z axis is offset by $p/2$ in Figure 23. This is the result of the cosine term in equation 5.46, which yields nulls at phase values of $\pm p/2$. The equation defining the separatrix can be found to be

$$n_s^2(z_s) = 2\,|a|\,\left[1+\sin(z_s + f)\right], \tag{5.63}$$

where n_s and z_s are the values of phase velocity and phase of the separatrix respectively. The zeros of the separatrix occur at $z = -p/2$ and $3p/2$.

The 1 mm electron pulse overlaps many wavelengths of the 1 μm light, so that there is a uniform distribution of electrons within each wavelength of light. The optical phase f can be taken to be zero in the low gain limit.

Electrons will typically undergo only a fraction of an oscillation in phase space while traveling through the undulator. Figure 24 [Colson (b), pp. 28] shows 20 sample electrons starting from the resonance velocity (n = 0) traveling through an undulator as t goes from 0 to 1. At t = 0, the electrons are shown in yellow and turn to red by t = 1. Initially, all the electrons are evenly distributed in initial phases, as indicated by even spacing through z. The yellow line in the gain and f graphs of Figure 65 show the gain and phase evolution as $t = 0 \rightarrow 1$, as predicted by weak field theory.

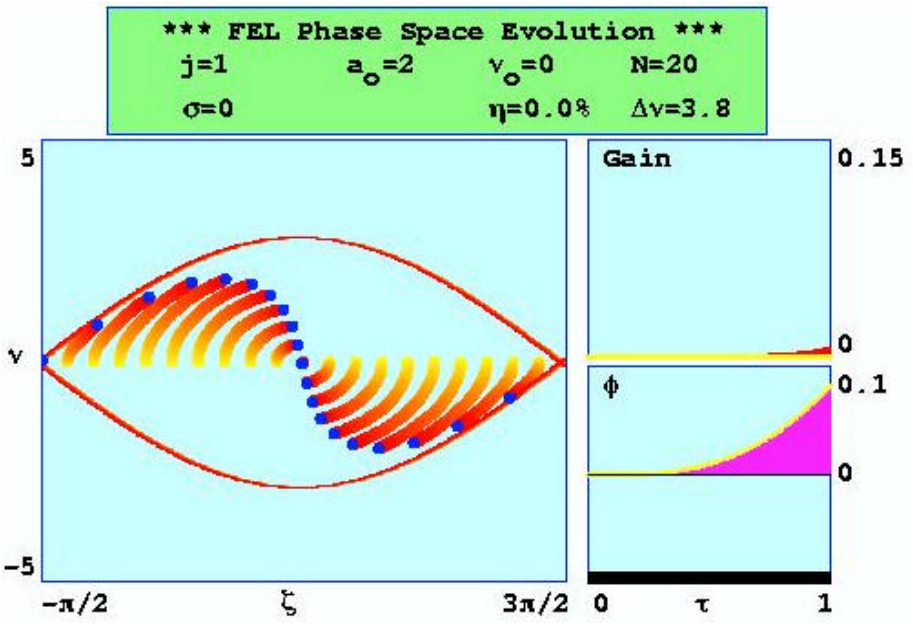

Figure 24. FEL phase space evolution at resonance

Those electrons between the phases $-p/2 \rightarrow p/2$ are seen to absorb energy from the light pulse and have a increasing phase velocities. Likewise, those electrons between the phases $p/2 \rightarrow 3p/2$ are seen to give up energy from the light pulse, ending up with lower phase velocities. This energy exchange matches what is predicted by the real portion of equation 5.49, which represents the changes in optical field amplitude,

$$\dot{a} = -j\left\langle \cos(z) \right\rangle \tag{5.64}$$

Energy transfer can then be observed qualitatively on a phase space plot by determining where in z the electrons bunch. In Figure 24, the electrons are bunched around $z = p/2$, with the same number of electrons ending at higher energies as those ending below. There is therefore no change in the average electron energy. For low gain, the optical phase evolution through an FEL is represented by

$$\dot{f} = \frac{j\left\langle \sin(z) \right\rangle}{|a|}. \tag{5.65}$$

Equation 5.65 shows that electron bunching at $z = p/2$ results in large changes in the optical phase, while Equation 5.64 predicts no change in amplitude of $|a|$ when electron bunching occurs at $z = p/2$.

To achieve gain or growth of the optical amplitude $|a|$, electron bunching must occur near $z = p$, whereas to achieve a large shift in optical phase, electron bunching near $\pm p/2$ is desired. Where bunching occurs is determined by the initial phase velocity of the electrons entering the undulator. Figure 25 [Colson (b), pp. 29] shows an FEL phase space plot with 200 electrons that have an initial phase velocity $n_0 = 3$ instead of $n_0 = 0$. Notice that the electrons bunch closer to p, resulting in much more gain than that achieved in Figure 24 (where $n_0 = 0$), with almost no optical phase shift.

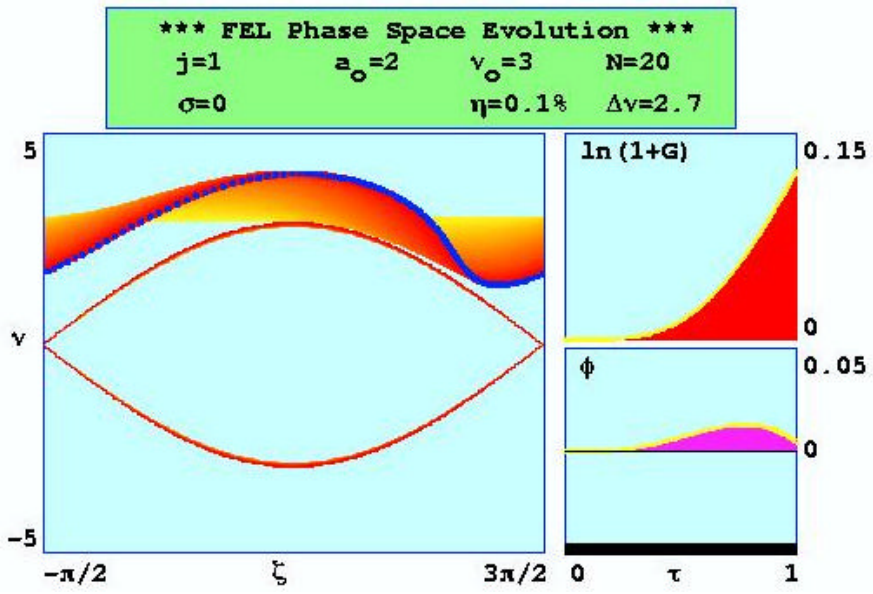

Figure 25. FEL phase space evolution above resonance

Figure 26 [Colson (b), pp. 31] shows FEL optical gain and phase spectra as a function of initial electron phase velocity for weak fields. These graphs plot the final optical gain and phase shift at the end of the undulator (t = 1) as a function of n_0. Weak fields are defined as optical fields with $|a| < p$. The peak weak field gain is seen to be at $n_0 \approx 2.6$, while the maximum phase shift occurs near resonance.

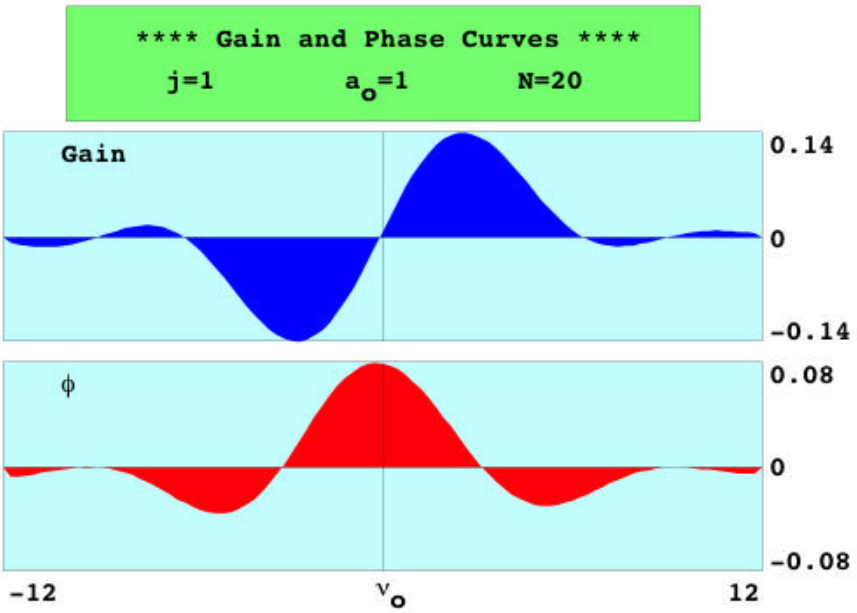

Figure 26. Weak field FEL gain and phase spectra

2. Strong Field FEL Phase Space - Saturation

As the optical field strength a increases after many repeated passes in the FEL oscillator, they reach the strong field regime and saturation. The height of the separatrix also increases as $2\sqrt{|a|}$ as the optical field increases. When the separatrix extends above n_0, electrons begin to get trapped within the separatrix. As these trapped electrons rotate in closed orbits in phase space, they can over-rotate through z and begin absorption of energy from the light wave. Figure 27 [Colson (b), pp. 32] shows over-bunching of the electrons with optical field a_0 = 20 in the strong field regime. Notice that the gain has peaked, and is beginning to decline. In this strong field simulation, a peak gain of only 0.02 was achieved, compared to 0.14 gain in the weak field simulation of Figure 25.

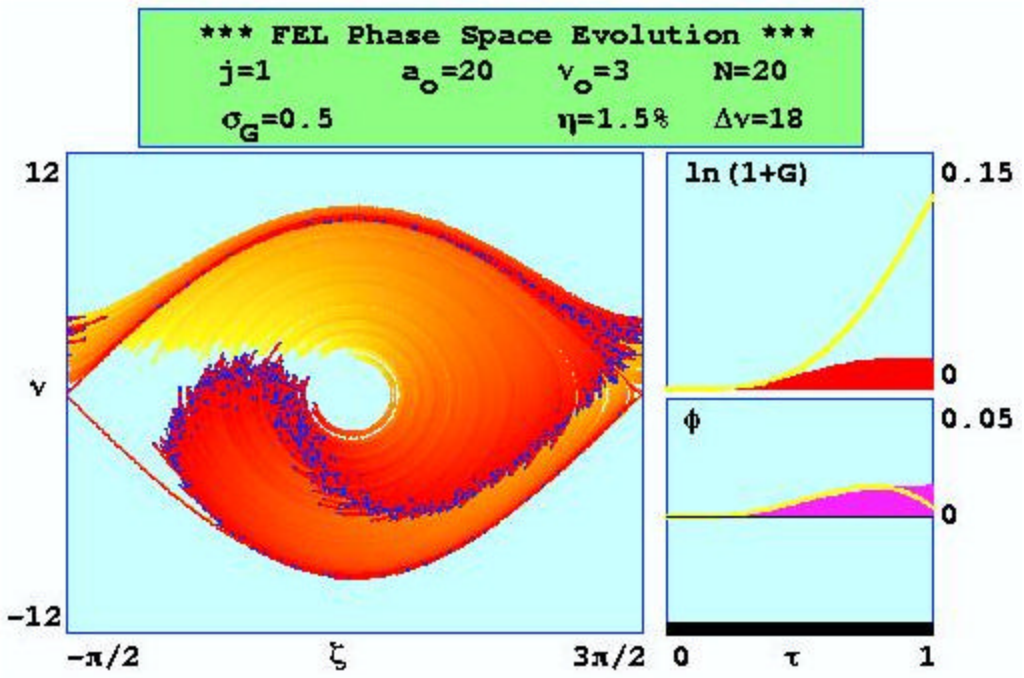

Figure 27. Strong field FEL phase space evolution

Saturation occurs when the separatrix height is greater than n_0 and there is no further growth in gain. Note that saturation does not limit power growth - power will continue to increase as long as gain is positive. But, it will occur more slowly until the gain equals mirror loss and a steady-state is reached.

3. High Current FEL Phase Space

In deriving equation 5.62 for a low-gain FEL, it was assumed that the optical field amplitude and phase were approximately constant. In a high current FEL, where $j >> 1$, the compact optical field equation 5.49 (reprinted below) shows that neither $\left[\mathrm{Re}(a)\right]$ nor $\left[\mathrm{Im}(a)\right]$, nor the amplitude $|a|$ or phase f, are constant

$$\frac{\partial}{\partial t} a = \boxed{\overset{\circ}{a} = -j\left\langle e^{-iz} \right\rangle} \quad . \tag{5.49}$$

The change in the optical field and therefore gain in a high current FEL grow exponentially [Colson (c), pp. 26], and are given by

$$\left|a(t)\right| \approx \frac{a_0}{3}\, e^{\left(\frac{j}{2}\right)^{1/3}\frac{\sqrt{3}t}{2}}, \tag{5.66}$$

$$f(t) \approx \frac{t}{2}\left(\frac{j}{2}\right)^{1/3}, \tag{5.67}$$

$$G(t) \approx \frac{1}{9}\, e^{\left(\frac{j}{2}\right)^{1/3}\sqrt{3}t}. \tag{5.68}$$

Figure 28 shows typical high current FEL gain and phase spectra. Note that there is significant gain and phase shift at resonance, in contrast to the low current FEL.

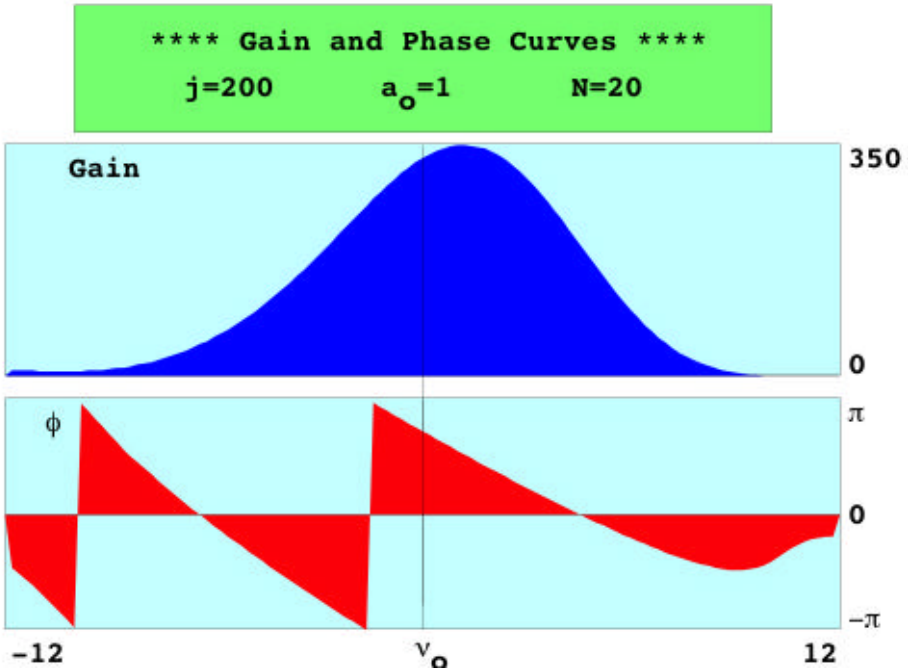

Figure 28. High current FEL gain and phase spectra

Phase space plots in Figure 29 for j = 200 (>> p) illustrate what is happening in a high current FEL. An electron beam on resonance (n_0 = 0) will begin to bunch near the relative phase $z + f = \pi/2$, just as in a low current FEL. Recall that bunching at $\pi/2$ will drive the optical phase f by nearly $\pi/2$, but not the amplitude of a. This optical phase growth results in the electrons that bunched naturally at $\pi/2$ seeing the optical phase move around the bunch so that near the midpoint of the undulator, $z + f \approx \pi$. Electrons bunching atrelative phase $z + f \approx p$ result in maximum optical amplitude growth, with exponential gain through the remainder of the undulator. Extremely high gains of many hundreds of percent per pass can then occur. Notice that by the end of the undulator (t = 1), the optical phase has shifted by $\approx 2\pi/3$, and the gain is nearly 350. The breaks in the yellow theory lines of the gain and optical phase plots mark the transition from using weak field theory to theory which describes exponential growth.

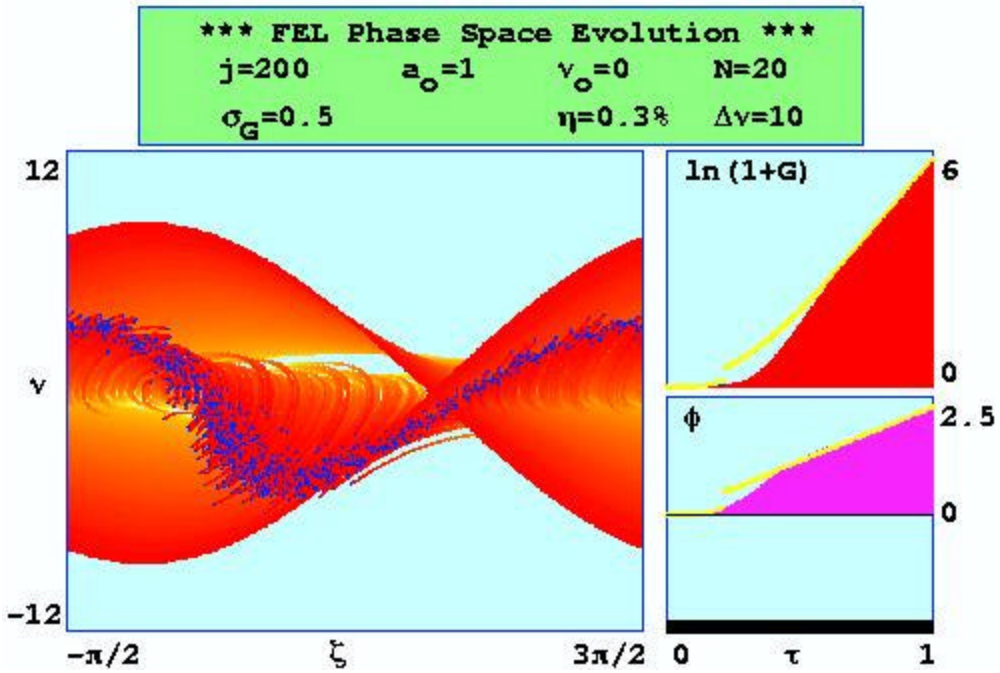

Figure 29. High current FEL phase space evolution

THIS PAGE INTENTIONALLY LEFT BLANK

VI. SHORT RAYLEIGH LENGTH SIMULATIONS

A. SHORT RAYLEIGH LENGTH

For the high-power FEL described in Section IV, 20-30% of the optical power escapes the cavity mirrors at each pass. In a 1 MW FEL, several MW of optical power would strike each mirror while the weapon is firing. In the 1 μm wavelength regime, optical intensities on the order of hundreds of kW/cm^2 can cause mirror damage on even the best reflecting surfaces. Avoiding mirror damage can be accomplished in several ways. Better mirror technology can be developed that allows higher optical intensities without damage. Alternatively, the power of the laser could be reduced; however, a low-power laser would take longer to kill a missile. More light can be let out per pass resulting in less energy stored within the cavity. This would require higher gain per pass for startup. But no remedies could reduce the intensity at the mirrors by the large amount needed. Growth of the optical beam diameter occurs naturally through diffraction, and a large optical beam spread over a short distance can be accomplished by using a short Rayleigh length.

The rate of optical spreading is characterized by the Rayleigh length Z_0, which is the distance a beam of light must propagate for the cross-sectional area of the mode waist to double. Mathematically,

$$Z_0 = \frac{p\ W_0^2}{l}, \tag{6.1}$$

where W_0 is the radius of the beam waist, located at the optical focus. The curvature of the cavity mirrors determines the focal length regardless of spot size. Within a resonating cavity, the optical mode shape is fixed by the separation of the resonator mirrors S and the mirror radii of curvature R_m. For a fixed resonator length, the closer the cavity mirrors are to concentric ($R_m = S/2$), the smaller Z_0 and W_0 become. The mode radius $W(z)$ will increase as the beam propagates in the z direction as

$$W^2(z) = W_0^2\left(1+\left(\frac{z}{Z_0}\right)^2\right), \tag{6.2}$$

where $W(z)$ is the waist at a distance z away from the waist.

FELs are usually designed to optimize the mode overlap with the electrons throughout the whole undulator. In a typical design, the Rayleigh length is approximately half of the undulator length L. In a low gain FEL, W_0 is typically only a few millimeters and is usually located at the center of the undulator to minimize the optical mode volume. In order to maintain optical intensities below damaging levels at the mirrors, the optical beam must be allowed to spread to several centimeters in radius

The Naval Postgraduate School has conducted several simulations of short Rayleigh length FEL operation. Results from JLAB's 100 kW upgrade design, expected to be commissioned in 2005/2006, are presented below for use in studying the physics of a short Rayleigh length FEL design. The proposed parameters for JLAB's 100 kW FEL are

Electron Beam Energy	E_e	210 MeV
Pulse Repetition Rate	W	750 MHz
Peak Current	I_{pk}	270 A
Electron Pulse length	l_e	0.1 mm
Electron Beam Radius	r_e	0.3 mm
Undulator Periods	N	36
Undulator length	L	288 cm
Undulator Parameter	K	1.7
Undulator wavelength	l_0	8 cm
Cavity Length	S	32 m
Resonator Quality Factor	Q	4.2 (21% transmission)
Optical Wavelength	l	1.06 μm

Dimensionless parameters are again useful for a broad application study. Normalizing transverse lengths to $\sqrt{L l / p}$ (= 0.986 x 10^{-4} m for the 100 kW parameters above) and longitudinal lengths to L (= 2.88m). The dimensionless optical waist $w(t)$ and Rayleigh length z_0 are given by

$$w(t) = \sqrt{z_0 + \frac{(t - 1/2)^2}{z_0}} \tag{6.3}$$

$$\text{and} \qquad z_0 = \frac{Z_0}{L}. \tag{6.4}$$

Using 21% transmission, and assuming 2% total edge loss, 435 kW of power must impinge on each mirror to obtain 100 kW of output. Figure 30 illustrates the reduction in power densities on the mirrors of the TJNAF FEL for dimensionless Rayleigh lengths of z_0 = 0.1, 0.2, 0.3, 0.4, and 0.5.

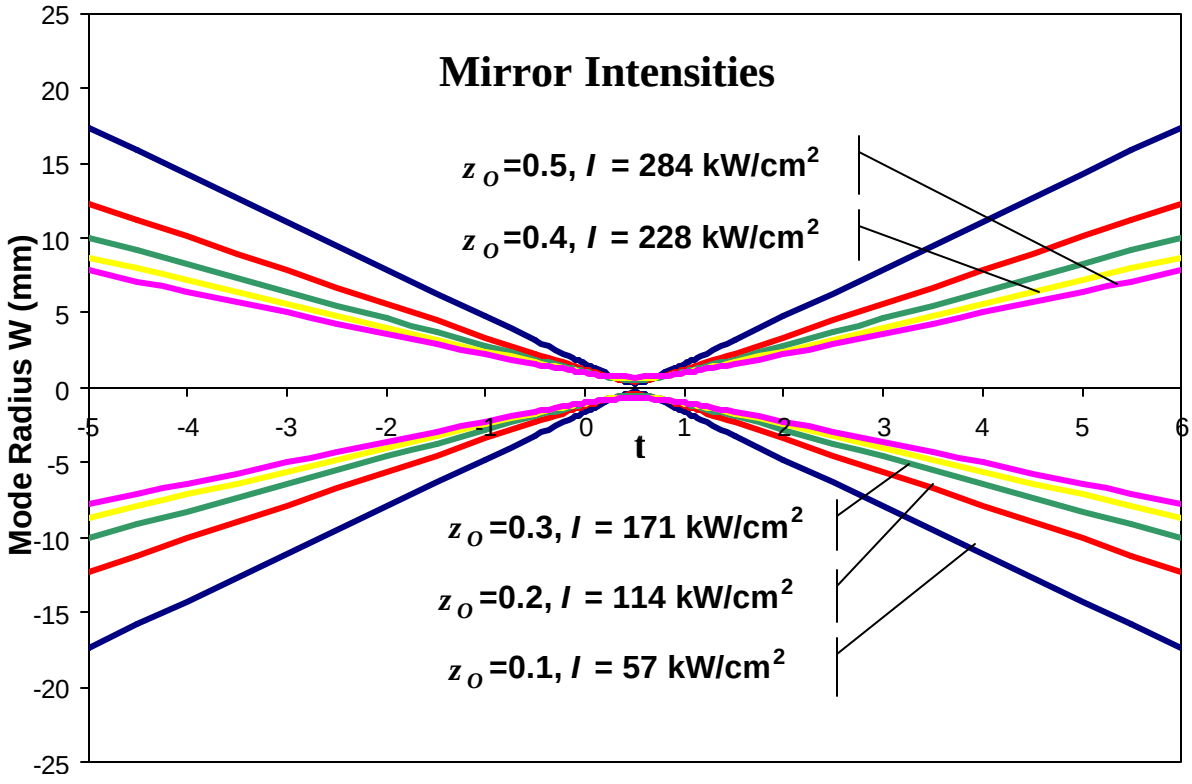

Figure 30. Spot Size Picture

B. TRANSVERSE WAVEFRONT SIMULATION

Changes of Rayleigh length alter the optical mode shape throughout the undulator. If the optical beam waist narrows to less than the electron beam cross-section, some electrons will not participate in the energy exchange process in portions of the undulator. Those electrons which remain within the optical mode, however, will be exposed to a much more intense electrical field from the focused optical beam. These multiple competing effects will alter the initial gain and final steady state power of the FEL.

In order to study the effects of short Z_0 on the gain and final efficiency, we use a three-dimensional (x, y, t) simulation that follows the development of a single optical

wavefront in the presence of the electron beam through an undulator. This self-consistent simulation uses the pendulum equation to describe electron motion, and the optical wave equation to describe the optical field propagation. While the trends developed by this simulation are reliable, the simulated extraction efficiency will be slightly higher than expected since real systems send electron *pulses* through the undulator rather than a continuous beam. Gain and efficiency are slightly reduced from those achieved if a continuous beam of electrons were used. This phenomenon, called the short pulse effect in an FEL, is accounted for in a separate simulation.

Figure 31 presents a simulation output used to determine the FEL gain in weak optical fields Figure 32 shows the same system after reaching steady-state high power in order to determine the extraction efficiency. A table of the dimensionless parameters used for this simulation is shown in the upper right hand block of the output figures. Parameters varied in this study include z_0, n_0, a_0, Q, s_x and s_y, the dimensionless electron beam radius in the x and y dimensions. Both Figures 31 and 32 are simulations using the dimensionless Rayleigh length of $z_0 = 0.1$ and dimensionless electron beam radius of $s_x = s_y = 0.3$. Note that for the extraction efficiency simulation (Figure 32), $Q = 4.2$, representing 21% cavity losses per pass, and the initial optical field strength $a_0 > \pi$, indicating strong initial optical fields. The weak field simulation (Figure 31) has essentially no cavity losses ($Q = 1 \times 10^{10}$) and an initial field strength near zero ($a_0 = 0.001$).

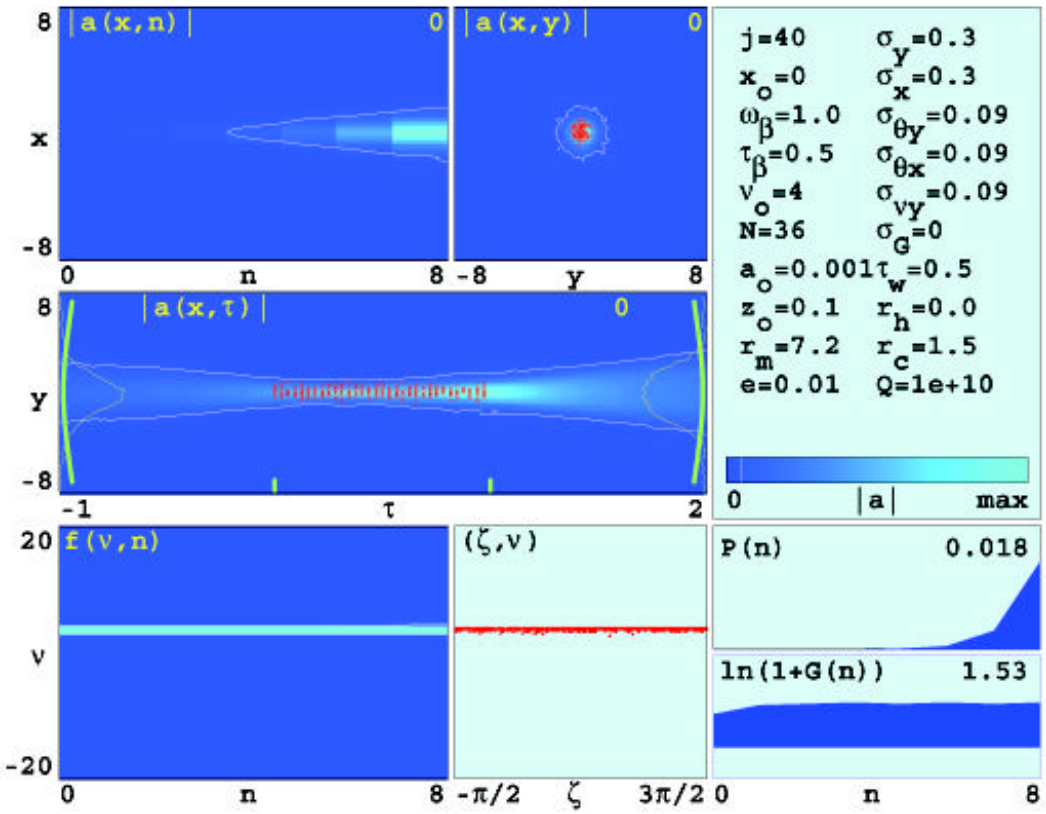

Figure 31. Weak Field Gain Simulation

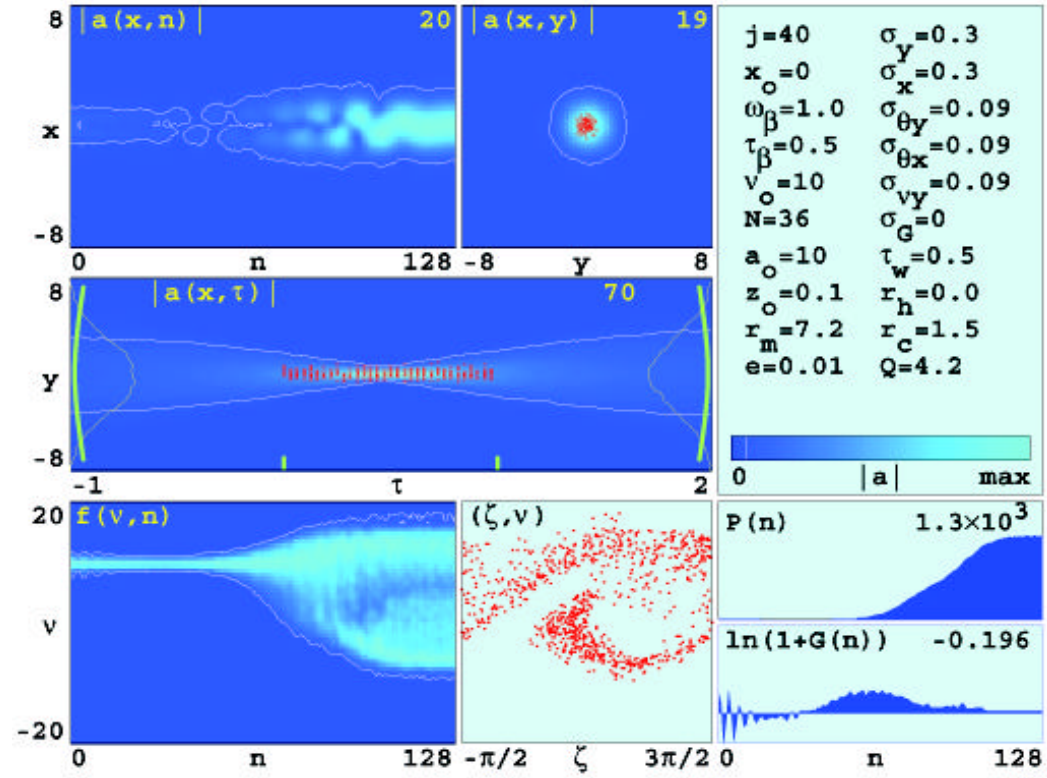

Figure 32. Extraction Efficiency Simulation

These simulations have been run over many values of n_0 near resonance to determine the peak values of gain and efficiency shown. Figures 31 and 32 represent the highest values of gain and extraction efficiency found for $z_0 = 0.1$ and $s_x = s_y = 0.3$.

The plot in the upper left of Figures 31 and 32, $|a(x,n)|$, tracks optical mode intensity at $t = 1$ over time, as viewed in the transverse direction. In Figure 31, the pulse has passed over the undulator $n = 8$ times, while $n = 128$ passes were used in Figure 32. The top center plot, $|a(x,y)|$, and the center plot, $|a(x,t)|$, show the optical mode shape after the final pass through the undulator. The top center plot is an end-view of the optical pulse as it exits the undulator at $t = 1$, while the center plot is a side view. In all of these plots, the red indicates electrons, while the yellow contour lines show the boundary of 5% of the peak optical field strength. Additionally, the middle plot also shows the optical intensity on either end of the diagram. Notice that the optical pulse on the mirrors extends outside of the contour lines, and the contour lines appear to begin to squeeze in near the mirrors. The contour lines are 5% of the largest optical field on the entire plot, not 5% of the optical field at that location in t. Notice also that many electrons are outside of the optical pulse's high intensity areas near the middle of the undulator where the optical pulse is strongest. For computational purposes, the mirror separation was shortened to three times the undulator length instead of the actual separation of 11 times the undulator length. The additional resonator length does not contribute to the optical field development, and is not significant for FEL operation, but only serves to allow the light to expand without interactions. To save computational time, the light is reflected sooner at $t = -1$ and $t = 2$. The lower left plot, *f(v,n)*, presents the electron phase velocity distribution at $t = 1$ after n passes of light through the undulator. The final electron phase-space plot is presented in the lower center. The bottom right hand corner shows the development of gain *G(n)* and dimensionless optical power *P(n)*. The numbers in the upper right corner of these plots give the peak magnitude of gain or power, while the final values are recorded as data (not shown) in the output file.

C. EFFECTS ON WEAK FIELD GAIN

Low field gains are studied to ensure that the laser will be able to take a field from spontaneous emission and develop it to a high enough field strength that substantial energy exchange can occur. Fields must not only be amplified, but must overcome the losses resulting from cavity transmission and mirror edge losses, which are assumed to total 23% for JLAB's FEL. In the low power regime, power will rise exponentially at a steady gain until either saturation is reached or the beams exit the undulator.

The goal of the gain simulations is to capture the FEL wavefront evolution during this power rise with constant gain, and ensure the gain is > 23% during this period. Figure 31 captures a very high gain ($\ln(1+G(n)) = 1.53$) of G 3.62, well in excess of the 0.23 that must be overcome for optical field growth. Notice that the lower left plot shows virtually no change in n throughout the simulation because the electron energy is approximately constant when little energy is being given to the weak optical field.

Figure 33 plots gain G versus initial electron phase velocity v_0 for the Rayleigh lengths z_0 = 0.1, 0.2, 0.3, 0.4, and 0.5. All initial gain simulations were run with an electron beam size $s_x = s_y = 0.3$. Peak gain for Rayleigh lengths z_0 = 0.1 to 0.4 occurred at an initial electron phase velocity of $v_0 = 4$ and at $v_0 = 3$ for $z_0 = 0.5$. These simulations indicate the shorter Rayleigh length improves gain for JLAB's FEL design, with all values of Rayleigh length tested achieve substantially more than the 0.23 gain required for optical field growth to saturation. Recall, however, that this simulation does not consider short-pulse effects, and therefore gives higher than expected values for gain.

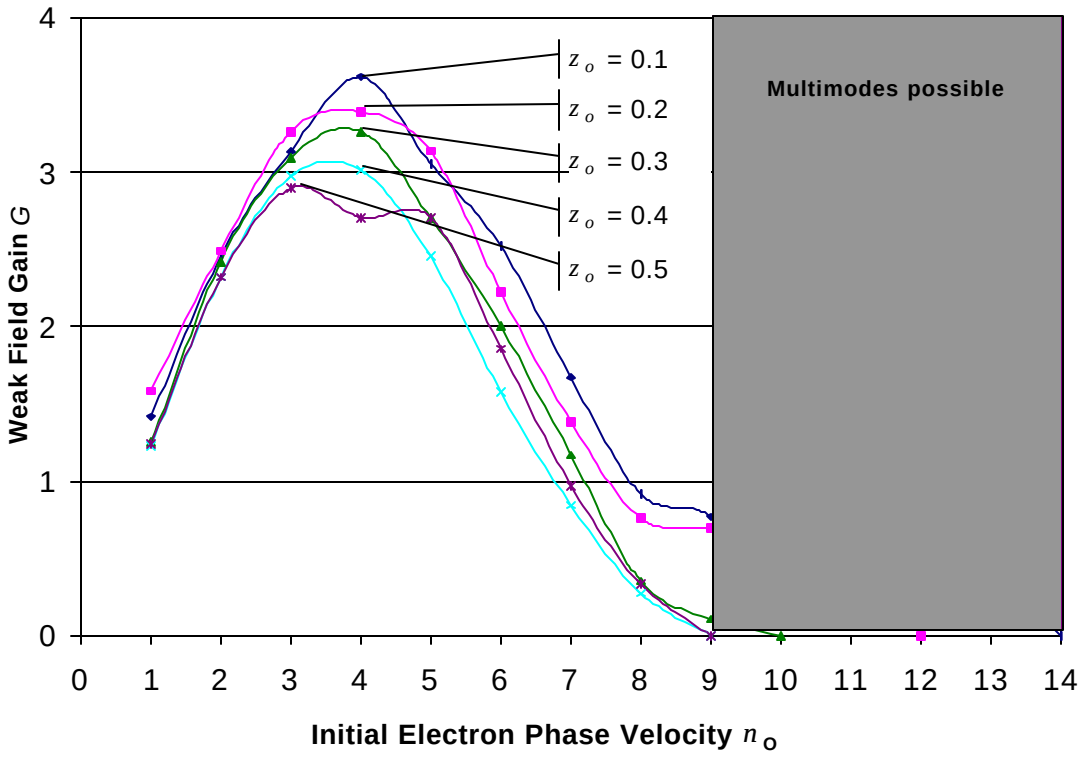

Figure 33. Weak Field Gain Simulation Results

D. EFFECTS ON FINAL OUTPUT POWER

Having determined that the short Rayleigh length design will start up, a determination of final steady state efficiency h is desired. The TJNAF proposed 100 kW FEL will operate with an electron beam power of 14 MW, and requires an extraction efficiency of $h > 0.7\%$ to reach the 100 kW output.

Extraction efficiency simulations use 21% mirror transmission (Q = 4.2) and 1% edge loss. Figure 32 shows that after 128 passes, power has reached a final steady state level, with final gain near zero. Notice that a_0 was started at 10, a value > π, which implies strong initial fields. The number in the upper right corner of the three optical field diagrams of Figure 32 give the peak optical field strength within each picture. The intense optical field of 70 in the longitudinal cross-section (middle picture) has been reduced to 19 by the end of the undulator. The reduction in optical field strength is due to the short Rayleigh length, which has allowed the beam to spread by a factor of 5 in the last half of the undulator length. The lower electron phase velocity distribution and phase

space plot show a substantial drop in the average electron energy, although some electrons end up higher than initial n_0.

Figure 34 plots the extraction efficiency h versus the initial electron phase velocity v_0 for the Rayleigh lengths of z_0 = 0.1, 0.2, 0.3, 0.4, and 0.5. All initial efficiency simulations were run with an electron beam size s_x = s_y = 0.3. Peak efficiency occurred at higher values of v_0 as the Rayleigh length was shortened. All the values of the Rayleigh length tested achieved more than the 0.7% efficiency required to achieve 100 kW. Recall, again however, that this simulation does not consider short-pulse effects, and therefore gives higher than expected values for final efficiency.

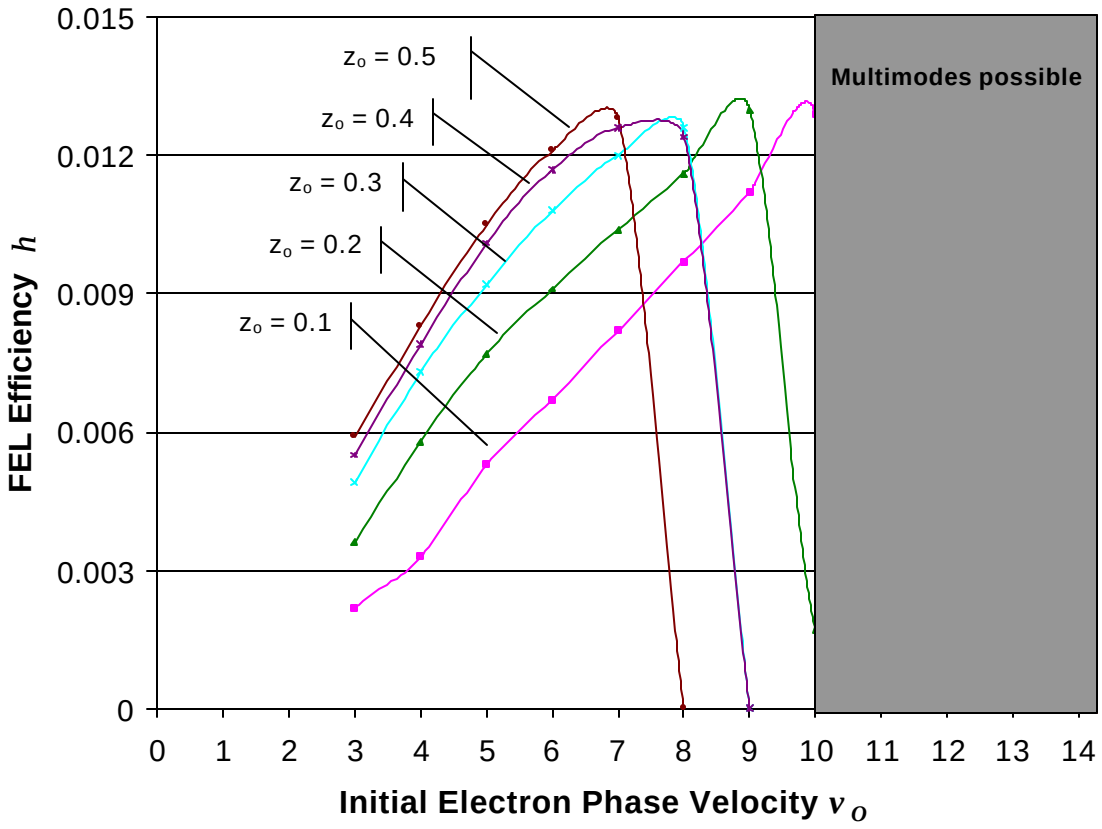

Figure 34. Strong Field Efficiency Simulation Results

E. VARYING ELECTRON BEAM SIZE

Given the change in the filling factor F and the existence of portions of the electron beam outside the optical mode waist for short Rayleigh lengths, it is reasonable to consider the effect of varying the electron beam radial coordinates s_x and s_y.

The values of the weak field gain and extraction efficiency determined above are all found using $s_x = s_y = 0.3$. Figure 35 shows weak field gain versus electron beam radius at Rayleigh lengths of z_0 = 0.1, 0.2, 0.3, 0.4, and 0.5. Gains are plotted for the peak electron phase velocity result found previously for each value of z_0 at each value of s_{xy}.

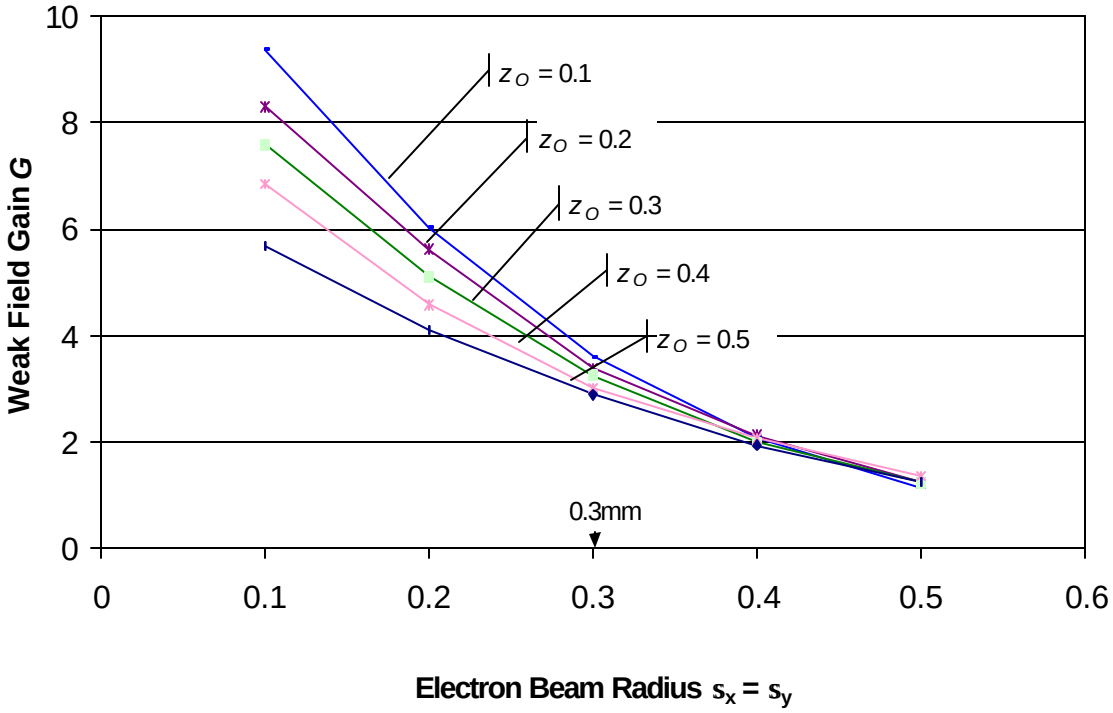

Figure 35. Weak Field Gain vs. Electron Beam Radius

As electron beam radius increased, gain decreased for all values of z_0. Apparently, the effect of utilizing a higher fraction of electrons in the optical mode waist is the dominant effect, increasing performance.

Similarly, Figure 36 presents a plot of the peak values of efficiency for each value of z_0 versus the electron beam radius.

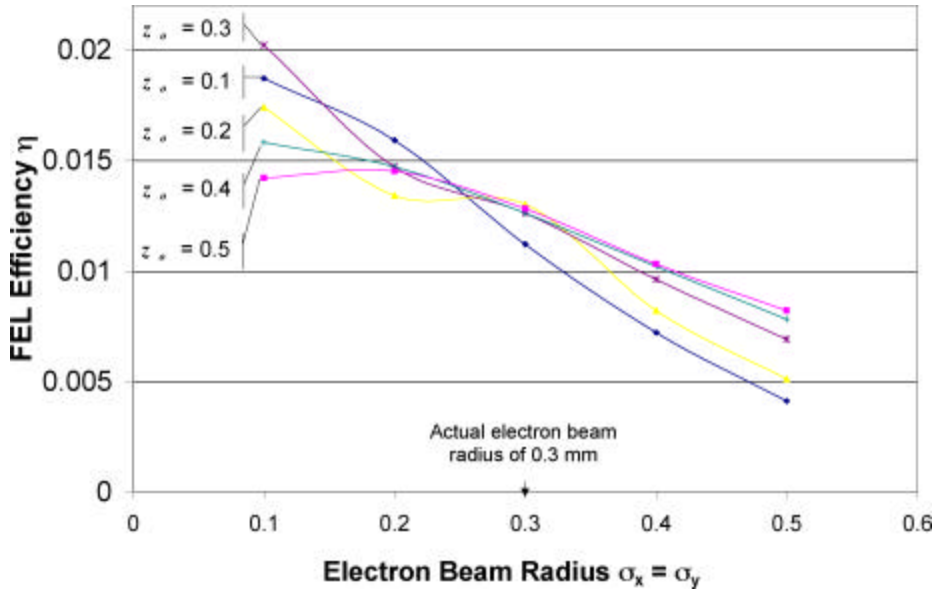

Figure 36. FEL Efficiency vs. Electron Beam Radius

In Figure 36, the general trend is for the FEL efficiency to increase as electron beam radii s_x and s_y decreases. While computing limitations prevented exploring s_x and s_y smaller than 0.1, Figure 36 shows the rolling off of efficiency as s_x and s_y is reduced below 0.3. Figure 37 shows the maximum efficiency obtained for each Rayleigh length at any tested value of s_x and s_y.

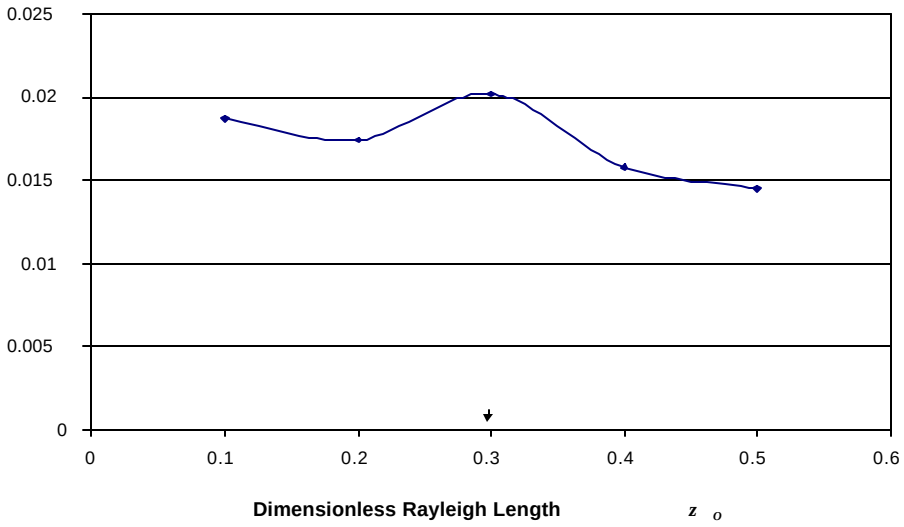

Figure 37. Peak FEL Efficiency vs. Rayleigh Length at Any Electron Beam Radius

In Figures 36 and 37, it is clear that the maximum efficiency for the FEL occurs at z_0 = 0.3, in agreement with the predicted maximum filling factor occurring at $z_0 = 1/(2\sqrt{3}) \approx 0.3$ [Colson, (c)].

F. JEFFERSON NATIONAL LABORATORY SHORT RAYLEIGH LENGTH EFFORTS

JLAB is commissioning a 10 kW FEL that has a design with an identical undulator to the 100 kW parameters given in section V above. This laser is meant to allow further study of the effects that short Rayleigh length and higher power have on laser operation. Pending successful operation of the 10 kW design, JLAB intends to upgrade their 10 kW FEL to 100 kW by the addition of an accelerator module and by raising the operating frequency from 75 MHz to 750 MHz. The simulations presented here predict that utilizing a short Rayleigh length FEL can substantially reduce intensity levels at the mirror. The decreases in gain and efficiency still allow the 100 kW goal to be attained. Although not presented within this thesis, simulations that account for the short pulse effects also indicate that the required weak field gain of > 23% and extraction efficiency of > 0.7% should be achieved in JLAB's 100 kW design.

VII. SHIPBOARD VIBRATION EFFECTS ON SHORT RAYLEIGH LENGTH FEL OPERATION

A. RESONATOR CAVITY STABILITY AND SHORT RAYLEIGH LENGTH

Lasers used in a naval application are regularly subjected to operational conditions which industrial and laboratory equipment may never face. While at sea, ships will undergo hogging, flexing, and vibrations which cannot be completely isolated from the FEL. In order to maintain the precise timing and alignment required between the electron pulse and the optical wave, FEL oscillators require extremely precise mirror separations and alignment. Offsets within microns of the desired cavity length are sufficient to prevent operation of an FEL. While shock mounting can reduce many vibrations from coupling to the mirror surfaces within an FEL cavity, complete decoupling is not achievable. In particular, near-concentric cavities, such as those required by short Rayleigh length FEL cavities, operate near the limits of stability in a cold cavity [Siegman]. (A cold cavity is a resonating cavity that has no method of producing gain, i.e. no electron beam.) Small vibrations could create mirror offsets or tilts, which allow the optical mode to rotate. The FEL, however, is not a cold cavity; the electron beam interaction with the optical wave provides gain. This gain encourages optical mode stability so that the light maintains overlap with the gain medium (in this case the electron beam).

B. SIMULATION TECHNIQUE

The impact of shipboard vibrations on the 1 MW system described in Section IV.B have been explored through use of a modified version of the three-dimensional transverse wavefront evolution simulation (described previously in Section VI.B) which allows one end mirror to be tilted. A constant mirror tilt maintained throughout the simulation is adequate to account for mirror vibrations. The highest frequency the FEL mirror can sustain is on the order of tens of kHz. With 23% losses per pass, a typical photon of light is in the 12m cavity for less than 0.1 μsec, a very small fraction of a complete 10kHz oscillation, which takes 100ms to complete. To the light pulse, the mirror appears steady but tilted through any small fraction of oscillation. The question

then becomes at what amplitude of vibration, translated into mirror tilt, can the FEL maintain power levels sufficient for weapon applications. Normalized mirror tilt angles q_m in the simulation are related to an actual mirror angle q by

$$q_m = \frac{q}{\sqrt{l/pL}} = \frac{q}{730\ \mu\text{rad}} \tag{6.1}$$

for l = 1 μm and L = 60 cm.

Figure 38 shows the output of the wavefront evolution simulation for q_m = 0.25 (q ≈ 180 μm) with initial electron phase velocity v_0 = 10. The simulation angle q_m = 0.25 corresponds to an actual mirror tilt of 200 μrad, resulting in about half (54%) of the power level observed when no mirror tilt is present. Active mirror alignment systems are currently used which hold mirror vibrations to less that 0.1 μrad, 1/2000 of the mirror tilt angle used for the simulation shown in Figure 38.

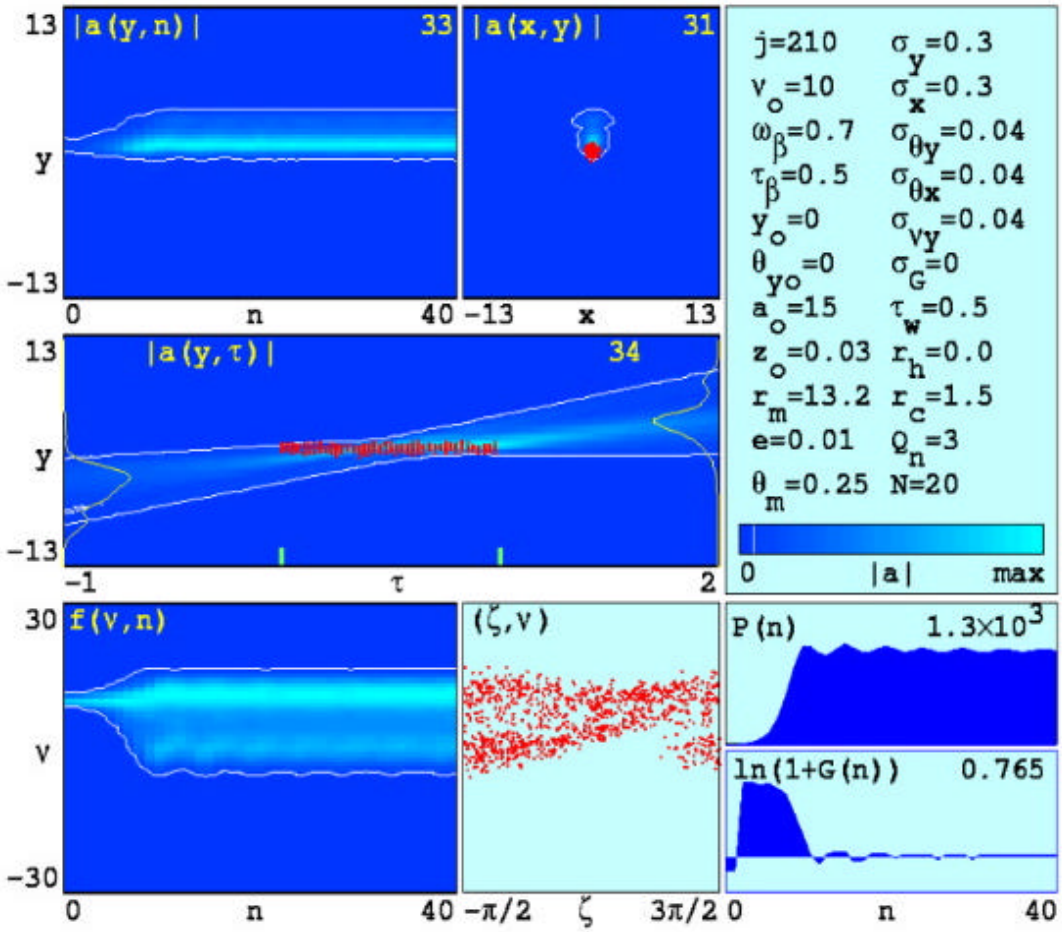

Figure 38. Mirror Tilt Simulation Results

In the center image $|a(y, t)|$ the optical mode rotation is clearly seen. The rotation is extremely exaggerated since 180 cm are shown on the t-axis, compared to 12 mm shown in the y-axis. Notice the rotation of the optical beam is such that the edge of its intensity peak remains contained in the right side of the electron beam. This is where the electrons are heavily bunched, and the laser is operating at saturation. This effect is clearly illustrated in the upper right picture $|a(x, y)|$, which shows the end view of the optical mode at the end of the undulator.

Due to the extremely high power generated by a 1 MW laser and the relatively short (≈12m) resonator cavity desirable for shipboard use, a Rayleigh length of $z_0 = 0.03$ (1.8 cm) is necessary to reduce optical intensities at the resonator mirrors to acceptable levels.

C. SIMULATION RESULTS

With no significant reduction in power found for mirror tilt angles up to 2 mrad, further simulations were conducted to determine how much tilt could be sustained with continued operability.

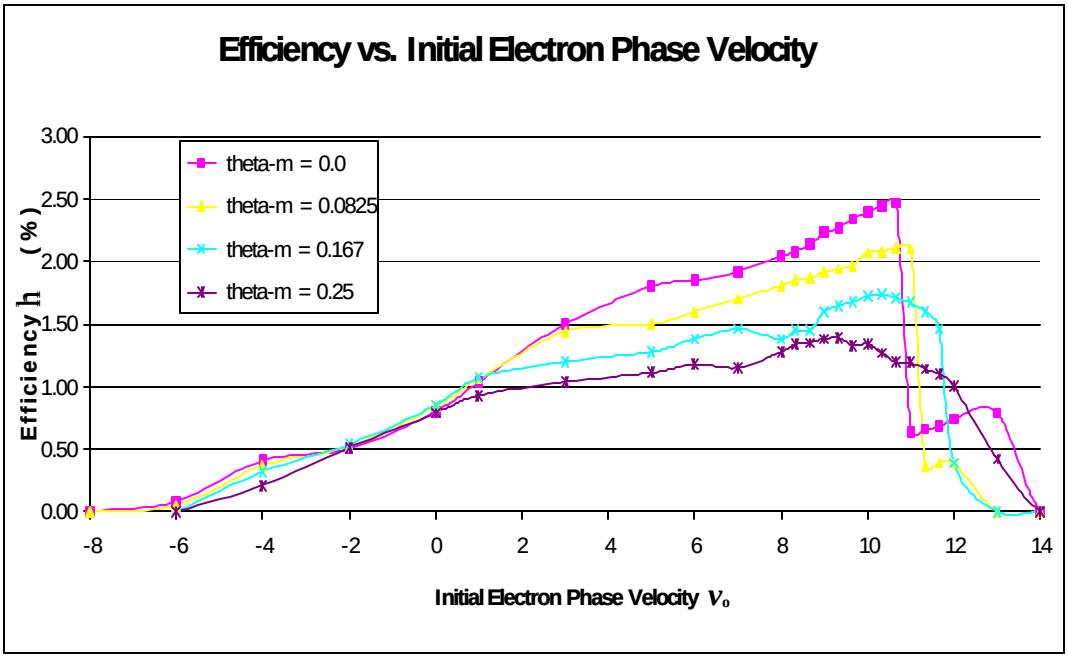

Figure 39. Efficiency vs. Initial Electron Phase Velocity as a Function of Mirror Tilt q_m

Figure 39 shows FEL efficiency h as a function of initial phase velocity v_0 for mirror tilts q_m = 0, 0.0825, 0.167, and 0.25 (corresponding to real offset angles q = 0, 67, 133, and 200 μrad). Similar data points were collected for q_m = 0.325, 0.4, and 0.5 (q = 260, 320, and 400 μrad). The peak efficiency found for each value of q_m is plotted in Figure 40.

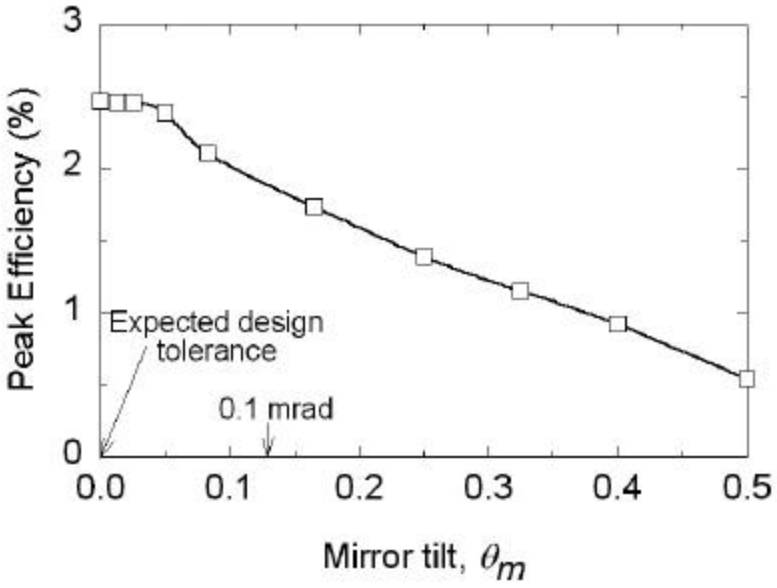

Figure 40. 1 MW Efficiency vs. Mirror Tilt

Efficiency decreases as the mirror tilt increases. Beyond 60 μrad, the efficiency decreases linearly. Modern active mirror alignment systems can maintain mirror tilts less than 0.1 μrad. Perhaps the most important feature in Figure 40 is that for mirror tilts less than the currently achievable limit of 0.1 μrad, there is no noticeable change in the FEL efficiency. Simulations conducted for the proposed 100 kW FEL at TJNAF [Crooker, 2002] yield similar results, presented in Figure 41. Notice, however, the linear drop in efficiency occurs much sooner, at approximately 2 μrad, in the 100 kW simulations.

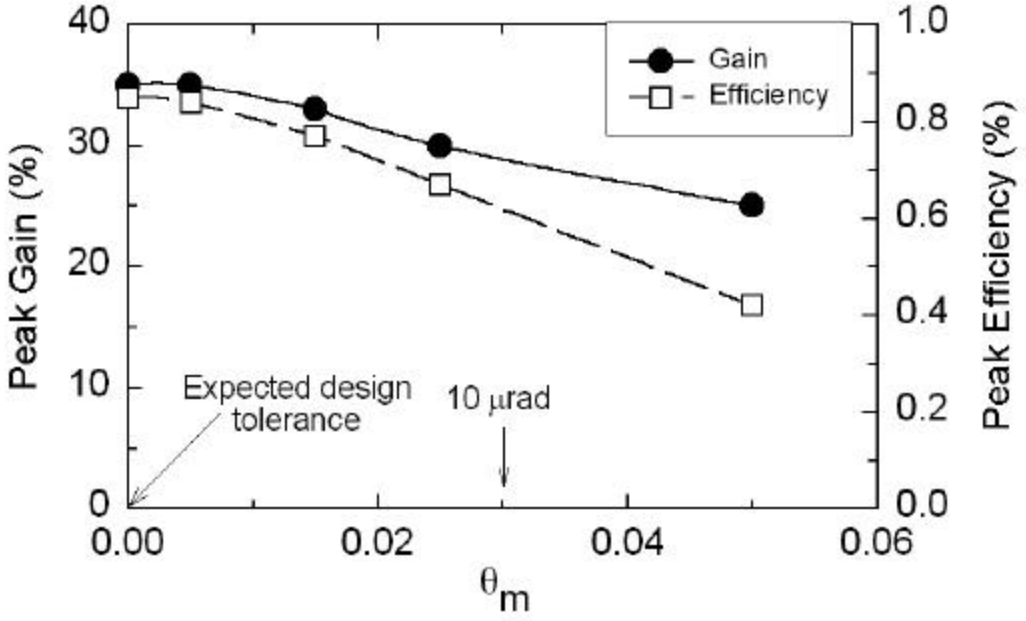

Figure 41. 100 kW Tilted Mirror Efficiency and Gain

D. INTERPRETATIONS AND CONCLUSIONS

Mirror rotations induced by shipboard vibrations will not affect the output power of an FEL when an active alignment system is used to maintain mirror tilt less than 20 μrad. The stabilizing effect of the electron beam in the FEL resonator cavity prevents the optical mode from rotating away from the gain medium, thus allowing continued operation at high powers. A comparison of the results of the 100 kW simulations with the 1 MW simulations indicate that greater values of the dimensionless current j substantially raise the mirror tilt operating tolerance of an FEL.

THIS PAGE INTENTIONALLY LEFT BLANK

VIII. CONCLUSION

Defending a ship against modern ASCMs is challenging. A combination of long-range and short-range missiles are used to engage incoming ASCMs, with PHALANX gunnery system used in a point defense role to destroy any ASCMs that slip through the anti-missile missiles and get within 2,000 meters of the ship. At such close ranges, if the PHALANX does destroy the missile, many missile fragments may strike the ship, which could still cause severe damage. Directed energy weapons can provide target engagement at the speed of light, moving the ASCM destruction range away from the ship so that fragments will not hit the ship. In addition to point defense duties, an HEL's ability to precisely deliver damage makes the HEL a capable offensive weapon against many asymmetric threats. The HEL optics can also serve as a high-resolution visual surveillance device.

The all-electric FEL can theoretically be scaled up to a MW class laser capable of naval weaponization. In the Navy's pursuit of a MW class laser, Thomas Jefferson National Accelerator Facility is commissioning a 10 kW FEL, with plans to upgrade to 100 kW in 2005. The high power levels of a MW class laser could easily damage the mirrors. JLAB's 10 kW FEL, and later the 100 kW FEL, are designed to explore the use of a short Rayleigh length to lower the optical intensities on the mirrors. Simulations show that a short Rayleigh length will significantly reduce optical intensities at the mirror without significant degradation of laser performance.

Shipboard application of an FEL poses problems to a laser that are not typically encountered in a laboratory setting. An FEL resonator, which must be tuned within microns of length, will be subject to shipboard motions, vibrations, and contortions. Simulations show that the high current necessary in a MW class FEL acts to stabilize the optical mode through oscillations that result in mirror tilting. When used in conjunction with an active mirror alignment system, output power is not affected.

The capabilities of a directed energy weapon are different from any other Navy system. The ability to strike a lethal blow at the speed of light with such precision would provide a new force in point defense, as well as a quick-response precision weapon in the

fight against anti-symmetric threats. With continued research into the effects of high-power short Rayleigh length, and in creating compact laser components, a MW class system is achievable within a decade.

APPENDIX A AN INTRODUCTION TO PHASE SPACE

Phase space plots are commonly used when examining systems that have periodic motions, such as a pendulum or a planet in orbit about a star. Both the planet and a simple pendulum exchange kinetic and potential energy between themselves and the source of gravitational pull. Since the equations of motion of electrons in an FEL undulator are mathematically the same as those of a pendulum, phase space diagrams are useful to graphically represent the electron's energy exchange just as it does that of a pendulum. The FEL electrons, however, are exchanging their kinetic energy with the energy contained in the optical field.

Figure 42 [Colson (b), pp. 24] is a phase space plot of a pendulum in closed orbit. In closed orbits, the pendulum does not have enough energy to swing over the top, but rocks back and forth.

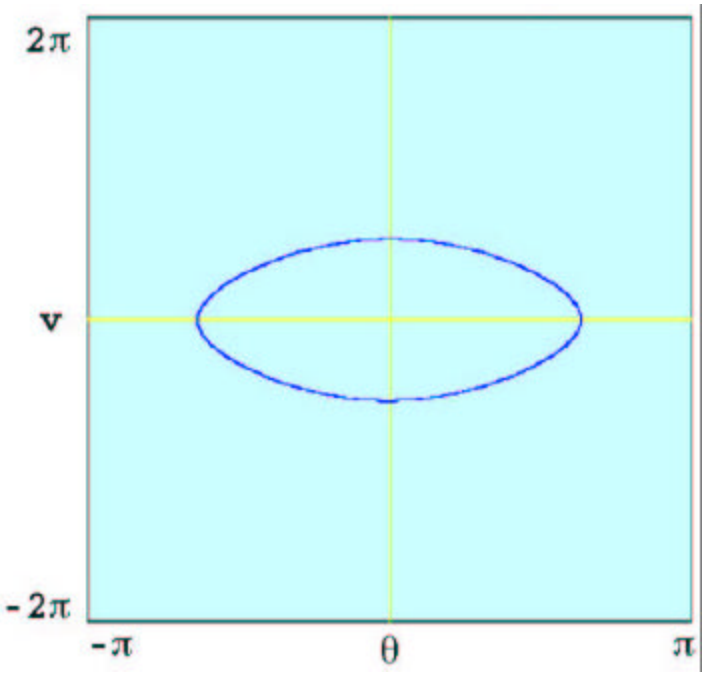

Figure 42. Simple pendulum closed-orbit phase space plot

Notice the axes of the plot are the phase velocity $n = \dot{q}$ versus the phase position q. If the pendulum is initially released from an initial angle q_0, it will fall and begin to rock back

and forth. In Figure 42, the pendulum initial position is q_0 , with angular velocity $n = \dot{q} = 0$ just as the pendulum is dropped. The pendulum begins travel from $q_{max}= 2$ with $\dot{q} < 0$, shown as the downward arc, until it reaches $q_{max}= -2$, where it reverses direction and begins to fall with $\dot{q} > 0$, shown as the upper arc. In a system where no energy is lost from the pendulum, the same phase space path will be made by the pendulum forever. If the pendulum were to lose energy to friction, it would slow down and not swing quite as far outward. In a phase space plot, this would be illustrated as the path spiraling in on itself, ending at $q = \dot{q} = 0$. Similarly, if you were to give the pendulum a well timed push, causing it to swing out farther, the path would open up to a wider ellipse shape, having larger peak values for both q and $\dot{q}$.

If you were to give the pendulum enough energy so that it makes it exactly to the top of its swing and stops, the path formed on a phase space plot is called the separatrix, and is shown in Figure 43 [Colson (b), pp. 26].

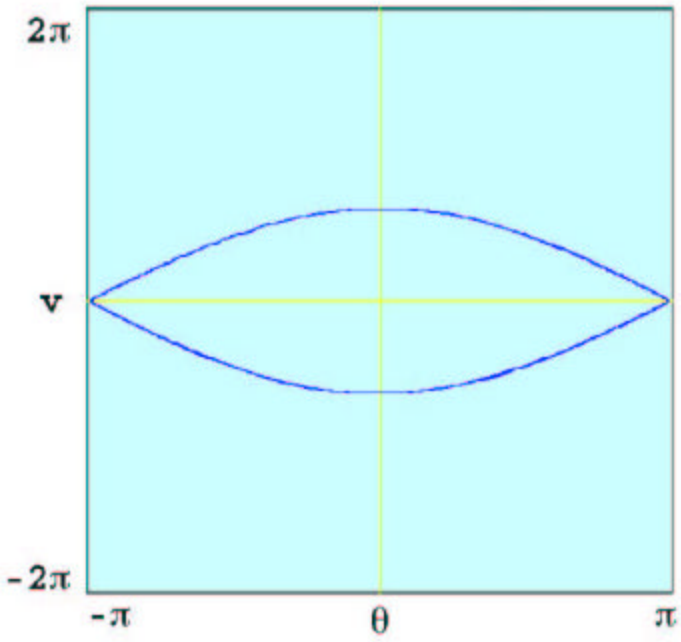

Figure 43. Pendulum separatrix

If any more energy is given to this pendulum, it will begin looping over the top. If no energy is lost to friction, it will never change directions. Open orbits are formed when the pendulum has enough energy to loop over the top. These are illustrated on a phase space plot by a path passing over the top of the separatrix for $\dot{q} > 0$, or a line passing underneath the bottom for $\dot{q} < 0$. Figure 44 [Colson (b), pp. 25] shows an example of an open orbit illustrating a pendulum passing over the top in the $\dot{q} > 0$ direction.

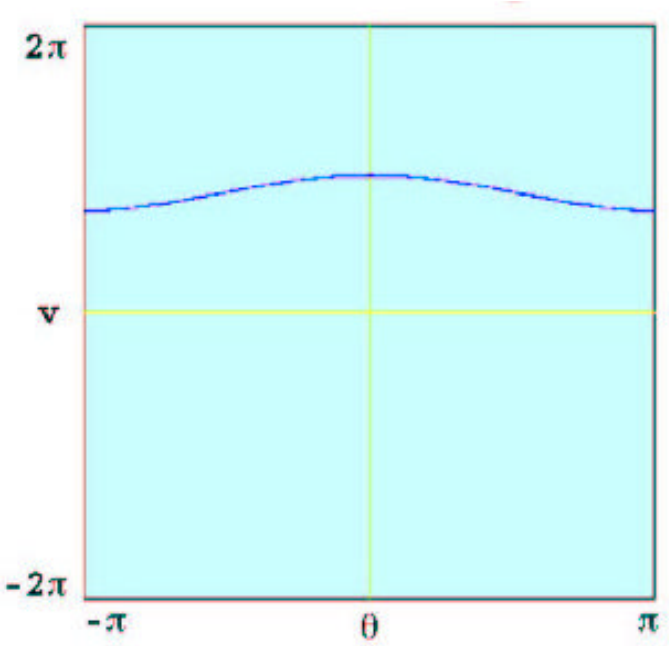

Figure 44. Simple pendulum open-orbit phase space plot

THIS PAGE INTENTIONALLY LEFT BLANK

LIST OF REFERENCES

1. Anderberg, Bengt, Major General (Swedish Army), *High-Energy Laser Weapons* excerpted from pp.107-137 of *Laser Weapons: The Dawn of a New Military Age*, *f*1992)
2. Blau, Joseph, *Multimode Simulations of Free Electron Lasers,* (March 2002)
3. Colson, W. B., Naval Postgraduate School,
    a. *FEL Theory ppt*., (15 October 2002)
    b. *FEL Modeling and Simulation*, PPT presentation at 2002 DEPS symposium
    c. *Classical Free Electron Laser Theory*, Chapter 5 in *Free Electron Laser Handbook*, (December 1990)\
    d. *PH 4911 Notes*, (2002)
4. Crooker, P. P.; Campbell, T., LT (USN); Ossenfort, W., LT (USN); Miller, S., LT (USN); Blau, J.; Colson, W.; *A Study of the Stability of a High-Power Free Electron Laser Utilizing a Short Rayleigh Length,* FEL 2002 Conference Paper, September 2002
5. DSBTF (Defense Science Board Task Force), *High Energy Laser Weapon Systems Applications,* (June 2001)
6. Eash, Joseph J. III, *The Tactical High-Energy Laser – The Implications For Future Warfare Of Engaging Targets At The Speed of Light*, Armed Forces Journal International, (October 2000)
7. FAS, Federation of American Scientists, Military Analysis Network http://www.FAS.org, (September 2002)
    a. *AN/SLQ-49 Chaff Buoy System*, (December, 1998)
    b. *AN/SLQ-49 Electronic Warfare (EW) system*, (June 1999)
8. GAO (Government Accounting Office), *Comprehensive Strategy Needed to Improve Ship Cruise Missile Defense*, Letter Report, 07/11/2000, GAO/NSIAD-00-149
9. Griffiths, David J., *Introduction to Electrodynamics*, 2nd edition, (1989)
10. HELERP (High Energy Laser Executive Review Panel), *High Energy Laser Program Annual Report to Congress*, (15 February 2001)
11. HELTAWG (High Energy Laser Technology Area Working Group), *High Energy Laser Program Annual Report to Congress* Background Documentation, (February 2001)
12. Jackson, *Classical Electrodynamics,* 2nd Edition, (October 1975)

13. Jane's Information Group
    a. *Jane's Land-Based Air Defense*, Fourteenth Edition (2001)
    b. *Jane's Naval Weapons Systems*, Online Edition (2002)
    c. *Jane's Fighting Ships*, Online Edition (2002-2003)
    d. *Jane's Radar and Electronic Warefare Systems*, Online Edition (2002-2003)
    e. *Jane's Major Warships*, Online Edition (1997)
    f. *Jane's Electro-Optic Systems*, Online Edition (2002-2003)
    g. *Jane's Strategic Weapon Systems*, Online Edition (April 2002)
14. JLAB.org, Thomas Jefferson National Accelerator Facilities, http://www.jlab.org/FEL/feldescrip.html, (October, 2002)
15. Kittle, C. *Introduction to solid State Physics*, 5th Edition, (1976)
16. LANL.gov, Los Alamos National Laboratory, http://www.lanl.gov/orgs/ibdnew/DTIN/open/UsrFac/userfac03.html, (September, 2002)
17. McWhite, James D., email to NSSC, (fwd by CDR Roger McGinnis), *Navy After Next – All Electric Ship Studies, New Info of FEL Requirements*, (2 July 2001)
18. Natter, Robert, Admiral, USN, *Memo to CNO SerN00/080*, (24 April 2001)
19. NFF (Navy Fact File),
    a. *Phalanx Close-In Weapons System*, (13 September 1999)
    b. *RIM-116A Rolling Airframe Missile (RAM)*, (20 May 2002)
    c. *Sparrow Missile*, (17 September 2002)
    d. *Standard Missile System*, (2002)
20. Neil, George, Thomas Jefferson National Accelerator Facilities, per e-mail
21. Ng, Ivan, *A Free Electron Laser Weapon For Sea Archer*, (December 2001)
22. Ossenfort, W., Blau, J., Campbell, T., Colson, W. B., Ng, I., Benson, S. V., Neil, G. R., Shinn, M. D., *Simulation of the 100 kW TJNAF FEL Using a Short Rayleigh Length*, Nuclear Instruments and Methods in Physics Research, A 483 (2002), 142-145
23. (RCA) Solid State Division of RCA, Inc., *Electro-Optics Handbook*, (1974)
24. Dr. Josef Shwartz and Schnurr, *Nautilus Project – Tactical High Energy Laser Advanced concept Technology Demonstration*, (February 2001)
25. A. E. Siegman, *Lasers*, Chapter 19, (1986)
26. Stock, Robert D., *Computer Simulations for a Maritime FEL*, presented at 2001 Free Electron Later Development for Naval Applications Conference, (5 July 2001)

27. Todd, Alan, Advanced Energy Systems
    a. and Colson, Bill, *High-Power, Compact, Free-Electron Laser Concepts* (2002)
    b. per e-mail to Bill Colson (17 May 2001)
    c. *High-Power FEL Point Designs (ppt)*, (July 2002)
    d. per fax to Bill Colson (19 October 2002)
28. Welch, General, USAF and Mr. Latham, *MEMORANDUM FOR THE CHAIRMAN, DEFENSE SCIENCE BOARD* (August 2, 2001)
29. White, *21st Century Air Defense – Tactical High Energy Laser*, Air Defense Artillery Magazine Online (Summer 1998)

THIS PAGE INTENTIONALLY LEFT BLANK

INITIAL DISTRIBUTION LIST

1. Defense Technical Information Center
   Ft. Belvoir, Virginia

2. Dudley Knox Library
   Naval Postgraduate School
   Monterey, California

3. Dr. Fred Dylla
   TJNAF
   Newport News, VA

4. CDR Roger McGinnis, USN
   Naval Sea Systems Command, Code SEA 53R
   Washington Navy Yard, DC

5. Dr. George Neil
   TJNAF
   Newport News, VA

6. Dr. Alan Todd
   Advanced Energy Systems, Inc.
   Princeton, NJ

7. Dr. Gil Graff
   Office of Naval Research, Code 351
   Arlington, VA

8. Michael B. Deitchman
   Office of Naval Research, Code 351
   Arlington, VA

9. Professor William B. Colson
   Naval Postgraduate School
   Monterey, California

10. Professor Robert L. Armstead
    Naval Postgraduate School
    Monterey, California

11. Professor Peter P. Crooker
    Naval Postgraduate School
    Monterey, California

12. Professor Joseph A. Blau
Naval Postgraduate School
Monterey, California

13. Chairman, Physics Department
Naval Postgraduate School
Monterey, California

14. Lieutenant William J. Ossenfort Jr, USN
Naval Submarine School
Groton, Connecticut